

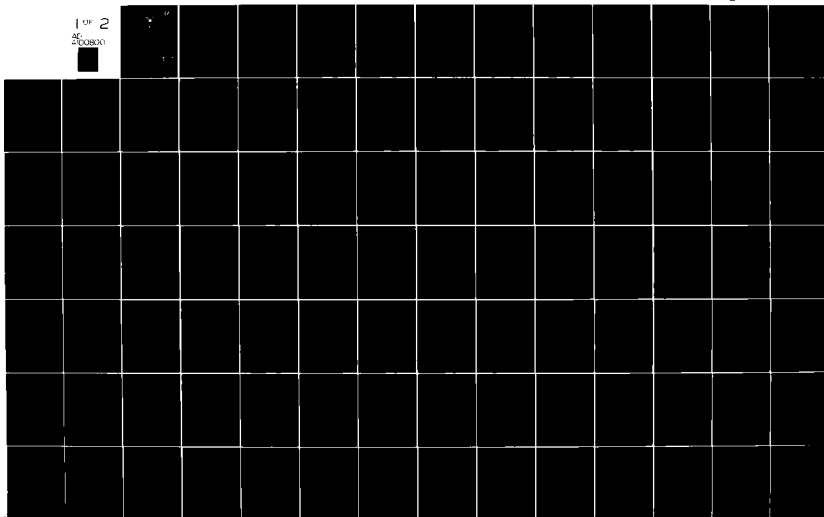
AD-A100 800

AIR FORCE INST OF TECH WRIGHT-PATTERSON AFB OH SCHOOL--ETC F/8 20/6
PHASE ESTIMATION TECHNIQUES FOR ACTIVE OPTICS SYSTEMS USED IN R--ETC(11)
DEC 80 F P ROJAS
AFIT/8EO/EE/80D-8

UNCLASSIFIED

ML

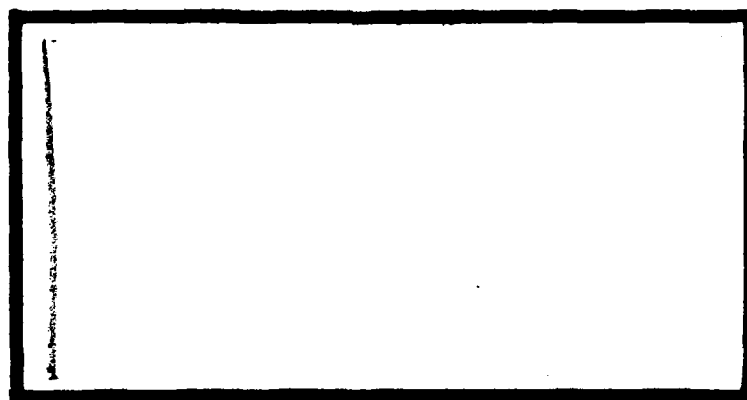
1 OF 2
26 000000



NDAC

AD A100800

①
LEVEL II



DTIC FILE COPY

DTIC
ELECTE
JUL 1 1981
S D

DEPARTMENT OF THE AIR FORCE
AIR UNIVERSITY (ATC)
AIR FORCE INSTITUTE OF TECHNOLOGY

Wright-Patterson Air Force Base, Ohio

DISTRIBUTION STATEMENT A

Approved for public release;
Distribution Unlimited

81 6 30 036

AFIT/GEO/EE/80D-4

Accession For	
NTIS GRA&I	<input checked="checked" type="checkbox"/>
DTIC TAB	<input type="checkbox"/>
Unannounced	<input type="checkbox"/>
Justification	
By	
Distribution/	
Availability Codes	
Dist	Avail and/or Special
A	

PHASE ESTIMATION TECHNIQUES FOR ACTIVE
OPTICS SYSTEMS USED IN REAL-TIME
WAVEFRONT RECONSTRUCTION.

14
THESIS

AFIT/GEO/EE/80D-4

FERNANDO P. ROJAS
1st Lt 4 USAF

14
DTIC
ELECTE

JUL 1 1981

D

Approved for public release; distribution unlimited

015225

AFIT/GEO/EE/80D-4

PHASE ESTIMATION TECHNIQUES FOR ACTIVE
OPTICS SYSTEMS USED IN REAL-TIME
WAVEFRONT RECONSTRUCTION

THESIS

Presented to the Faculty of the School of Engineering
of the Air Force Institute of Technology
Air University
in Partial Fulfillment of the
Requirements for the Degree of
Master of Science

by

FERNANDO P. ROJAS, B.S.

1st Lt USAF

Graduate Electro-Optics

December 1980

Approved for public release; distribution unlimited

Preface

The work of this thesis was prompted by a paper published in 1975 by J. C. Wyant on the subject of phase estimation for wavefront correction systems. His technique for estimating the phase differentials measured from lateral shearing interferometry on an optical wavefront had the form of a simple and appealing algorithm. The need for a closer examination of Wyant's technique from a statistical point of view was a motivating factor for the work of this thesis, as was also the possibility of obtaining improved performance from joint processing of multiple measurements performed by real-time wavefront correction systems.

I would like to thank Capt. Stanley R. Robinson for suggesting the topic and giving me initial advice and encouragement. I would also like to thank the members of my thesis committee, Dr. Peter S. Maybeck and Lt Col Ronald J. Carpinella, for accepting reading of this paper and for offering their comments and constructive criticism. I also appreciate useful conversations with 2Lt Martin B. Mark who worked on a related topic. I also thank M. Sally Lindsay for her typing of this thesis.

Finally, I would like to extend my gratitude to my thesis advisor, Capt. James M. Moore, whose guidance and encouraging advice throughout this work are greatly appreciated.

Fernando P. Rojas

Contents

	Page
Preface	ii
List of Figures	v
List of Tables	vii
List of Symbols	viii
Abstract	xiv
I. Introduction	1
System Description	1
Problem Statement	2
Approach	4
Scope and Assumptions	4
II. The Shearing Interferometer	7
Output Field	8
Detector Signal	10
III. Phase Estimation Preliminaries	12
Signal Model	14
Maximum A Posteriori and Maximum Likelihood Estimation Theories	20
IV. Phase Estimation in White Gaussian Noise	22
Maximum A Posteriori Estimate	25
Maximum Likelihood Estimate	34
Performance of the Estimators	38
Verification of the MAP and ML Estimators	58
V. Phase Estimation in Shot Noise	73
Maximum A Posteriori and Maximum Likelihood Estimates	74
Performance of the Phase Estimators in Shot Noise	80
VI. Joint Processing of Array Signals for Wavefront Estimation	88
Multidimensional Estimator Formulation	89
Wavefront Estimation from the Shearing Interferometers	94
Estimator Performance	109

Contents (Continued)

	Page
VII. Conclusions and Recommendations	114
Conclusions	114
Recommendations	117
Bibliography	119
Vita	121

List of Figures

Figure		Page
1	A Typical Real-Time Wavefront Correction System	3
2	A Two Shearing-Interferometer Sensor Used with Wavefront Correction Systems	8
3	Expanded View of the X-Channel Interferometer	9
4	Phase Distribution at the Aperture Seen by Detectors in the Back Focal Plane	13
5	Equivalent Correlator Model of the CCD Detector	15
6	Photon Count Processor for MAP Estimation of θ	32
7	The Error Variance as a Function of Algorithm Form	45
8	Relationship between γ_k and k as a Product	46
9	Relative MSE Improvement Compared to the Error in Three Subintervals	50
10	MAP Simulation Results - Single Phase at Different SNR's	60
11	MAP Simulation Variance - Single Phase at Different SNR's	62
12	MAP Simulation Results - Multiple Phase Angles at a Fixed SNR	63
13	MAP Simulation Variance - Multiple Phase Angles at a Fixed SNR	64
14	MAP Simulation Run with Improved Phase Variance	65
15	MAP Simulation Error Using Improved Phase Variance	66
16	ML Simulation Results - Single Phase at Different SNR's	68

List of Figures (Continued)

Figure		Page
17	ML Simulation Variance - Single Phase at Different SNR's	69
18	ML Simulation Results - Multiple Phase Angles at a Fixed SNR	70
19	ML Simulation Variance - Multiple Phase Angles at a Fixed SNR	71
20	Correlator-Summer Model for Joint Processing	95
21	Arrangement of Two Detector Arrays to Measure $(m+1) \times (n+1)$ Phase Points with $(m+1) \times n$ X- and $m \times (n+1)$ Y-Detectors	98
22	Arrangement of Detector Column Array for Joint Processing	100
23	Phase Estimate Distribution Over the Aperture	104
24	Phase-Detector Grid for Joint Processing of Four Detectors to Estimate Four Wavefront Phases	106
25	Correlator-Summer to Estimate Four Phases	107
26	Underlying Mechanism to Estimate ϕ_1 and ϕ_3	108
27	The Form of the Matrix $\underline{D}_a(u, \phi)$	111

List of Tables

Table		Page
I	Examples of the Maximum A Posteriori Phase Estimator Form for k Observations	35
II	Examples of the Maximum Likelihood Phase Estimator Form for k Observations	37
III	Examples of the MAP Phase Estimator Error Variance for Large SNR	48
IV	Examples of the MAP Phase Estimator Form Under Multimode Shot Noise Conditions . . .	81
V	Examples of the ML Phase Estimator Under Multimode Shot Noise Conditions	82

List of Symbols

Roman Letter Symbols

a	DC amplitude of detector signal (amps)
a_i	Equivalent of a_p in transformed coordinate system
a_p	$p^{(th)}$ element of the vector \underline{a}
\hat{a}_p	Estimated value of a_p
\underline{a}	Vector of parameters (phases)
A	Constant $A(\bar{r}_d)$ A constant used in Eq. (4-19) Same as r_1 in Eq. (7-1)
A_d	Detector area
A_o	Defined by Eq. (5-23)
$A(\bar{r}_a)$	Amplitude of optical field
b	AC amplitude of detector signal (amps)
B	Same as r_2 in Eq. (7-1) A gain factor in Eq. (7-2)
B_n	Bandwidth parameter in Eq. (4-75)
B_o	Optical bandwidth of the receiver
c	Same as b
C	Same as r_3 in Eq. (7-1)
CCD	Charge-coupled device
CDC	Control Data Corporation
CRB	Cramer-Rao (lower) bound
d	Same as a
D	Same as r_4 in Eq. (7-1)
D_s	Number of spatial modes
$\underline{D}(t, \underline{a})$	Defined by Eq. (6-23)

$D_j(\underline{a})$	Defined by Eq. (6-15)
E_a	Energy in (0,T) of the ac component of the detector signal (Joul)
$E[\]$	Statistical expectation
$E[\ \]$	Conditional expectation
f	Focal length
$f_{n(t)} n(t)$	Probability density function of the noise process
f_o	Optical frequency (Hz)
$f_{\underline{r}}(\underline{r})$	Marginal probability density function of \underline{r}
$f_{\underline{r},\theta}(\underline{r},\theta)$	Joint probability density function of \underline{r} and θ
$f_{r_j \theta}(r_j \theta)$	Conditional probability density function of r_j
$f_{\underline{r} \theta}(\underline{r} \theta)$	Conditional probability density function of \underline{r}
$f_{\underline{R} \underline{a}}(\underline{R} \underline{a})$	Conditional probability density function of \underline{a}
$f_{\theta}(\theta)$	A priori probability density function of θ
$f_{\theta \underline{r}}(\theta \underline{r})$	A posteriori probability density function of θ
FORTRAN	Formula translation
$F(\theta)$	Defined by Eq. (4-26)
$g(t)$	A function of time in Eq. (4-19)
h	Planck's constant (Joul-sec)
$h(t)$	A function of time in Eq. (4-19)
i_b	Background noise current (dc) (amps)
i_d	DC component of detector dark current (amps)
$I_d(\bar{r}_d, t)$	Optical field intensity at detector plane
$I_{mp}(dB)$	Improvement in error variance
IMSL	International Mathematical and Statistical Library
j	Index of observables in \underline{r}

κ	Row index of detector array
k	Boltzmann's constant in Eq. (4-3) (Joul/°K)
	Number of observations made in (O,T)
k_o	Defined in Table I and Eq. (4-53)
k_l	Defined in Table IV
k_p	Defined in Table I
k_q	Defined in Table IV
\underline{k}_a	Phase covariance matrix
$k_{pq,rs}$	Elements of \underline{k}_a
l	Column index of detector array
l.i.m.	Limit in the mean - defined by Eq. (3-11)
L	Interferometer lense
m	Number of rows in detector array
$m(t)$	Noise in X-shear array detectors
M	Magnification constant of interferometer
$M_{\kappa l}$	Noise power spectral density of $\kappa l^{(th)}$ X-shear array detector (watt/Hz per ohm)
MAP	Maximum A posteriori
ML	Maximum likelihood
MS	Mean square
MSE	Mean square error
MMSE	Minimum mean square error
n	Number of columns in detector array
	Dummy variable in Eq. (4-1)
n_j	Noise counts
$n(t)$	White Gaussian noise
$n_c(t)$	Filtered white Gaussian noise

N	Scale factor relating τ and T
N_{kl}	Same as M_{kl} in Y-shear array
N_o	Same as N_{kl} and M_{kl}
N_{ob}	Background power spectral density (watt/Hz per ohm)
p	Index in ϕ and a
P_j	Random number
q	Electronic charge (coul)
r_j	Elements of \underline{r}
\underline{r}	Photoelectron counts in (O,T)
\bar{r}_a	Polar coordinates of a point in the aperture plane
\bar{r}_d	Polar coordinates of detector plane
$r(t)$	Detector output current (amps)
$\hat{r}(t)$	Approximate value of $r(t)$ from orthogonal expansion
R_e	Equivalent detector resistance
\underline{R}	Total number of photoelectron counts in (O,T) from detector array
\underline{R}_B	CRB bounds matrix
s_d	Shear distance
$s_j(\theta)$	Signal component of r_j
$s(t,\theta)$	Signal component of $r(t)$
SNR	Signal-to-noise ratio
t_j	Initial time of j th time subinterval
t_{j+1}	Final time of j th time subinterval
T	Observation time interval
	Superscript for matrix transpose
T_o	Detector temperature ($^{\circ}K$)

U	A constant used in Eqs. (4-40) and (4-41)
v	Tangential velocity of interferometer reticule
V	A constant used in Eqs. (4-40) and (4-41)
$V_a()$	Asymptotic variance
$V_{ar}()$	Variance
$w(t)$	Same as $r(t)$
\underline{W}	Noise matrix
$x(t,\theta)$	Same as $s(t,\theta)$
X	Direction of shear
$y(t,\theta)$	Same as $s(t,\theta)$
Y	Direction of shear
$z(t)$	Same as $r(t)$

Greek Letter Symbols

α_j	Defined by Eq. (3-26)
β_j	Defined by Eq. (3-27)
γ	Fringe visibility
γ_k	Defined by Eq. (4-59)
$\delta(\bar{r}-\bar{r}')$	Spatial incoherent process
$\delta(t-t')$	White stationary process
$\Delta\phi(\bar{r}_a)$	Wavefront difference function
η	Detector quantum efficiency
ϵ_r	Error function
ξ_ψ	Root mean square error
$\xi(\bar{r}_{a,t})$	Defined by Eq. (2-2)
λ_b	Background noise count rate (photons/sec)
λ_d	Dark current count rate (photons/sec)

$\lambda(t)$	Detector count rate (photons/sec)
$\lambda_{sn}(t)$	Signal shot noise count rate (photons/sec)
Λ	Likelihood ratio
μ_j	Photon counts in $(t_j, t_j + \tau)$
π	Conventional meaning of pi
ρ_i	Parameter in Eq. (4-75)
$\phi_i(P)$	Element of $\underline{\phi}_i$
$\underline{\phi}$	Phase vector
$\underline{\phi}_i$	Vector for phase orthonormal expansion
$\phi(\bar{r}_a \pm M\bar{s}_d)$	Phases measured by detector located at $-\bar{r}_d$
	Elements of $\underline{\phi}$
$\underline{\psi}(t)$	Basis functions for signal orthogonal expansion
σ^2	Phase variance
$\underline{\zeta}(t)$	Set of complete orthonormal functions
τ	Modulation period
	Used to signify $t_j + \tau = t_{j+1}$
ω	Modulation frequency of detector field
θ	Constant phase difference
$\theta(\bar{r}_{a,t})$	Phase difference

Other Symbols

$[]^T$	Matrix transpose
$()!$	Factorial

Abstract

Wavefront estimation from shearing interferometry measurements is considered in detail. Two analyses are presented, which involve the estimation of constant phase from single detector and detector array measurements. The single detector analysis is carried out in a discrete mode to obtain algorithms based on photon counting as the alternate means for use under low light level conditions. The method used follows the Maximum A Posteriori and Maximum Likelihood estimation theories. This is done for measurements made in both white Gaussian noise and Poisson shot noise limited conditions. The results so obtained are trigonometric relationships between the phases and the photon counts. The theoretical performance results show a strong signal-to-noise ratio dependence. Simulation results show that signal-to-noise ratios of 17 dB or better are needed to produce adequate estimates. Both theory and simulation show that an estimate improvement is obtained as more photon counts are performed, and in the limiting case, the ideal form is a current measurement. In this sense, although photon counting seems to be inferior to current measuring, the error variance is only 1.65 dB larger in the worst case, where three photon counts are performed.

The ML estimator was found to be computationally simpler than the MAP estimator, and with similar performance for SNR's in the order of 10 dB and higher.

An extension of the single detector analysis is made, using only the Gaussian noise assumption, to derive an algorithm that jointly estimates the phase distribution over an optical wavefront. The procedure is based on a parametric dependence between the measurements performed by adjacent detectors, and on the a priori knowledge available through a covariance matrix. An algorithm for processing continuous waveform measurements is developed, but no computer simulation is included due to difficulties encountered in solving the feedback system equations.

PHASE ESTIMATION TECHNIQUES FOR ACTIVE
OPTICS SYSTEMS USED IN REAL-TIME
WAVEFRONT RECONSTRUCTION

I Introduction

Reconstruction of a wavefront in real time is of particular interest to the Air Force because of the need to compensate for atmospheric disturbances and target variations that adversely affect laser weapons systems. Wavefront correction systems of diverse complexity are employed to maximize the irradiance of the laser on a target. The laser beam is continuously shaped in real time by means of mirrors to reconstruct the detected wavefront of the target's radiation. Actually, the complex conjugate field is reconstructed to propagate back to the target a wavefront with the same characteristics but in complementary form. Prior to such reconstruction, the phase distribution of the wavefront must be estimated over the region of space enclosed by the aperture of the receiving system. The most common method used for measuring the phasefront is shearing interferometry. The search for improved phase estimation techniques using the outputs of shearing interferometers constitutes the basis of this thesis. The shearing interferometer will be discussed in Chapter II.

System Description

Active optics systems have been widely described in the literature and only a brief description is necessary

for the purpose of this paper. Detailed systems descriptions are given by Hardy (Ref 3), Hudgin (Ref 5), Rimmer (Ref 10) and Martoni (Ref 7:1) among many. The system operation basically consists of wavefront detection, phasefront estimation, and beam control. Figure 1 shows a simplified block diagram of a typical system. In such a system, a reflecting telescope is used both as entrance aperture for the optical radiation from the target, and as exit aperture for the laser beam. Both input and output wavefronts travel the same path in opposite directions. Part of the incoming field is deflected off onto a phasefront sensor usually composed of two shearing interferometers. The output of this sensor is translated into control commands which actuate deformable mirrors off which the laser beam is reflected onto the target. Since this is done in real time, the atmosphere induces on the laser wavefront the reverse distortion effects induced on the detected field. The radiation reaching the target has, therefore, been adjusted for maximum irradiance.

Problem Statement

There is an issue expressed by the Weapons Laboratory that when the target radiance is low, the detectable field is not strong enough to perform phasefront estimation based on continuous signal measurements. A phase estimation technique was proposed by J. C. Wyant in 1975 (Ref 16:2624), based on detector processing of photon counts observed

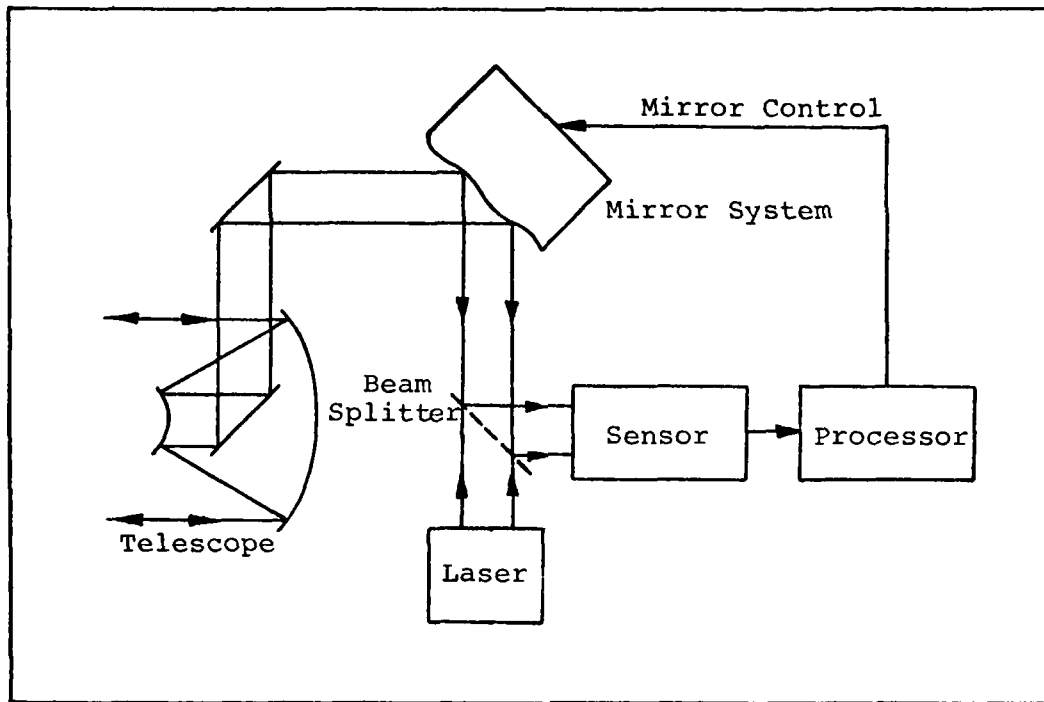


Fig 1. A Typical Real-Time Wavefront Correction System
(Adapted from Ref 7)

during short time intervals. Although his assumption is shot noise limited detection, his results are free from noise considerations, and the simplicity of the resulting algorithm motivates one to investigate more deeply into his technique. The overall wavefront is obtained from a mapping of independent phase estimates over the aperture of the system.

The purpose of this paper is to explore the photon counting technique from a statistical point of view and to examine in detail the effects of receiver and signal shot noises in order to determine the extent to which this procedure can be applied efficiently. Joint processing of multiple detectors has also been considered within the

scope of this work in an attempt to obtain improved results over linear mappings currently used to estimate the wavefront over the region of interest.

Approach

The basic approach to the problem is based on countable observables obtained by decomposing the continuous output of a detector into discrete components. The problem reduces to classical parameter estimation theory and will be carried out using the concepts of Maximum A Posteriori and Maximum Likelihood estimation theories. To fulfill the purpose of this approach, it is assumed that specially designed detectors are available, based on the promising future of charge-coupled devices (CCD) (Ref 13:Chapter 12), which are capable of integrating the detected field signal over short periods of time and dumping the contents into the registers of a computer. Such a receiver can be represented mathematically with a time correlator to be described later in Chapter III.

Scope and Assumptions

In this thesis, the wavefront process will be considered slow varying in time such that a stepwise approximation to the actual variation can be performed. The phase in each step of length T will be constant and the analysis of the problem will be limited to a single observation interval $(0, T)$. An extension to sequential estimation over successive intervals can then be performed using Gauss-

Markov parameter models. That will not be considered in this thesis. Constant phase is, therefore, the basic assumption of the forthcoming developments. The disturbance induced by the atmosphere will be modeled as an additive noise phase to the target wavefront. There is no need to distinguish between the target and noise induced phases because the reverse disturbance effects produced on the laser wavefront by the atmosphere cancel the noise component. Therefore, they will be lumped together into a single parameter θ , where θ is a random variable. The probabilistic descriptions of θ will be fitted to the ones given by Gaussian and uniform probability density functions in the interval $(-\pi, \pi)$. Other than for ease in estimator derivation, the Gaussian model is chosen considering that for slow varying wavefronts, the phase variations are more likely to be concentrated about the zero value and less likely as the phase value increases. On the other hand, because the sensor output is a sinusoidal variation, the uniform density is also a logical choice since the phases are equally likely in the interval $(-\pi, \pi)$.

Estimation of θ will be analyzed in the presence of noise from two points of view: predominant detector noise and predominant signal shot noise processes. Chapter IV is devoted to the analysis of the detector limited case, where the noise is modeled as a continuous white Gaussian random process. Chapter V is devoted to the analysis in signal induced noise, where the noise is modeled as a discrete

Poisson count process. A mixed mode of continuous and discrete processes will not be considered in this paper, but deserves future attention. An extension of the Gaussian noise analysis is performed in Chapter VI where the same concepts are applied to joint processing of two plane detector arrays. Finally, Chapter VII makes a summary of results and conclusions, and presents suggestions for further study.

II The Shearing Interferometer

The wavefront sensor of interest in this thesis consists of two ac heterodyne, lateral shearing interferometers. This sensor configuration is depicted in Figure 2. The field entering the system is beamsplit into two channels. Each channel has a shearing interferometer composed of two confocal lenses which constitute a Fourier transform pair. The field at the common focal point is the Fourier transform of the received field. The Fourier transform field is sampled with a radial grating displaced off the optic axis and rotating with velocity v and period τ . An expanded view is shown in Figure 3.

If the aperture is located at the front focal plane of lense L_1 , the field observed at the back focal plane of lense L_2 is sheared into a number of components laterally displaced from each other by an equal distance Ms_d , known as the shear distance, where s_d is a parameter of the interferometer determined by v , and M is a magnification factor determined by the ratio of the lenses in the system. The field components so displaced interfere with each other, and the modulated output is observed in the form of an interferogram spread over a detector array. It is this slowly but continuously changing interferogram that contains the wavefront phase information being sought.

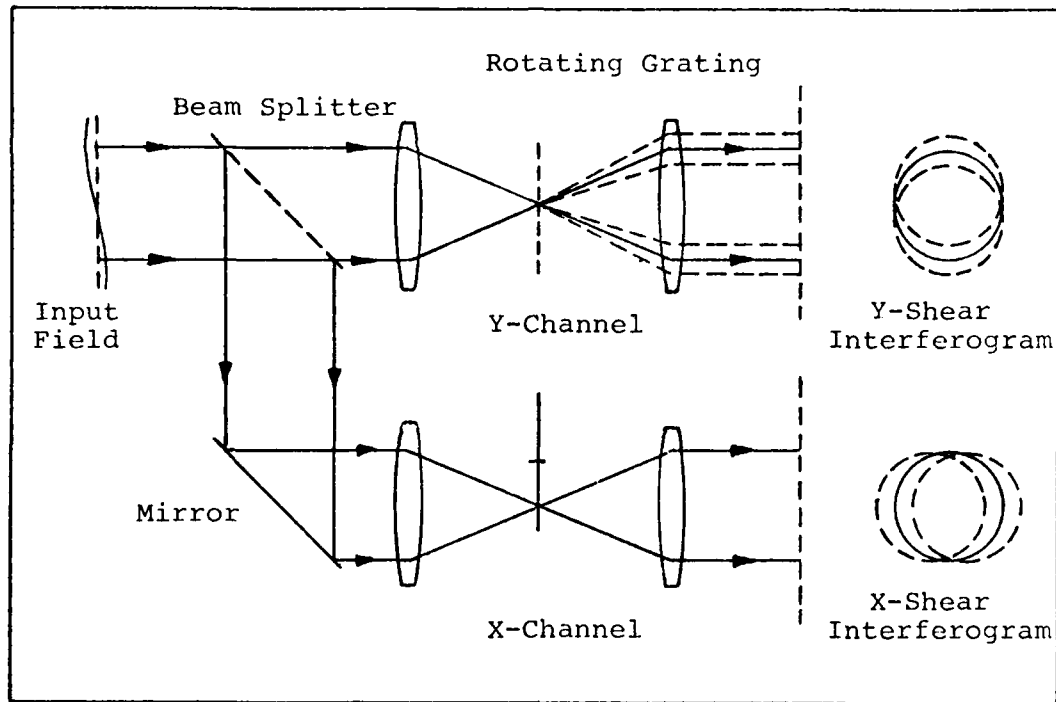


Fig 2. A Two Shearing-Interferometer Sensor Used with Wavefront Correction Systems (Adapted from Ref 3)

Output Field

The sheared field at the focal plane takes on slightly different forms for broadband (white light) and monochromatic fields. However, the same equation is applicable in both cases when the shear is small. Thus, for spatially coherent, white light aperture fields when the shear distance Ms_d is small, the detector field intensity is given by (Ref 6:58,61)

$$\begin{aligned}
 I_d(\bar{r}_d, t) = & \left(\frac{1}{4} + \frac{2}{\pi} \right) M^2 [A(\bar{r}_a)]^2 \\
 & + \frac{2}{\pi} M^2 [A(\bar{r}_a)]^2 \cos \xi(\bar{r}_a, t) \sin(\omega t + \theta(\bar{r}_a, t))
 \end{aligned}$$

for $0 \leq t \leq T$, (2-1)

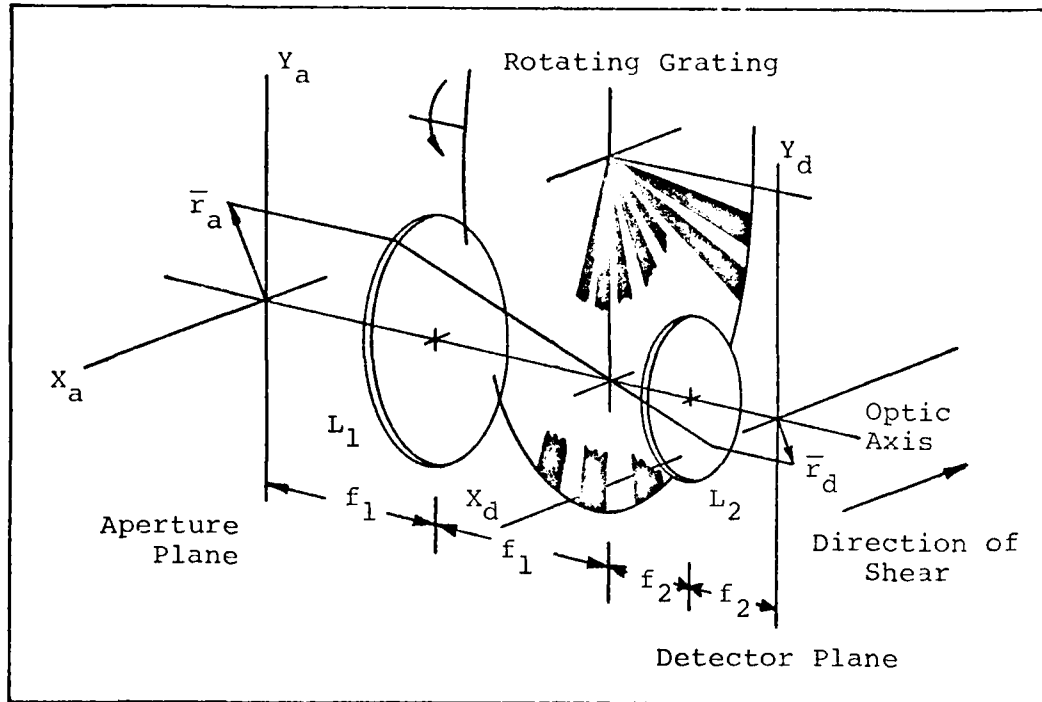


Fig 3. Expanded View of the X-Channel Interferometer
(Adapted from Ref 6)

where

$$\xi(\bar{r}_{a,t}) = \frac{\phi(\bar{r}_a - M\bar{s}_{d,t}) + \phi(\bar{r}_a + M\bar{s}_{d,t})}{2} \cdot \phi(\bar{r}_{a,t}) \quad (2-2)$$

and

$$\theta(\bar{r}_{a,t}) = \frac{\phi(\bar{r}_a - M\bar{s}_{d,t}) - \phi(\bar{r}_a + M\bar{s}_{d,t})}{2} \quad (2-3)$$

are phase functions in terms of the phases at locations $\pm M\bar{s}_d$ from \bar{r}_a . The term $A(\bar{r}_a)$ is the amplitude of the aperture field at location $\bar{r}_a = M\bar{r}_d$ shown in Figure 3. For slow varying fields over the aperture and constant intensity, Eq. (2-1) can be simplified to (Ref 7:10,6:59)

$$I_d(\bar{r}_{d,t}) = \left(\frac{1}{4} + \frac{2}{\pi}\right) M^2 A^2 + \frac{2M^2 A^2}{\pi} \sin(\omega t + \theta(\bar{r}_{a,t})) \quad (2-4)$$

The frequency

$$\omega = \frac{2\pi}{T} \quad (2-5)$$

is the fundamental modulation frequency of the detector field (Ref 6:41). Double frequency and higher order frequency terms have been dropped from Eqs. (2-1) and (2-4), anticipating subsequent signal processor filtering.

Detector Signal

The output $r(t)$ of a detector at location \bar{r}_{d_1} in the back focal plane is computed from the received field intensity $I_d(\bar{r}_{d,t}, \theta(\bar{r}_{a,t}))$ and the detector noise as follows:

$$r(t) = s(t, \theta(t)) + n(t), \text{ at } \bar{r}_d \in \text{Aperture}, \quad (2-6)$$

where (Ref 2:54-55)

$$s(t, \theta(t)) = \frac{\eta}{hf_0} \int_{A_d} I_d(\bar{r}_{d,t}, \theta(M\bar{r}_{d,t})) d\bar{r}_d$$

$$\text{for } \theta(\bar{r}_{d,t}) \text{ constant over } A_d, \quad (2-7)$$

is the signal current. The constant η/hf_0 is a detector conversion factor, A_d is the area of the detector, and $I_d(\bar{r}_{d,t}, \theta(\bar{r}_{d,t}))$ is the field of the detector given by Eq. (2-4) at location $\bar{r}_{d_1} = \bar{r}_{a_1}/M$. The assumption made here is that the field intensity at \bar{r}_{d_1} is constant over the detector area. If the observation time is short enough such that the phase is approximately constant in the interval $(0, T)$ to

fit the assumptions of Chapter I, the time dependence of the phase can be dropped. The interval T is assumed to be much larger than the period τ of the modulated field.

Equation (2-6) becomes

$$r(t) = s(t, \theta) + n(t), \quad 0 \leq t \leq T \quad (2-8)$$

where

$$s(t, \theta) = a + b \sin(\omega t + \theta) \quad (2-9)$$

is the output signal of one detector, and

$$a \triangleq \frac{g\eta}{hf_o} \left(\frac{1}{4} + \frac{2}{\pi} \right) M^2 A^2 A_d \quad (2-10)$$

$$b \triangleq \frac{g\eta}{hf_o} \left(\frac{2M^2 A^2}{\pi} \right) A_d \quad (2-11)$$

Chapter III further models the detector signal in order to pursue the photon count approach established in Chapter I.

III Phase Estimation Preliminaries

Reconstruction of the wavefront requires knowledge of the phase distribution of the optical field within the aperture. However, the knowledge provided by the shearing interferometers is in the form of a phase difference between two points along the line of shear as given by Eq. (2-3). In the simplest form, the problem is of phase difference estimation from the measurement of a single detector. The phase difference is known as the wavefront difference function given by (Refs 6:49 and 7:16)

$$\Delta\phi(\bar{r}_a) = \phi(\bar{r}_a - M\bar{s}_d) - \phi(\bar{r}_a + M\bar{s}_d) \quad (3-1)$$

where $\phi(\bar{r}_a - M\bar{s}_d)$ and $\phi(\bar{r}_a + M\bar{s}_d)$ are the phases at the aperture which we ultimately want to estimate. The components of the wavefront difference function in cartesian coordinates are given by

$$\phi(\bar{r}_a - M\bar{s}_d) = \phi(X_a - Ms_{dx}, Y_a), \quad \text{X-shear} \quad (3-2)$$

$$= \phi(X_a, Y_a - Ms_{dy}), \quad \text{Y-shear} \quad (3-3)$$

$$\phi(\bar{r}_a + M\bar{s}_d) = \phi(X_a + Ms_{dx}, Y_a), \quad \text{X-shear} \quad (3-4)$$

$$= \phi(X_a, Y_a + Ms_{dy}), \quad \text{Y-shear} \quad (3-5)$$

Figure 4 illustrates the phase distribution described by Eqs. (3-2)-(3-5). The shear distances are usually made equal so that $s_{dx} = s_{dy} \frac{\Delta}{s_d}$. When $M = -1$ (\bar{r}_d and \bar{s}_d are

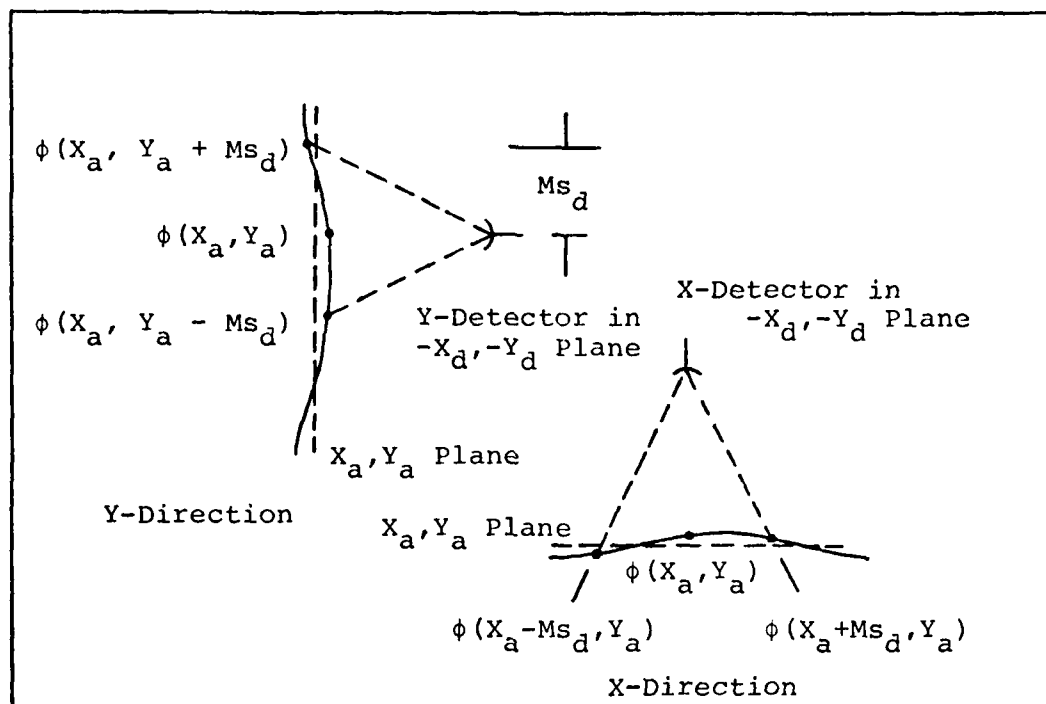


Fig 4. Phase Distribution at the Aperture Seen by Detectors in the Back Focal Plane

also negative), the wavefront difference function measured at the detector plane gives information of the phase points located one shear distance s_d away on each side of the detector. To estimate the actual phases ϕ , the information must be collected from all detectors. This will be addressed in Chapter VI. Chapters IV and V will concentrate on the estimation of the phase difference $\theta(\vec{r}_d)$ from one detector only. Prior to considering the estimation problem, a signal model must be found using the hypothetical CCD photon counting detector.

Signal Model

A signal model is developed in this section to estimate the phase difference θ measured by each detector following the integration approach with CCD devices. This is equivalent to saying that the output of each detector is sampled by a correlator structure as shown in Figure 5. In this correlator model, the observation $r(t)$, which represents the cathode current, is sampled by a vector of K orthogonal basis functions

$$\underline{\psi}(t) = [\psi_1(t) \dots \psi_j(t) \dots \psi_k(t)]^T, \quad (3-6)$$

(the superscript T means transpose of the matrix) where each basis function $\psi_j(t)$ is given by

$$\begin{aligned} \psi_j(t) &= \frac{1}{q}, \quad t_j \leq t \leq t_{j+1} \\ &= 0, \quad \text{otherwise,} \end{aligned} \quad (3-7)$$

with q being the electron charge and t_j a sequence of k equal-length, non-overlapping time subintervals in one observation interval of length T . The resulting output is a vector of k observations

$$\underline{r} = [r_1 \dots r_j \dots r_k]^T \quad (3-8)$$

which represent photon counts in the time subinterval (t_j, t_{j+1}) . With the signal represented in this manner, the following equalities are true:

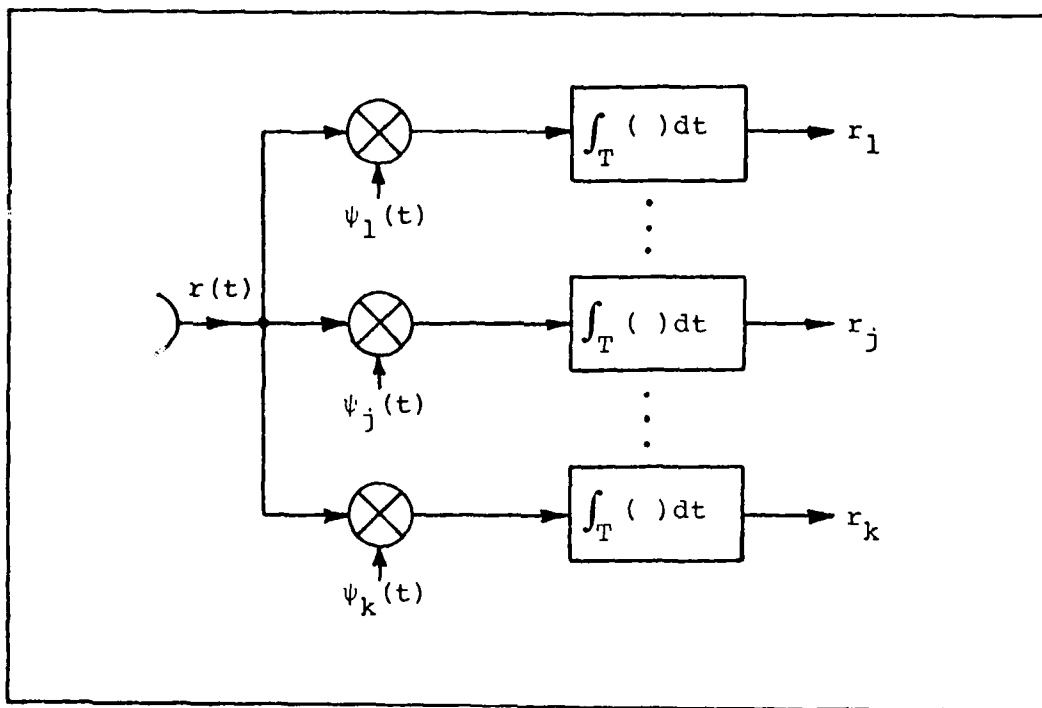


Fig 5. Equivalent Correlator Model of the CCD Detector

$$\int_{t_1}^{t_1+T} \psi_i(t) \psi_j(t) dt = \frac{T}{q^2 k} , i = j$$

$$= 0 , i \neq j \quad (3-9)$$

and

$$\hat{r}(t) = \text{l.i.m.}_{k \rightarrow \infty} \frac{q^2 k}{T} \sum_{j=1}^k r_j \psi_j(t) , \quad (3-10)$$

is satisfied. This condition known as the Cauchy criterion for convergence of random sequences (Ref 8:262) is satisfied by the choice of the t_j 's as non-overlapping time subintervals. Equations (3-9) and (3-10) are the tools needed in the forthcoming parameter estimation analysis.

This analysis will be the classical discrete observation problem with generalizations to the continuous observation form using Eq. (3-10). For this purpose and to define t_j properly, the observation period is divided into k equal subintervals (t_j, t_{j+1}) . The functions $\psi_j(t)$ are, therefore, identical except for their sequential position in time. In order to simplify the derivation let the initial time be $t_1 = -T/2k$ and the final time t_1+T be $t_k = (2k-1)T/2k$ for any interval T . Thus, the integration limits for the j th subinterval are

$$t_j = \frac{(2j-3)T}{2k} \quad (3-12)$$

and
$$t_{j+1} = \frac{(2j-1)T}{2k} . \quad (3-13)$$

The correlation operation

$$r_j = \int_0^T r(t) \psi_j(t) dt , \quad (3-14)$$

indicated in Figure 5 is then given by

$$\begin{aligned} r_j &= \int_{t_j}^{t_{j+1}} \frac{r(t)}{q} dt \\ &= \int_{t_j}^{t_{j+1}} \frac{s(t, \theta)}{q} dt + \int_{t_j}^{t_{j+1}} \frac{n(t)}{q} dt , \end{aligned} \quad (3-15)$$

which can be conveniently defined as

$$r_j = s_j(\theta) + n_j , \quad (3-16)$$

where

$$s_j(\theta) = \frac{1}{q} \int_{t_j}^{t_{j+1}} s(t, \theta) dt \quad (3-17)$$

and

$$n_j = \frac{1}{q} \int_{t_j}^{t_{j+1}} n(t) dt \quad (3-18)$$

with t_j and t_{j+1} given by Eqs. (3-12) and (3-13). Because the observation $r(t)$ has the form of an electrical current, the correlation functions of Eq. (3-7) were selected so that r_j , $s(\theta)$, and n_j have the physical interpretation of photons, both signal and noise, counted in each observation subinterval (t_j, t_{j+1}) . The sum $\sum_{j=1}^k r_j$ corresponds to the total photons counted in the observation interval (t_1, t_1+T) . If the functional form of $s(t, \theta)$ given by Eq. (2-9) is substituted into Eq. (3-17), the signal in discrete form becomes

$$s_j(\theta) = \frac{1}{q} \int_{t_j}^{t_{j+1}} [a + b \sin(\omega t + \theta)] dt, \quad (3-19)$$

for $\theta(t)$ constant over T .

The integration indicated by Eq. (3-19) yields

$$\begin{aligned} s_j(\theta) = & \frac{a}{q} [t_{j+1} - t_j] \\ & + \frac{b}{\omega} [\cos(\omega t_j + \theta) - \cos(\omega t_{j+1} + \theta)]. \end{aligned} \quad (3-20)$$

If the observation interval is several times the modulation period so that many frequency cycles are observed each time,

then they are related by

$$N = \frac{T}{\tau} \quad (3-21)$$

where τ is as in Eq. (2-5). With the identity of Eq. (3-21) substituted into Eq. (3-20), the signal equation becomes

$$s_j(\theta) = \frac{aT}{qk} + \frac{bT}{2\pi qN} [\cos(\frac{\pi N}{k}(2j-3)+\theta) - \cos(\frac{\pi N}{k}(2j-1)+\theta)] , \quad (3-22)$$

where the definitions of Eqs. (3-12) and (3-13) were used as integration limits. However, in order to preserve the phase information, a small shear distance is required (Refs 6:41 and 16:2622). For small shear, the modulation frequency ω must be low relative to the optical field frequency such as 25 kilohertz (Ref 4:363). Thus, typically $\tau = 0.04$ milliseconds and N can range from unity to a very large number depending on how fast the phase changes in time. For simplicity and to check with Wyant's results, let $N = 1$ so that Eq. (3-22) becomes

$$s_j(\theta) = \frac{aT}{qk} + \frac{bT}{2\pi q} [\cos(\frac{\pi}{k}(2j-3)+\theta) - \cos(\frac{\pi}{k}(2j-1)+\theta)] . \quad (3-23)$$

Although Eq. (3-23) gives an exact expression for the photon counts in terms of θ , it is not in a workable form. It is therefore necessary to expand the cosine functions to obtain

$$s_j(\theta) = \frac{aT}{qk} + \frac{bT}{2\pi q} \left\{ [\cos \frac{\pi}{k}(2j-3) - \cos \frac{\pi}{k}(2j-1)] \cos \theta - [\sin \frac{\pi}{k}(2j-3) - \sin \frac{\pi}{k}(2j-1)] \sin \theta \right\}. \quad (3-24)$$

Equation (3-24) is the expression that will be used to represent the signal-generated photon counts. For ease in further derivations, Eq. (3-24) can be more compactly written as

$$s_j(\theta) = \frac{aT}{qk} + \frac{bT}{2\pi q} [\alpha_j \cos \theta - \beta_j \sin \theta], \quad (3-25)$$

where

$$\alpha_j = \cos \frac{\pi}{k}(2j-3) - \cos \frac{\pi}{k}(2j-1) \quad (3-26)$$

$$\beta_j = \sin \frac{\pi}{k}(2j-3) - \sin \frac{\pi}{k}(2j-1). \quad (3-27)$$

With the above signal model completed, the estimation procedure to obtain $\hat{\theta}(\underline{r})$ will be considered next. The "hat" over $\theta(\underline{r})$ indicates that this is just an estimate of θ , and the argument " \underline{r} " indicates that the estimate is in terms of the observation vector \underline{r} of Eq. (3-8). The estimate $\hat{\theta}(\underline{r})$ will be performed based on the criteria of Maximum A Posteriori and Maximum Likelihood estimation. Before applying these criteria to find the phase estimates in Chapters IV, V, and VI, these concepts will be briefly explained in the following section.

Maximum A Posteriori and Maximum Likelihood Estimation Theories

Estimation of the phase difference θ measured by a single detector at a fixed location \bar{r}_d and time t , and of the actual phases ϕ measured over the aperture by two detector arrays will be made applying the concepts of Maximum A Posteriori (MAP) and Maximum Likelihood (ML) estimation theories. The MAP and ML estimates of θ are those values $\hat{\theta}(\underline{r})$ for which the probability of having found the correct θ after the measurement is made is maximum. This is equivalent to maximizing the a posteriori probability density function of θ conditioned on the observations. Let this a posteriori density be represented by

$$f_{\theta|\underline{r}}(\theta|\underline{r}) , \quad (3-28)$$

and let it be maximized by the proper choice of $\hat{\theta}(\underline{r})$. With the condition that the maximum occurs within the range of θ , maximization is obtained by setting

$$\frac{\partial}{\partial \theta} [f_{\theta|\underline{r}}(\theta|\underline{r})] = 0 . \quad (3-29)$$

An equivalent and sometimes more convenient form of Eq. (3-29) is given by

$$\frac{\partial}{\partial \theta} [\ln f_{\theta|\underline{r}}(\theta|\underline{r})] = 0 . \quad (3-30)$$

By using the Baye's rule substitution

$$f_{\theta|\underline{r}}(\theta|\underline{r}) = \frac{f_{\underline{r}|\theta}(\underline{r}|\theta)f_{\theta}(\theta)}{f_{\underline{r}}(\underline{r})} \quad (3-31)$$

In Eq. (3-30), the necessary but not sufficient condition for the MAP estimate is found to be (Ref 14:58)

$$\left. \frac{\partial}{\partial \theta} [\ln f_{\underline{x}|\theta}(\underline{x}|\theta) + \ln f_{\theta}(\theta)] \right|_{\text{MAP}} = 0 . \quad (3-32)$$

Because θ is in the argument of a sine function, it is modulo 2π . The ML estimate of the phase is then found by modeling the a priori density $f_{\theta}(\theta)$ as uniform within the range of θ , which is the interval $(-\pi, \pi)$. The ML estimate is, therefore, given by (Ref 14:65)

$$\left. \frac{\partial}{\partial \theta} [\ln f_{\underline{x}|\theta}(\underline{x}|\theta)] \right|_{\text{ML}} = 0 . \quad (3-33)$$

Equations (3-32) and (3-33) are the equations for MAP and ML parameter estimation. The parameter so found is the one with highest probability of being the true value. There, of course, may be false solutions, and an error is associated with each estimate. The errors will be treated in the next chapters after the solution algorithms have been found. The problem of estimating $\theta(\bar{r}_{a,t})$ in the presence of noise will be addressed next; first, it will be investigated in the context of a Gaussian problem where the only noise is due to thermal noise limited detectors, and then in the context of a Poisson problem when the shot noise is the predominant noise source. The approach, however, will be the same in both Gaussian and Poisson cases: photon counting as the only alternative under low light level conditions.

IV Phase Estimation in White Gaussian Noise

When the output field of the interferometer is received by a detector array with predominant thermal noise, the noise is adequately modeled by a zero-mean, stationary white Gaussian process described by the probability density (Ref 8:360)

$$f_{n(t)}(n) = [2\pi\sigma_n^2]^{-1/2} \exp[-n^2/2\sigma_n^2] , \quad (4-1)$$

where the variance is given by

$$\sigma_n^2 = \frac{N_o}{2T} . \quad (4-2)$$

The process has a double-sided, flat power spectral density $\frac{N_o}{2}$ over and beyond the spectral region of interest. If the noise is described in the form of a random current, additive to the current output of the detector, the spectral density is given by (Ref 8:361)

$$\frac{N_o}{2} = \frac{2kT_o}{R_e} \quad (\text{watts per hertz -- per ohm}) , \quad (4-3)$$

where k is the Boltzmann constant, T_o is the operating temperature and R_e is the equivalent resistance of the detector. On a per-ohm basis, $\frac{N_o}{2}$ has the units of energy. The correlation function of the noise process is the inverse Fourier transform of the power spectral density. For stationary white noise it is given by

$$E[n(t)n(t')] = \frac{N_o}{2} \delta(t-t') . \quad (4-4)$$

On a per-ohm basis, the correlation function has the units of power. The first order statistics are given by

$$E[n(t)] = 0 . \quad (4-5)$$

Before applying the concepts of MAP and ML estimation, it is necessary to obtain the density function of the observation vector \underline{r} conditioned on the parameter θ , as required by Eqs. (3-32) and (3-33). Therefore, the following development is made:

Referring to Eqs. (3-14) and (4-6)

$$E[n_j] = \int_T dt \ E[n(t)]\psi_j(t) = 0 . \quad (4-6)$$

Referring to Eqs. (3-9) and (4-4)

$$\begin{aligned} E[n_j^2] &= \int_T dt \int_T dt' E[n(t)n(t')]\psi_j(t)\psi_j(t') \\ &= \int_T dt \int_T dt' \left[\frac{N_0}{2} \delta(t-t')\psi_j(t)\psi_j(t') \right] \\ &= \frac{N_0}{2} \int_T \psi_j^2(t) dt = \frac{N_0 T}{2q^2 k} \end{aligned} \quad (4-7)$$

Therefore,

$$E[r_j] = s_j(\theta) \quad (4-8)$$

$$\text{Var}[r_j] = \text{Var}[n_j] = \frac{N_0 T}{2q^2 k} . \quad (4-9)$$

In addition to the variance and the mean of r_j , it is necessary to demonstrate that r_j and r_q are uncorrelated. Thus,

$$\begin{aligned} \text{cov}[r_j, r_q] &= E[(r_j - E[r_j])(r_q - E[r_q])] \\ &= E[(r_j - s_j(\theta))(r_q - s_q(\theta))] \\ &= E[n_j n_q] . \end{aligned} \quad (4-10)$$

Further evaluating Eq. (4-10)

$$\begin{aligned} E[n_j n_q] &= \int_T dt \int_T dt' E[n(t)n(t')] \psi_j(t) \psi_q(t') \\ &= \int_T dt \int_T dt' \left[\frac{N_0}{2} \delta(t-t') \psi_j(t) \psi_q(t') \right] \\ &= \frac{N_0}{2} \int_T \psi_j(t) \psi_q(t) dt = 0, \quad j \neq q . \end{aligned} \quad (4-11)$$

Therefore, from Eqs. (3-16), (4-6), and (4-11)

$$\text{cov}[r_j, r_q] = E[n_j n_q] = 0, \quad j \neq q, \quad (4-12)$$

which implies that r_j and r_q are uncorrelated. The probabilistic description of r_j given θ is the description of $n_j = r_j - s_j(\theta)$, which is also Gaussian since n_j is a linear operation on $n(t)$. The conditional density of the observation can be written as

$$f_{r_j|\theta}(r_j|\theta) = [2\pi N_o T / 2q^2 k]^{1/2} \exp \left[- \frac{(r_j - s_j(\theta))^2}{2(N_o T / 2q^2 k)} \right]. \quad (4-13)$$

Because the observations r_j are uncorrelated and conditionally Gaussian, they are independent. Therefore, the observation vector has a conditional density function given by

$$\begin{aligned} f_{\underline{r}|\theta}(\underline{r}|\theta) &= \prod_{j=1}^k f_{r_j|\theta}(r_j|\theta) \\ &= \left[\frac{q^2 k}{\pi N_o T} \right]^{k/2} \exp \left[- \frac{q^2 k}{N_o T} \sum_{j=1}^k (r_j - s_j(\theta))^2 \right]. \end{aligned} \quad (4-14)$$

Maximum A Posteriori Estimate

The MAP estimate of a parameter θ observed in noise is based, as indicated by Eq. (3-32), on the conditional density of the observations \underline{r} given θ , as well as on the a priori density of θ . Considering first the conditional density of \underline{r} given θ , the following procedure is developed:

From Eq. (4-14),

$$f_{\underline{r}|\theta}(\underline{r}|\theta) = \left[\frac{q^2 k}{\pi N_o T} \right]^{k/2} \exp \left[- \frac{q^2 k}{N_o T} \sum_{j=1}^k (r_j^2 - 2r_j s_j(\theta) + s_j^2(\theta)) \right] . \quad (4-15)$$

The natural logarithm of Eq. (4-15) is

$$\begin{aligned} \ln f_{\underline{r}|\theta}(\underline{r}|\theta) &= \frac{k}{2} \ln \frac{q^2 k}{\pi N_o T} - \frac{q^2 k}{N_o T} \sum_{j=1}^k (r_j^2 - 2r_j s_j(\theta) + s_j^2(\theta)) \\ &= \frac{2q^2 k}{N_o T} \sum_{j=1}^k r_j s_j(\theta) - \frac{q^2 k}{N_o T} \sum_{j=1}^k s_j^2(\theta) \\ &\quad - \frac{q^2 k}{N_o T} \sum_{j=1}^k r_j^2 + \frac{k}{2} \ln \frac{q^2 k}{\pi N_o T} . \end{aligned} \quad (4-16)$$

The derivative of Eq. (4-16) with respect to θ is

$$\begin{aligned} \frac{\partial}{\partial \theta} \ln f_{\underline{r}|\theta}(\underline{r}|\theta) &= \frac{2q^2 k}{N_o T} \sum_{j=1}^k r_j \frac{\partial}{\partial \theta} s_j(\theta) \\ &\quad - \frac{2q^2 k}{N_o T} \sum_{j=1}^k s_j(\theta) \frac{\partial}{\partial \theta} s_j(\theta) . \end{aligned} \quad (4-17)$$

By substituting Eq. (4-17) into Eq. (3-32), a general expression for the MAP estimate is obtained and is given by

$$\frac{2q^2 k}{N_o T} \sum_{j=1}^k [r_j - s_j(\theta)] \frac{\partial}{\partial \theta} s_j(\theta) + \frac{\partial}{\partial \theta} [\ln f_{\theta}(\theta)] = 0 . \quad (4-18)$$

The solution of Eq. (4-18) when the appropriate expressions for $s_j(\theta)$ and $f_{\theta}(\theta)$ are substituted for yields $\hat{\theta}(\underline{r})|_{\text{MAP}}$.

Before doing this, it is interesting to observe what happens when k becomes very large. It is very simple to prove that if

$$g(t) = \lim_{k \rightarrow \infty} \frac{1}{A} \sum_{j=1}^k g_j \phi_j(t)$$

$$\text{and} \quad h(t) = \lim_{k \rightarrow \infty} \frac{1}{A} \sum_{j=1}^k h_j \phi_j(t) , \quad (4-19)$$

where $\phi_i(t)$ are orthogonal functions such that

$$\int_0^T \phi_i^2(t) dt = \frac{1}{A}$$

$$\text{and} \quad \int_0^T \phi_i(t) \phi_j(t) dt = 0 , \quad i \neq j , \quad (4-20)$$

$$\text{then} \quad \lim_{k \rightarrow \infty} \frac{1}{A} \sum_{j=1}^k g_j h_j = \int_0^T g(t) h(t) dt . \quad (4-21)$$

With the help of Eqs. (4-19)-(4-21) and the orthogonal relation of Eq. (3-10), Eq. (4-18) becomes ($t_1 \rightarrow 0$ as $k \rightarrow \infty$)

$$\frac{2}{N_0} \int_0^T [r(t) - s(t, \theta)] \frac{\partial}{\partial \theta} s(t, \theta) dt + \frac{\partial}{\partial \theta} [\ln f_{\theta}(\theta)] = 0 . \quad (4-22)$$

Equation (4-22) is the general expression for the MAP estimate $\hat{\theta}$ of a parameter θ in a continuous waveform $r(t)$ observed in white Gaussian noise (Ref 14:275).

Returning to Eq. (4-18), the substitution for $s_j(\theta)$ given by Eq. (3-25) is made to obtain $\hat{\theta}(\underline{r})$ as follows:

From Eq. (3-25)

$$s_j(\theta) = \frac{aT}{qk} + \frac{bT}{2\pi q} [\alpha_j \cos \theta - \beta_j \sin \theta] . \quad (4-23)$$

Its phase derivative is

$$\frac{\partial}{\partial \theta} s_j(\theta) = - \frac{bT}{2\pi q} [\alpha_j \sin \theta + \beta_j \cos \theta] . \quad (4-24)$$

Equation (4-18) can now be written as

$$\begin{aligned} \frac{2q^2 k}{N_o T} \sum_{j=1}^k \left\{ \left(r_j - \frac{aT}{qk} - \frac{bT}{2\pi q} [\alpha_j \cos \theta - \beta_j \sin \theta] \right) \right. \\ \left. - \frac{bT}{2\pi q} [\alpha_j \sin \theta + \beta_j \cos \theta] \right\} \\ + \frac{\partial}{\partial \theta} [\ln f_\theta(\theta)] = 0 . \end{aligned} \quad (4-25)$$

In order to simplify notation, let a new function $F(\theta)$ be defined as

$$F(\theta) \triangleq \frac{\partial}{\partial \theta} [\ln f_\theta(\theta)] . \quad (4-26)$$

After some algebraic manipulation of Eq. (4-25), the following MAP estimate of θ is obtained:

$$\begin{aligned} \sum_{j=1}^k \left\{ \left[r_j - \frac{aT}{qk} \right] \alpha_j \sin \hat{\theta}(\underline{r}) + \left[r_j - \frac{aT}{qk} \right] \beta_j \cos \hat{\theta}(\underline{r}) \right\} \\ - \frac{bT}{2\pi q} \sum_{j=1}^k \left\{ \left(\frac{\alpha_j^2 - \beta_j^2}{2} \right) \sin 2\hat{\theta}(\underline{r}) + \alpha_j \beta_j \cos 2\hat{\theta}(\underline{r}) \right\} \\ - \frac{\pi N_o}{qkb} F(\theta) = 0 , \end{aligned} \quad (4-27)$$

where α_j and β_j are defined by Eqs. (3-26) and (3-27). Although Eq. (4-27) defines $\hat{\theta}(\underline{r})|_{\text{MAP}}$, as is, it is not in final form. The second summation in Eq. (4-27) vanishes for all values of k except for $k = 2$. This was determined on a computer check and will be used without a rigorous proof. Therefore, Eq. (4-27) becomes

$$\sum_{j=1}^k \left[r_j - \frac{aT}{qk} \right] \alpha_j \sin \hat{\theta}(\underline{r}) + \sum_{j=1}^k \left[r_j - \frac{aT}{qk} \right] \beta_j \cos \hat{\theta}(\underline{r}) - \frac{\pi N_0}{qkb} F(\theta) = 0 ; \quad k \geq 3 , \quad (4-28)$$

where the constraint that $k \geq 3$ is imposed on the estimator because for $k = 1$, the two sums vanish.

Now, the conditions for which the second summation in Eq. (4-27) vanishes are to be investigated. For that to happen, it is required that

$$\sum_{j=1}^k \frac{(\alpha_j^2 - \beta_j^2)}{2} = 0 \quad (4-29)$$

and
$$\sum_{j=1}^k \alpha_j \beta_j = 0 . \quad (4-30)$$

Substitution of the expressions given by Eqs. (3-26) and (3-27) for α_j and β_j into Eqs. (4-29) and (4-30) yields

$$\sum_{j=1}^k \left\{ \left[\cos \frac{\pi}{k}(2j-3) - \cos \frac{\pi}{k}(2j-1) \right]^2 - \left[\sin \frac{\pi}{k}(2j-3) - \sin \frac{\pi}{k}(2j-1) \right]^2 \right\} = 0 , \quad (4-31)$$

and
$$\sum_{j=1}^k \{ [\cos \frac{\pi}{k}(2j-3) - \cos \frac{\pi}{k}(2j-1)]$$

$$[\sin \frac{\pi}{k}(2j-3) - \sin \frac{\pi}{k}(2j-1)] \} = 0 . \quad (4-32)$$

By carrying out the operations indicated by Eqs. (4-31) and (4-32), it is found that the conditions for a vanishing term are

$$\begin{aligned} \sum_{j=1}^k \{ \cos \frac{2\pi}{k}(2j-3) + \cos \frac{2\pi}{k}(2j-1) \\ - 2\cos \frac{2\pi}{k}(2j-2) \} = 0 \end{aligned} \quad (4-33)$$

and
$$\begin{aligned} \sum_{j=1}^k \{ \sin \frac{2\pi}{k}(2j-3) + \sin \frac{2\pi}{k}(2j-1) \\ - 2\sin \frac{2\pi}{k}(2j-2) \} = 0 . \end{aligned} \quad (4-34)$$

The question is, for what values of k do Eqs. (4-33) and (4-34) hold? The easiest way to find out is by computing the summations for a number of k 's. This was done on the computer for $k = 1$ to $k = 28$ with the assuring result that only for $k = 2$ both sums do not equal zero. It was also observed (and will be used without a rigorous proof) that

$$\sum_{j=1}^k \alpha_j = \sum_{j=1}^k \beta_j = 0 \quad (4-35)$$

for all k .

Therefore, Eq. (4-28) simplifies even further to yield the final result of the discrete MAP estimate of θ as

$$\sum_{j=1}^k \alpha_j r_j \sin \hat{\theta}(\underline{r}) + \sum_{j=1}^k \beta_j r_j \cos \hat{\theta}(\underline{r}) - \frac{\pi N_0}{qkb} F(\theta) = 0, \quad k \geq 3. \quad (4-36)$$

For the particular case when the phase θ is a Gaussian random variable with variance less than 0.8 rad^2 , the density function is practically given by

$$f_{\theta}(\theta) = [2\pi\sigma_{\theta}^2]^{-1/2} \exp[-\theta^2/2\sigma_{\theta}^2], \quad (4-37)$$

in the interval $(-\pi, \pi)$. Then,

$$F(\theta) = \frac{\partial}{\partial \theta} [\ln f_{\theta}(\theta)] = -\frac{\theta}{\sigma_{\theta}^2}. \quad (4-38)$$

By letting $\theta = \hat{\theta}(\underline{r})$, Eq. (4-36) becomes

$$\hat{\theta}(\underline{r}) = \frac{qkb\sigma_{\theta}^2}{\pi N_0} \left\{ -\sum_{j=1}^k \beta_j r_j \cos \hat{\theta}(\underline{r}) - \sum_{j=1}^k \alpha_j r_j \sin \hat{\theta}(\underline{r}) \right\}. \quad (4-39)$$

Equation (4-39) is the MAP estimate of a Gaussian phase θ in terms of discrete observations. The MAP estimate is, therefore, a function of the detector noise $\frac{N_0}{2}$ given by Eq. (4-3), the variance σ_{θ}^2 of the random phase and the amplitude b of the signal. Equation (4-39) is of the form

$$x = U \cos x + V \sin x \quad (4-40)$$

and cannot be reduced any further. It can be implemented in the form of a photon processor as shown in Figure 6.

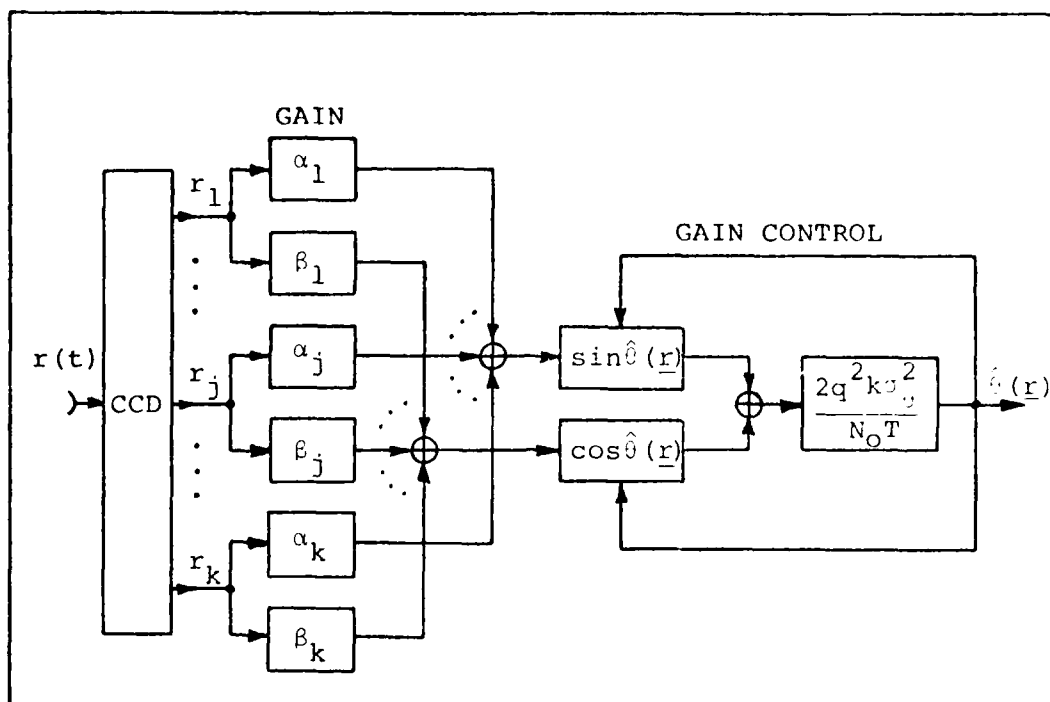


Fig 6. Photon Count Processor for MAP Estimation of θ

Equation (4-40) can, however, be solved numerically on the computer. An effective way is to expand the sine and cosine functions into series and solve the resulting polynomial iteratively as a predictor-corrector algorithm. A fifth order expansion (three terms in each function) results in reasonably good solutions up to 0.7 radians, but it gives gross errors for higher phase angles. On the other hand, a seventh order expansion (four terms in each function) proved to give very accurate results regardless of the phase value. Thus, using four terms in the expansion of the trigonometric functions of Eq. (4-40) (Ref 12:472), the following polynomial is obtained:

$$5040U + 5040(V-1)x - 2520Ux^2 - 840Vx^3 + 210Ux^4 + 42Vx^5 - 7Ux^6 - Vx^7 = 0 \quad (4-41)$$

Equation (4-41) has seven roots. It was solved using a subroutine from the International Mathematical and Statistical Library (IMSL) package available for use with the CDC 6600/Cyber 74 computer system at the Air Force Institute of Technology. The real roots so found that satisfy Eq. (4-40) are the estimator solutions. It was found from several tests (no proof included) that the lowest root always gives the solution with the smallest error, and is therefore the sought MAP estimate. As an example, the solution to

$$x = 11.23108494624 \cos x - 38.93776905131 \sin x, \quad (4-42)$$

taken from an actual simulation run, is, using single precision,

$$x = 0.2740523040524 \text{ radians} \quad (4-43)$$

with a discrepancy of

$$7.920348821244E-9 \text{ radians}, \quad (4-44)$$

which is an extremely accurate result.

For the purpose of comparison, it is easily found using Eq. (4-22) that the MAP phase estimate from a continuous measurement is (Refs 11:189 and 15:129)

$$\hat{\theta} = \frac{2b_0^2}{N_0} \left\{ \left[\int_0^T r(t) \cos \omega t dt \right] \cos \hat{\theta} - \left[\int_0^T r(t) \sin \omega t dt \right] \sin \hat{\theta} \right\}. \quad (4-45)$$

In order to give an idea of the forms assumed by Eq. (4-39) for a specified number of observations, a few illustrative examples are given in Table I. Finally, in order not to disrupt the continuity of the present developments, verification of Eq. (4-39) through computer simulation is reserved for the last section of this chapter.

Maximum Likelihood Estimate

The ML estimate of a parameter θ observed in noise is based on the conditional density of the observations given θ only. This is performed when the statistical description of θ is not available (Ref 14:65). It is reasonable to assume that θ is equally likely to occur in the interval $(-\pi, \pi)$ not having any other a priori information. The density of θ is therefore modeled as

$$f_{\theta}(\theta) = \frac{1}{2\pi}, \quad -\pi \leq \theta \leq \pi$$

$$= 0, \text{ elsewhere,} \quad (4-46)$$

with zero mean value and variance $\pi^2/3$. From Eq. (4-46), it is found that $F(\theta) = 0$ (equivalent to a large σ_{θ}^2 in Eq. (4-37)), and the ML estimate is defined by Eq. (3-33).

TABLE I

Examples of the Maximum A Posteriori Phase
Estimator Form for k Observations

k	$\hat{\theta}(r_1 \dots r_k)$
3	$\frac{3\sqrt{3}}{4} (2r_1 - r_2 - r_3) k_o \cos \hat{\theta}(\underline{r}) - \frac{3}{2} (r_2 - r_3) k_o \sin \hat{\theta}(\underline{r})$
4	$\sqrt{2} (r_1 - r_3) k_o \cos \hat{\theta}(\underline{r}) - \sqrt{2} (r_2 - r_4) k_o \sin \hat{\theta}(\underline{r})$
6	$\frac{3\sqrt{3}}{4} [2(r_1 - r_4) + r_2 - r_3 - r_5 + r_6] k_o \cos \hat{\theta}(\underline{r})$ $- \frac{3}{2} (r_2 + r_3 - r_5 - r_6) k_o \sin \hat{\theta}(\underline{r})$
∞	$[\int_0^T r(t) \cos \omega t dt] k_p \cos \hat{\theta} - [\int_0^T r(t) \sin \omega t dt] k_p \sin \hat{\theta}$

$$k_o \triangleq \frac{q k b \sigma_{\theta}^2}{\pi N_o}$$

$$k_p \triangleq \frac{2 b \sigma_{\theta}^2}{N_o}$$

Equation (4-36) then becomes

$$\sum_{j=1}^k \alpha_j r_j \sin \hat{\theta}(\underline{r}) + \sum_{j=1}^k \beta_j r_j \cos \hat{\theta}(\underline{r}) = 0$$

for $k \geq 3$. (4-47)

Finally, Eq. (4-47) reduces to

$$\hat{\theta}(\underline{r}) \Big|_{ML} = \tan^{-1} \left[\frac{- \sum_{j=1}^k \beta_j r_j}{\sum_{j=1}^k \alpha_j r_j} \right], \quad k \geq 3. \quad (4-48)$$

Equation (4-48) is the ML estimate of the phase based on discrete observations. The condition that $k \geq 3$ is maintained since for $k = 1$, the tangent of $\hat{\theta}(\underline{r})$ is not defined (zero divided by zero) and for $k = 2$ the summations in Eqs. (4-29), (4-30), and (4-35) do not equal zero. Again for comparison, as k becomes very large and with $F(\theta) = 0$, Eq. (4-45) gives (Ref 15:129)

$$\hat{\theta} \Big|_{ML} = \tan^{-1} \left[\frac{\int_0^T r(t) \cos \omega t \, dt}{\int_0^T r(t) \sin \omega t \, dt} \right]. \quad (4-49)$$

Equation (4-49) is the ML phase estimate made from a continuous measurement.

Equation (4-48) takes on different forms for each value of k . In order to visualize how it changes, a few illustrative examples are given in Table II. These results agree with the findings of Wyant (Ref 16:264), which inspired the work of this thesis, although he assumed shot noise instead.

TABLE II

Examples of the Maximum Likelihood Phase
Estimator Form for k Observations

k	$\tan \hat{\theta}(r_1 \dots r_k)$
3	$\frac{\sqrt{3}}{3} \frac{2r_1 - r_2 - r_3}{r_2 - r_3}$
4	$\frac{r_1 - r_3}{r_2 - r_4}$
6	$\frac{\sqrt{3}}{3} \frac{2(r_1 - r_4) + r_2 - r_3 - r_5 + r_6}{r_2 + r_3 - r_5 - r_6}$
20	$\frac{0.3129(r_1 - r_{11}) + 0.2980(r_2 - r_{10} - r_{12} + r_{20})}{0.0967(r_2 + r_{10} - r_{12} - r_{20}) + 0.1839(r_3 + r_9 - r_{13} - r_{19})} \dots$ $\dots \frac{+0.2531(r_3 - r_9 - r_{13} + r_{19}) + 0.1839(r_4 - r_8 - r_{19} + r_{18})}{+0.2531(r_9 + r_8 - r_{14} - r_{18}) + 0.2976(r_5 + r_7 - r_{15} - r_{17})} \dots$ $\dots \frac{+0.0967(r_5 - r_7 - r_{15} + r_{17})}{+0.3129(r_6 - r_{16})}$
∞	$\frac{\int_0^T r(t) \cos \omega t \, dt}{\int_0^T r(t) \sin \omega t \, dt}$

He originally noted that $k \geq 3$, and proposed four integrations. The result corresponds to the entry for $k = 4$ in Table II.

Before proceeding to the algorithm verification, it is necessary to determine (or predict) how good an estimate can be obtained from Eqs. (4-36) and (4-48). Therefore, the question of performance remains to be addressed.

The conditions for which photon counting yields accurate estimates are to be investigated in the next sections.

Performance of the Estimators

One measure of performance of an estimator is generally given by the variance of the estimate with respect to the true value. This measure of performance is known as the Mean-Square Error (MSE), and in the case of unbiased estimates (zero-mean errors), it is the variance of the error itself.

For nonlinear estimates, the MS error is not simple to compute, and a lower bound on the error is sought instead. The most widely used bound is the one given by the Cramer-Rao inequality (Ref 14:66-73). An approximate MS error and the Cramer-Rao (lower) Bound (CRB) will be computed in this paper and a comparison will be made to establish the validity of the CRB bound to measure the performance of the joint estimation problem addressed in Chapter VI.

Mean-Square Error. The MSE of an estimate is defined as the expected value of the square error between the

estimate $\hat{\theta}(\underline{r})$ and the actual value of θ (Refs 14:64, 17:412).
Let the error be defined as

$$\epsilon_{\underline{r}} \triangleq (\theta - \hat{\theta}(\underline{r})) . \quad (4-50)$$

The exact MSE is then given by (Ref 14:56)

$$E[\epsilon_{\underline{r}}^2] = \int_{-\infty}^{\infty} d\theta \int_{-\infty}^{\infty} d\underline{r} (\theta - \hat{\theta}(\underline{r}))^2 f_{\theta, \underline{r}}(\theta, \underline{r}) . \quad (4-51)$$

The joint density is given by the product $f_{\underline{r}|\theta}(\underline{r}|\theta)f_{\theta}(\theta)$.
For the MAP estimate, $\hat{\theta}(\underline{r})$ and the two densities are given by Eqs. (4-39), (4-14), and (4-37). For the ML estimate, $\hat{\theta}(\underline{r})$ and the densities are given by Eqs. (4-48), (4-14), and (4-46). The direct computation of Eq. (4-51) is difficult to perform. However, an indirect computation suggested by Sage and Melsa (Ref 11:189) is performed here for discrete observations and yields a result that depends on the energy of the system for large signal-to-noise ratios. These derivations are developed in the following sections.

The MAP-MS Estimation Error. The MAP estimate of θ when the a priori density is Gaussian is, from Eq. (4-36),

$$\hat{\theta}(\underline{r}) = - \sum_{j=1}^k \beta_j r_j k_o \cos \hat{\theta}(\underline{r}) - \sum_{j=1}^k \alpha_j r_j k_o \sin \hat{\theta}(\underline{r}) , \quad (4-52)$$

where, from Table I,

$$k_o \triangleq \frac{q k b \sigma_{\theta}^2}{\pi N_o} . \quad (4-53)$$

If the expression for r_j given by Eq. (3-16) is substituted into Eq. (4-53), then the MAP estimate becomes, in terms of signal and noise,

$$\begin{aligned}\hat{\theta}(\underline{r}) = & - \sum_{j=1}^k \beta_j s_j(\theta) k_o \cos \hat{\theta}(\underline{r}) - \sum_{j=1}^k \beta_j n_j k_o \cos \hat{\theta}(\underline{r}) \\ & - \sum_{j=1}^k \alpha_j s_j(\theta) k_o \sin \hat{\theta}(\underline{r}) - \sum_{j=1}^k \alpha_j n_j k_o \sin \hat{\theta}(\underline{r}),\end{aligned}\quad (4-54)$$

where $s_j(\theta)$ is given by Eq. (3-25). After some processing of Eq. (4-54), the estimate becomes

$$\begin{aligned}\hat{\theta}(\underline{r}) = & - \frac{aT}{qk} k_o \sum_{j=1}^k \{ \beta_j \cos \hat{\theta}(\underline{r}) + \alpha_j \sin \hat{\theta}(\underline{r}) \} \\ & - \frac{bT}{2\pi q} k_o \sum_{j=1}^k \{ \beta_j \alpha_j \cos \theta \cos \hat{\theta}(\underline{r}) - \beta_j^2 \sin \theta \cos \hat{\theta}(\underline{r}) \\ & + \alpha_j^2 \cos \theta \sin \hat{\theta}(\underline{r}) - \alpha_j \beta_j \sin \theta \sin \hat{\theta}(\underline{r}) \} \\ & - k_o \sum_{j=1}^k \{ \beta_j n_j \cos \hat{\theta}(\underline{r}) + \alpha_j n_j \sin \hat{\theta}(\underline{r}) \}.\end{aligned}\quad (4-55)$$

The equalities of Eqs. (4-30) and (4-35) can now be substituted into Eq. (4-55). By setting $\sum_{j=1}^k \alpha_j \beta_j = \sum_{j=1}^k \alpha_j = \sum_{j=1}^k \beta_j = 0$ and expanding the products of $\sin \theta \cdot \cos \hat{\theta}(\underline{r})$ and $\cos \theta \cdot \sin \hat{\theta}(\underline{r})$ into sums, Eq. (4-55) becomes

$$\begin{aligned}
\hat{\theta}(\underline{r}) &= \frac{bT}{4\pi q} k_o \sum_{j=1}^k \{ \beta_j^2 [\sin(\theta + \hat{\theta}(\underline{r})) + \sin(\theta - \hat{\theta}(\underline{r}))] \\
&\quad - \alpha_j^2 [\sin(\theta + \hat{\theta}(\underline{r})) - \sin(\theta - \hat{\theta}(\underline{r}))] \\
&\quad - k_o \sum_{j=1}^k \{ \beta_j n_j \cos \hat{\theta}(\underline{r}) + \alpha_j n_j \sin \hat{\theta}(\underline{r}) \} \quad . \quad (4-56)
\end{aligned}$$

The error ϵ_r defined in Eq. (4-50) is expected to be small; otherwise, the estimate is meaningless. To insure this condition, the approximation

$$\sin(\theta - \hat{\theta}(\underline{r})) \approx \epsilon_r \quad (4-57)$$

can be used in Eq. (4-56). By observing from Eq. (4-29) that $\sum_{j=1}^k \alpha_j^2 = \sum_{j=1}^k \beta_j^2 = 0$, Eq. (4-56) can be transformed to yield an expression for the error; so, it becomes

$$\begin{aligned}
\epsilon_r &= \frac{\pi^2 N_o}{E_a \sigma_\theta^2} \gamma_k \hat{\theta}(\underline{r}) + \frac{2\pi q k}{bT} \gamma_k \\
&\quad \sum_{j=1}^k \{ \beta_j n_j \cos \hat{\theta}(\underline{r}) - \alpha_j n_j \sin \hat{\theta}(\underline{r}) \} \quad , \quad (4-58)
\end{aligned}$$

where new parameters have been defined as

$$\gamma_k \triangleq [k \sum_{j=1}^k \alpha_j^2]^{-1} \quad , \quad (4-59)$$

which is just a number that depends on the particular value of k , and

$$E_a \triangleq \frac{b^2 T}{2}, \quad t_1 \leq t \leq t_1 + T, \quad (4-60)$$

which is the ac component of the energy in the interval $(t_1, t_1 + T)$ of the signal of Eq. (2-9).

The first check to be made on the estimate $\hat{\theta}(\underline{r})$ using Eq. (4-58) is that for bias (Ref 17:404). Thus, by recalling from Eq. (4-7) that $E[n_j] = 0$, the conditional expectation of the error given θ is

$$E[\epsilon_r | \theta] = \frac{\pi^2 N_o}{E_a \sigma_\theta^2} \gamma_k E[\hat{\theta}(\underline{r}) | \theta]. \quad (4-61)$$

Solving for $E[\hat{\theta}(\underline{r}) | \theta]$ and noticing that $E[\theta | \theta] = \theta$, Eq. (4-61) gives

$$E[\hat{\theta}(\underline{r}) | \theta] = \theta [1 + \pi^2 N_o \gamma_k / E_a \sigma_\theta^2]^{-1}. \quad (4-62)$$

Thus, the conditional expected value of $\hat{\theta}(\underline{r})$ is a scaled version of the true value of θ . The estimate approaches the true value as the signal to noise energy ratio in $(t_1, t_1 + T)$, E_a/N_o , is made very large, which is expected when the measurement is made in the absence of noise. Thus, in the limiting case, and only in that case,

$$\lim_{E_a/N_o \rightarrow \infty} E[\hat{\theta}(\underline{r}) | \theta] = \theta, \quad (4-63)$$

and the MAP phase estimate is asymptotically unbiased (Ref 17:404).

The second computation to be made from ϵ_r is that of the MS error between $\hat{\theta}(\underline{r})$ and θ . The MS error is defined as the expected value of ϵ_r^2 . The first order statistics needed to asymptotically characterize the MSE are

$$E[\theta] = 0 \quad (4-64)$$

$$E[\hat{\theta}(\underline{r})] = E[E[\hat{\theta}(\underline{r})|\theta]] = 0 \quad (4-65)$$

$$E[\epsilon_r] = E[\theta] - E[\hat{\theta}(\underline{r})] = 0. \quad (4-66)$$

In such a case, large E_a/N_o , the MS error is both the variance of $\hat{\theta}(\underline{r})$ and the variance of ϵ_r which will be defined asymptotically as

$$\begin{aligned} V_a(\epsilon_r) &\triangleq \lim_{E_a/N_o \rightarrow \infty} \text{Var}(\epsilon_r) \\ &= \lim_{E_a/N_o \rightarrow \infty} E[\epsilon_r^2]. \end{aligned} \quad (4-67)$$

From Eq. (4-58) the second order moment of ϵ_r is given by

$$\begin{aligned} E[\epsilon_r^2] &= [\pi^2 N_o \gamma_k / E_a \sigma_c^2]^2 E[(\hat{\theta}(\underline{r}))^2] \\ &\quad + [2\pi q_k \gamma_k / bT]^2 \\ &\quad E[\{\sum_{j=1}^k (\beta_j n_j \cos \hat{\theta}(\underline{r}) + \alpha_j n_j \sin \hat{\theta}(\underline{r}))\}^2], \end{aligned} \quad (4-68)$$

where the identity $E[n_j] = 0$ was used. The second expectation term in Eq. (4-68) reduces to

$$\frac{N_o T}{2q^2 k} \sum_{j=1}^k \alpha_j^2,$$

where use of the identities of Eqs. (4-8), (4-29) and (4-30) was made. Finally, by using Eqs. (4-59) and (4-60), Eq. (4-68) becomes

$$E[\epsilon_r^2] = [\pi^2 N_o \gamma_k / E_a \sigma_\theta^2]^2 E[(\hat{\theta}(\underline{r}))^2] + \pi^2 N_o \gamma_k / E_a . \quad (4-69)$$

Equation (4-69) is the MS error of the phase estimate. The difficulty with this expression is that $E[(\hat{\theta}(\underline{r}))^2]$ must be evaluated from the density function of Eq. (4-14) (Ref 14:64). However, if the ratio E_a/N_o is made very large, the error variance becomes, from Eq. (4-67)

$$V_a(\epsilon_r) = \frac{\pi^2 N_o \gamma_k}{E_a} . \quad (4-70)$$

It will be beneficial to inquire what the effect of γ_k in Eq. (4-70) is as k varies from $k = 3$ to the limit where it becomes very large. A plot of γ_k versus k for large signal-to-noise ratio (SNR) is shown in Figure 7 as a normalized variance

$$\frac{V_a(\epsilon_r) E_a}{\pi^2 N_o} .$$

A plot of $\gamma_k k$; that is, $[\sum_{j=1}^k \alpha_j^2]^{-1}$, versus k is shown in Figure 8 to show how fast the (normalized) variance, γ_k , approaches linearity as k increases. From Figure 7 it is observed that γ_k tends to stabilize at around 0.051 as k becomes large. This corresponds to the asymptotic slope of the curve in Figure 8. Thus, equation (4-70) becomes

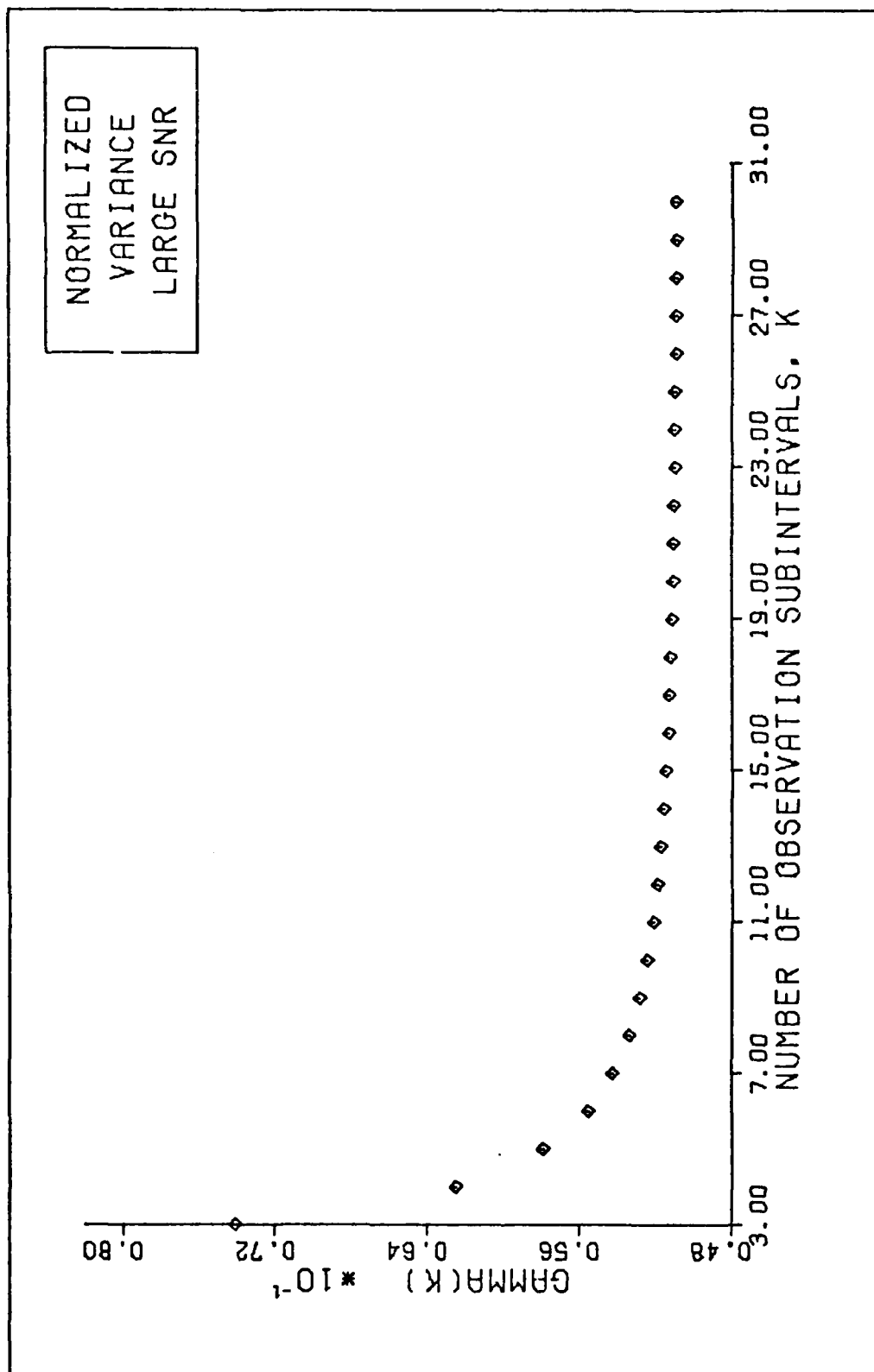


Fig 7. The Error Variance as a Function of Algorithm Form

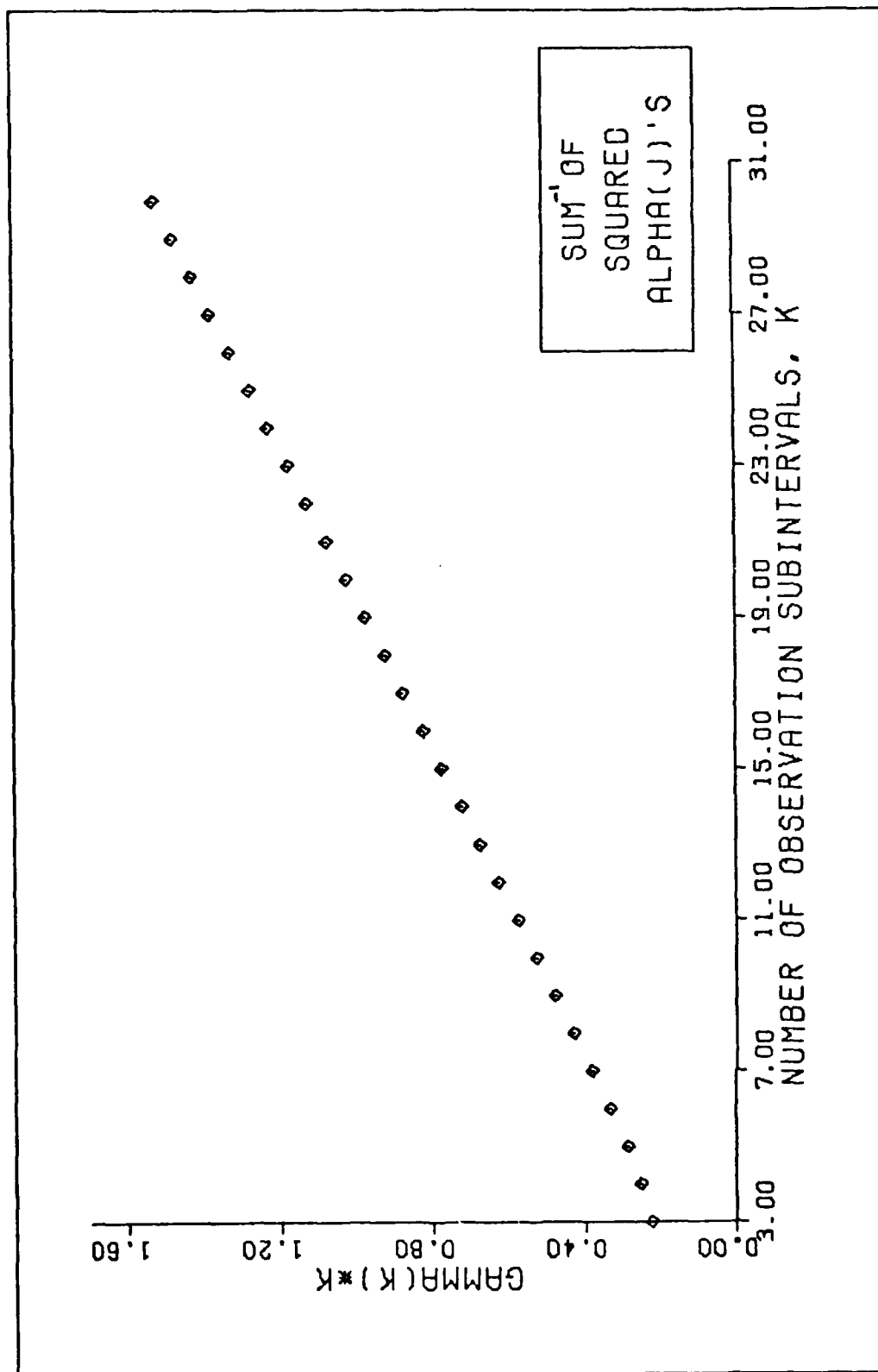


Fig 8. Relationship between γ_k and K as a Product

$$\begin{aligned}
\lim_{k \rightarrow \infty} V_a(\epsilon_r) &\approx \frac{0.051\pi^2 N_o}{E_a} \\
&= \frac{N_o}{2E_a} .
\end{aligned} \tag{4-71}$$

The MS error of a phase estimate for large signal-to-noise energy ratio in (t_1, t_1+T) is just a multiple of the inverse SNR scaled by a factor that depends on the number of the observation interval subdivisions, k . A few examples to illustrate Eq. (4-70) are given in Table III.

The ML-MS Estimation Error. The same procedure used in the previous section to determine the MAP-MS error can be used for the ML case. Using Eq. (4-48) as a starting point and substituting for r_j given by Eq. (3-16), it is found that the ML estimate is unconditionally unbiased; that is,

$$E[\hat{\theta}(\underline{r}) | \theta] = \theta . \tag{4-72}$$

This is easy to verify by observing that for ML, $\sigma_\theta^2 = \infty$ in the MAP equations. Thus, Eq. (4-69) reduces to Eq. (4-72) without any SNR restrictions. Completion of the procedure yields an unconditional error variance given by

$$V_{ar}(\epsilon_r) = \frac{\pi^2 N_o \gamma_k}{E_a} . \tag{4-73}$$

Again this is easily verified by letting $\sigma_\theta^2 = \infty$ in Eq. (4-69). A different procedure, however, carried out by Raemer (Ref 9:263,458) to compute directly the Root Mean-Square (RMS) error defined as

TABLE III

Examples of the MAP Phase Estimator
Error Variance for Large SNR

k	$V_a(\epsilon_r)$
3	$\frac{4\pi^2}{27} \frac{N_o/2}{E_a} = 1.462 \frac{N_o/2}{E_a}$
4	$\frac{\pi^2}{8} \frac{N_o/2}{E_a} = 1.2337 \frac{N_o/2}{E_a}$
5	$\frac{2\pi^2}{17.27} \frac{N_o/2}{E_a} = 1.1427 \frac{N_o/2}{E_a}$
6	$\frac{\pi^2}{9} \frac{N_o/2}{E_a} = 1.0966 \frac{N_o/2}{E_a}$
15	$\frac{2\pi^2}{19.45} \frac{N_o/2}{E_a} = 1.0147 \frac{N_o/2}{E_a}$
20	$\frac{2\pi^2}{19.57} \frac{N_o/2}{E_a} = 1.0082 \frac{N_o/2}{E_a}$
∞	$\frac{N_o/2}{E_a} = \frac{N_o/2}{E_a}$

$$\epsilon_{\psi} \triangleq [V_{ar}(\epsilon_r)]^{1/2}, \quad k = \infty, \quad (4-74)$$

where $\hat{\theta}(\infty)$ is as in Eq. (4-49) did show a SNR dependence of the ML estimate. By expanding the arc tangent in Eq. (4-49), Raemer obtained similar results with the condition of a large E_a/N_o ratio. Specifically,

$$\epsilon_{\psi}^2 \approx \frac{1}{4} \frac{1}{\rho_i B_n T} = \frac{N_o}{2E_a}, \quad (4-75)$$

where ρ_i and B_n were defined parameters of the signal and noise treated as narrowband processes. Therefore, the MAP and ML error variance are the same and approach zero when the signal is strong relative to the receiver noise. Thus, Table III is equally an ML comparison of the error variance in terms of the observations k . To show graphically the relative improvement of entries in Table III, define in logarithmic terms

$$\begin{aligned} I_{mp}(\text{dB}) &\triangleq 10 \log \left[\frac{V_{ar}(\epsilon_r) | k=3}{V_{ar}(\epsilon_r)} \right] \\ &= 10 \log (\gamma_3/\gamma_k). \end{aligned} \quad (4-76)$$

The relative improvement in decibels (dB) of the error ϵ_r with respect to the error in three subintervals is shown in Figure 9.

The important conclusion of this section is that in the presence of thermal (receiver) noise, the error in the phase estimate is strictly a function of the signal-to-noise

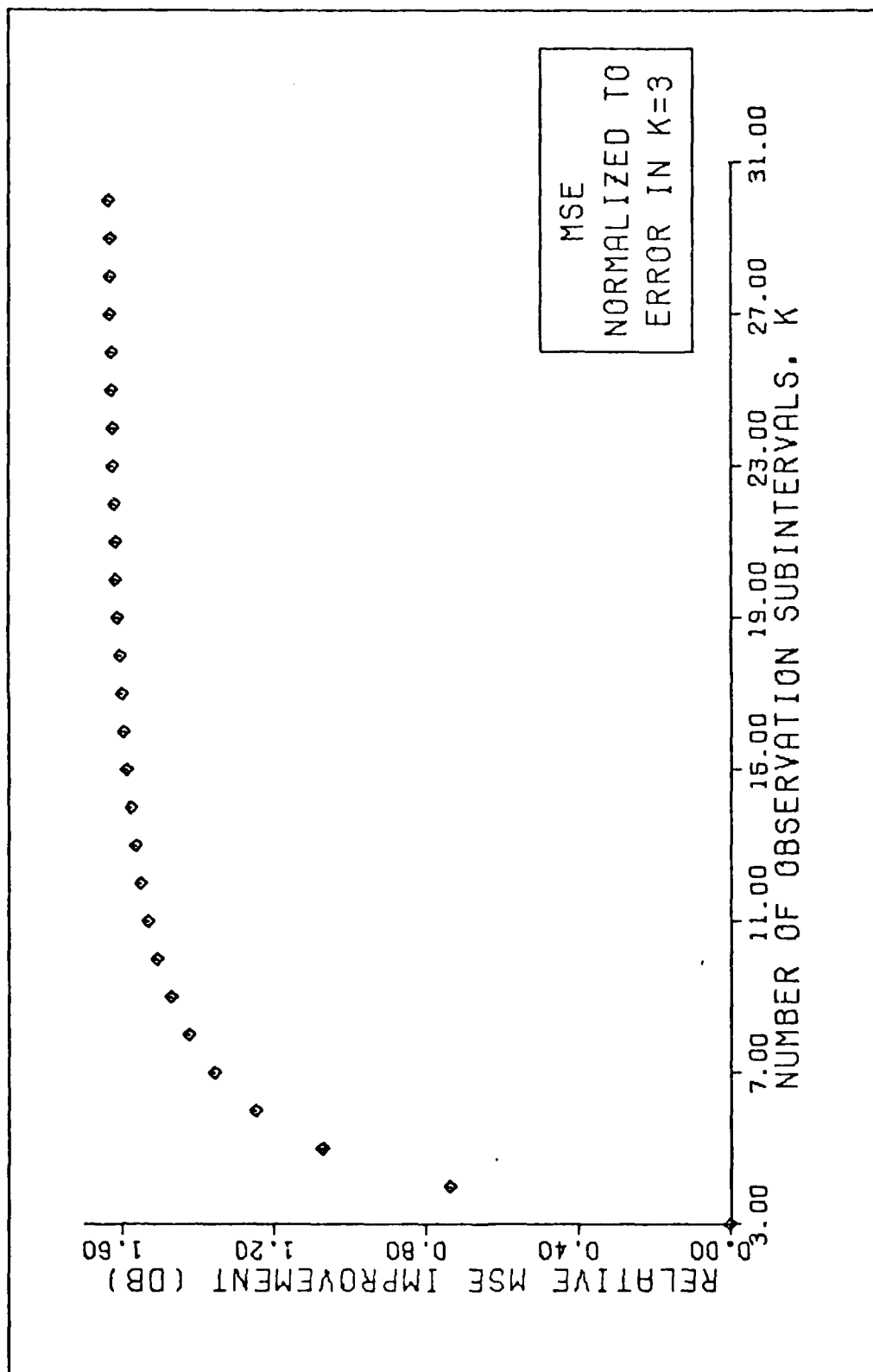


Fig 9. Relative MSE Improvement Compared to the Error in Three Subintervals

ratio. The ideal procedure is to perform a current measurement ($k = \infty$), for which the error is the inverse SNR multiplied by a factor of 1. The procedure is suboptimal if discrete photon counts are made ($k < \infty$), for which case the same error is scaled by an appropriate factor determined by k . Referring to the curve in Figure 9, the continuous current-based estimate offers an improvement of 1.65 dB over the discrete photon count based on only $k = 3$ integrations. Notice, however, that if the hypothetical CCD detectors can provide 15 or more integrations over T , then the improvement of a continuous measurement over photon counting is only 0.064 dB. Thus, provided the SNR restrictions are met, the photon counting algorithms offer a viable alternative for phase estimation when the signal levels are low.

Considering the extremes, when the SNR is low, neither a current measurement nor a photon count will yield an accurate phase estimate. On the other hand, in the absence of noise, the error is zero ($E_a/N_0 = \infty$) as expected from a perfect measurement. This is easily proven by substituting $r_j = s_j(\theta)$, given by Eq. (4-23), back into Eqs. (4-36) (with $F(\theta) = 0$) or (4-48). With the help of Eqs. (4-29), (4-30), and (4-35) the result obtained is $\hat{\theta}(\underline{r}) = 0$ as expected. This was also verified computationally.

The level of SNR to assure with a given certainty that an estimate is within a specified phase range has been addressed in the literature and will not be repeated here

(Ref 9:266). Instead, a general observation will be made from the results of the computer simulation discussed at the end of this chapter.

In order to complete the error analysis, it is desirable to inquire what the minimum MS error is, and the conditions under which it is attained. A good description is given by the Cramer-Rao bound on the minimum MSE although other bounds are also available (Ref 14:71). The Cramer-Rao approach will be considered in the next section.

Cramer-Rao Lower Bound on the Minimum MS Error. The lower limit on the value that the minimum MS error (MMSE) can have can be calculated without actually having to know the estimate. For the case of an unbiased estimate, the CRB bound is given by (Ref 14:72)

$$\begin{aligned} \text{CRB} &= \{E[(\frac{\partial}{\partial \theta} \ln f_{\underline{r}, \theta}(\underline{r}, \theta))^2]\}^{-1} \\ &= -\{E[\frac{\partial^2}{\partial \theta^2} \ln f_{\underline{r}, \theta}(\underline{r}, \theta)]\}^{-1} . \end{aligned} \quad (4-77)$$

For the case of a biased non-random parameter, a bound expression is given by Van Trees (Ref 14:147).

In order to use Eq. (4-77) in the problem at hand, it is necessary to work with the large SNR restriction, for which the estimate $\hat{\theta}(\underline{r})$ was shown to be asymptotically unbiased. Thus, the bound is given by

$$V_a(\epsilon_r) \geq \text{CRB} , \quad E_a/N_o \rightarrow \infty . \quad (4-78)$$

Before letting the SNR become very large let

$$V_{ar}(\epsilon_r) > CRB = -\{E[\frac{\partial^2}{\partial \theta} \ln f_{\underline{r}|\theta}(\underline{r}|\theta) + \ln f_{\theta}(\theta)]\}^{-1} \quad (4-79)$$

For the observation in white Gaussian noise, it is convenient to specialize Eq. (4-79) further before considering the phase problem. From Eq. (4-17)

$$\begin{aligned} \frac{\partial}{\partial \theta} \ln f_{\underline{r}|\theta}(\underline{r}|\theta) &= \frac{2q^2 k}{N_o T} \sum_{j=1}^k r_j \frac{\partial}{\partial \theta} s_j(\theta) \\ &\quad - \frac{2q^2 k}{N_o T} \sum_{j=1}^k s_j(\theta) \frac{\partial}{\partial \theta} s_j(\theta) . \end{aligned} \quad (4-80)$$

The second derivative of Eq. (4-80) with respect to θ is

$$\begin{aligned} \frac{\partial^2}{\partial \theta^2} \ln f_{\underline{r}|\theta}(\underline{r}|\theta) &= \frac{2q^2 k}{N_o T} \sum_{j=1}^k \left\{ [r_j - s_j(\theta)] \frac{\partial^2}{\partial \theta^2} s_j(\theta) \right. \\ &\quad \left. - \left(\frac{\partial s_j(\theta)}{\partial \theta} \right)^2 \right\} . \end{aligned} \quad (4-81)$$

The CRB bound then becomes

$$\begin{aligned} CRB &= - \left\{ \frac{2q^2 k}{N_o T} \sum_{j=1}^k E \left[(r_j - s_j(\theta)) \frac{\partial^2}{\partial \theta^2} s_j(\theta) \right. \right. \\ &\quad \left. \left. - \left(\frac{\partial s_j(\theta)}{\partial \theta} \right)^2 \right] + E \left[\frac{\partial^2}{\partial \theta^2} \ln f_{\theta}(\theta) \right] \right\}^{-1} . \end{aligned} \quad (4-82)$$

By observing that

$$r_j - s_j(\theta) = n_j$$

and

$$E[n_j] = 0 ,$$

the MAP error variance becomes in terms of the CRB bound

$$V_a(\epsilon_r) \geq \left\{ \frac{2q^2 k}{N_0 T} \sum_{j=1}^k \left(\frac{\partial s_j(\theta)}{\partial \theta} \right)^2 - E\left[\frac{\partial}{\partial \theta} F(\theta) \right] \right\}^{-1}, \quad k \geq 3 ,$$

$$\text{for } E_a/N_0 \rightarrow \infty . \quad (4-83)$$

Without the large SNR restriction, Eq. (4-83) is a general expression for the lower bound on the error variance of any unbiased estimate (Ref 17:412). The factor $\frac{q^2 k}{T}$ in Eq. (4-83) comes from the use of the orthogonal functions defined by Eqs. (3-7) and (3-9). In the limit as k becomes very large, Eq. (4-83) becomes

$$V_a(\epsilon_r) \geq \left\{ \frac{2}{N_0} \int_0^T \left(\frac{\partial s(t, \theta)}{\partial \theta} \right)^2 dt - E\left[\frac{\partial}{\partial \theta} F(\theta) \right] \right\}^{-1}$$

$$\text{for } E_a/N_0 \rightarrow \infty , \quad (4-84)$$

where use of Eqs. (3-10) and (4-21) was made. This is the result for the bound on the error of the estimate of a parameter measured in a continuous waveform regardless of algorithmic form (Ref 14:275). Returning to Eq. (4-83), from Eq. (4-24),

$$\left[\frac{\partial}{\partial \theta} s_j(\theta) \right]^2 = \left(\frac{bT}{2\pi q} \right)^2 \sum_{j=1}^k [\alpha_j \sin \theta + \beta_j \sin \theta]^2 . \quad (4-85)$$

By use of Eq. (4-85) in Eq. (4-83), the bound becomes

$$\begin{aligned}
 \text{CRB} &= \left\{ \frac{2q^2 k}{N_o T} \left(\frac{bT}{2\pi q} \right)^2 \sum_{j=1}^k [\alpha_j \sin \theta + \beta_j \cos \theta]^2 - E\left[\frac{\partial}{\partial \theta} F(\theta)\right] \right\}^{-1} \\
 &= \left\{ \frac{2Tk}{N_o} \left(\frac{b}{2\pi} \right)^2 \sum_{j=1}^k [\alpha_j^2 \sin^2 \theta + \beta_j^2 \cos^2 \theta + \alpha_j \beta_j \sin 2\theta] \right. \\
 &\quad \left. - E\left[\frac{\partial}{\partial \theta} F(\theta)\right] \right\}^{-1}, \quad k \geq 3. \quad (4-86)
 \end{aligned}$$

Invoking the identities of Eqs. (4-29) and (4-30) one more time, Eq. (4-86) can be simplified to

$$\begin{aligned}
 V_a(\epsilon_r) &\geq \left\{ \frac{kb^2 T}{4\pi^2 N_o / 2} \sum_{j=1}^k \alpha_j^2 - E\left[\frac{\partial}{\partial \theta} F(\theta)\right] \right\}^{-1} \\
 &\geq \left\{ \frac{E_a}{\pi^2 N_o \gamma_k} - E\left[\frac{\partial}{\partial \theta} F(\theta)\right] \right\}^{-1}, \quad k \geq 3,
 \end{aligned}$$

$$\text{for } E_a/N_o \rightarrow \infty. \quad (4-87)$$

Equation (4-87) is the lower bound on the MS error in the estimate of θ given by the Cramer-Rao inequality. It is a function of the ac component of the signal energy E_a , the noise energy N_o and the observation subinterval k represented by γ_k . It is also a function of the statistical description of θ represented by the density $f_\theta(\theta)$. In the particular case where the phase is modeled as a Gaussian random variable with the density given by Eq. (4-37), then

$$E\left[\frac{\partial}{\partial \theta} F(\theta)\right] = -\frac{1}{\sigma_\theta^2} . \quad (4-88)$$

The bound on the error variance becomes

$$\begin{aligned} V_a(\epsilon_r) &\geq \left[\frac{E_a}{\pi^2 N_o \gamma_k} + \frac{1}{\sigma_\theta^2} \right]^{-1} \\ &\geq \frac{\pi^2 N_o \gamma_k \sigma_\theta^2}{\pi^2 N_o \gamma_k \sigma_\theta^2 + E_a \sigma_\theta^2} , \quad k \geq 3 , \end{aligned}$$

$$\text{for } E_a/N_o \rightarrow \infty . \quad (4-89)$$

In the limiting case as k becomes very large, $1/\gamma_k \approx 19.6$ (see p. 44), so

$$\begin{aligned} \lim_{k \rightarrow \infty} \text{l.i.m. } V_a(\epsilon_r) &\geq \left[\frac{2E_a}{N_o} + \frac{1}{\sigma_\theta^2} \right]^{-1} \\ &\geq \frac{\sigma_\theta^2 N_o}{N_o + 2E_a \sigma_\theta^2} \end{aligned}$$

$$\text{for } E_a/N_o \rightarrow \infty . \quad (4-90)$$

Equation (4-90) gives the MAP lower bound on the error variance based on a continuous measurement. Finally, when the large SNR condition is used, Eq. (4-90) becomes

$$\lim_{E_a/N_o \rightarrow \infty} \{ \text{l.i.m. } V_{ar}(\epsilon_r) \} \geq \frac{N_o}{2E_a} . \quad (4-91)$$

This is precisely the result given by Eq. (4-71). Therefore, as the term E_a/N_o grows unbounded, the true error

variance approaches the CRB with equality; the MAP estimates $\hat{\theta}(\underline{r})$ and $\hat{\theta}$ are asymptotically efficient (Ref 14:276). Thus, the Cramer-Rao bounds are also given in Table III. The same observation is made for the ML-CRB on the error variance. For the ML-CRB, from Eq. (4-46),

$$E\left[\frac{\partial}{\partial \theta} F(\theta)\right] = 0, \quad (4-92)$$

and Eq. (4-77) reduces to (Ref 14:66)

$$\text{CRB} = -\{E\left[\frac{\partial^2}{\partial \theta^2} \ln f_{\underline{r}|\theta}(\underline{r}|\theta)\right]\}^{-1}. \quad (4-93)$$

Therefore the bound for the ML error is, from Eq. (4-89) as σ_θ^2 gets large,

$$V_a(\epsilon_r) \geq \frac{\pi^2 N_o \gamma_k}{E_a}, \quad k \geq 3, \quad (4-94)$$

or from Eq. (4-90),

$$\lim_{k \rightarrow \infty} V_a(\epsilon_r) \geq \frac{N_o}{2E_a}. \quad (4-95)$$

From Eq. (4-90) it is observed that when the signal is weak, the error is limited by the variance σ_θ^2 . But this is not the same result expressed by Eq. (4-69), and therefore the Cramer-Rao bound becomes meaningless in such a case.

In conclusion, the analysis made in the Gaussian noise context indicates that under thermal noise limited conditions, measurement of a phasefront cannot be made accurately except for large signal-to-noise ratios. For low light

levels conforming to this restriction, the photon counting technique is quite acceptable, but when the signal level permits, a current measurement is most appropriate. At this point, a verification of the algorithms derived in Eqs. (4-39) and (4-48), as well as a performance evaluation, is overdue. This was done in a computer simulation, and is presented in the following section.

Verification of the MAP and ML Estimators

A simulation program to test Eqs. (4-39) and (4-48) was written in FORTRAN and run on the CDC 6600 computer system. After the parameters for the simulation have been input, the program generates the signal counts $s_j(\theta)$, computed from the true phase input and Eq. (3-24), and adds white Gaussian noise counts n_j , computed from

$$n_j = \frac{P_j}{q} \left[\frac{N_0 T}{2k} \right]^{1/2}, \quad (4-96)$$

where P_j is a number from a zero-mean, unit-variance, Gaussian random number sequence, generated using a subroutine from the IMSL library. The program then estimates the phase based on the noise-corrupted measurements r_j using Eqs. (4-39), (4-41) and (4-48) as needed.

The parameters chosen for this simulation are a 25 kilohertz modulation frequency, a 0.04 millisecond observation period (required by the choice of $N = 1$ in Eq. (3-22)) and a signal level in the order of 1 microamp. Although the algorithm is independent of signal level (also verified

by using 10 milliamps) this number was entered to simulate the output of a detector under low signal levels. The number of counts r_j thus generated are of the order of 10^8 photoelectrons and below. In the 0.04 millisecond observation time used, this corresponds to less than 10^{13} photoelectrons per second, a rate which is in the category of low photon coherence. The simulation results are contained in Figures 10-19.

Simulation Results for the MAP Estimator. The MAP estimator simulation is a series of tests performed on Eq. (4-39) to verify its performance as an estimator. In these tests, Eq. (4-39) was used to estimate a known phase given different signal-to-noise ratios following the procedure outlined in the previous section. The tests were then repeated to estimate different phase angles at a fixed SNR. Several such tests were performed and the results presented here are typical. The first set is shown in Figure 10. These curves were obtained using a phase variance of 0.8 rad^2 , chosen as the safe maximum deviation for which Eq. (4-38) can be used to obtain Eq. (4-39); and using a test phase of 0.5234 radians (30°), which seemed a logical choice. The five curves shown are the phase estimates plotted as a function of the algorithmic form used (determined by k) for the indicated signal-to-noise ratios (10 dB to 30 dB). The same noise counts were used in each curve.

From this and other tests performed (by changing the noise seed to generate P_j), it is observed that the estimate

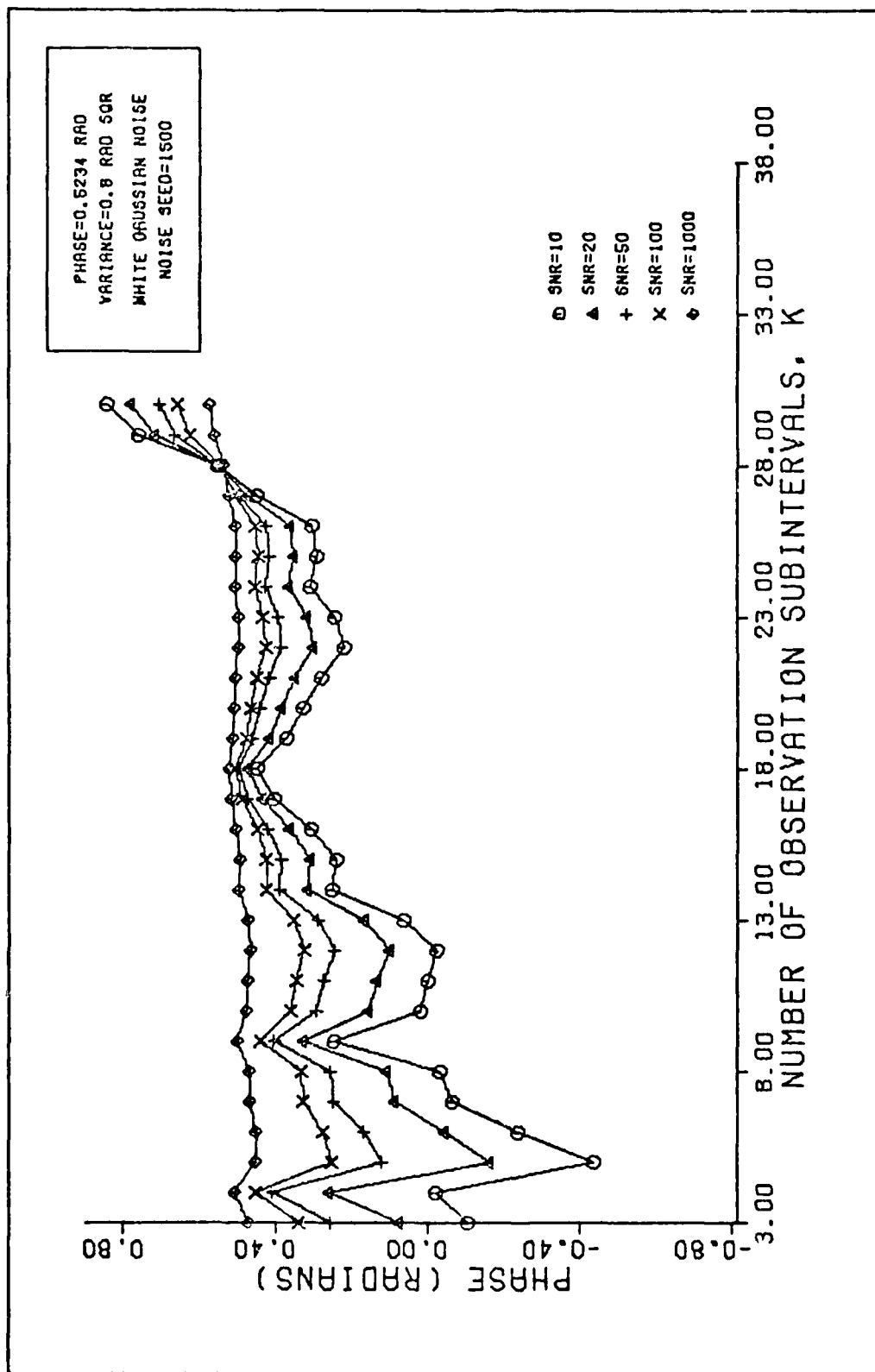


Fig 10. MAP Simulation Results - Single Phase at Different SNR's

deviations are larger for lower values of k , but improve as the SNR increases. Thus, for large SNR's, consider that to be 50 (17 dB) and above, the benefit of the simpler algorithm forms in Table I can be used to an advantage (less computation time). The same is true for the ML approach (see Table II). The variance of these estimates is shown in Figure 11.

Figure 12 is a plot of the estimates of five phase angles obtained with a SNR of 17 dB. They range from 0.2 radians (11.5°) to 1.4 radians (80°). No significant differences in the pattern are observed. A small discrepancy, however, had to be fixed in this particular plot; the phase estimate $\hat{\theta}(r_4)$ for $\theta = 1.4$ radians made by using four sub-intervals had a negative sign. This occurred both in the MAP and the ML test. However, it cannot be inferred that the estimator is more sensitive as the phase becomes larger. The variance of these estimates is shown in Figure 13. Both Figures 11 and 13 seem to confirm the theoretical prediction of Figure 7: improved performance as k (and SNR) $\rightarrow \infty$.

A test to check the effect of a smaller a priori phase variance σ_θ^2 was also run and is shown in Figure 14. The variance was chosen to be 0.274 rad^2 (the square of the test phase). A slight improvement was obtained with respect to the curves of Figure 10. The comparison can be made more easily by looking at the estimates variance shown in Figure 15. Here, the improvement is more obvious for the lower values of k , and in particular for the 10 dB curve; that is,

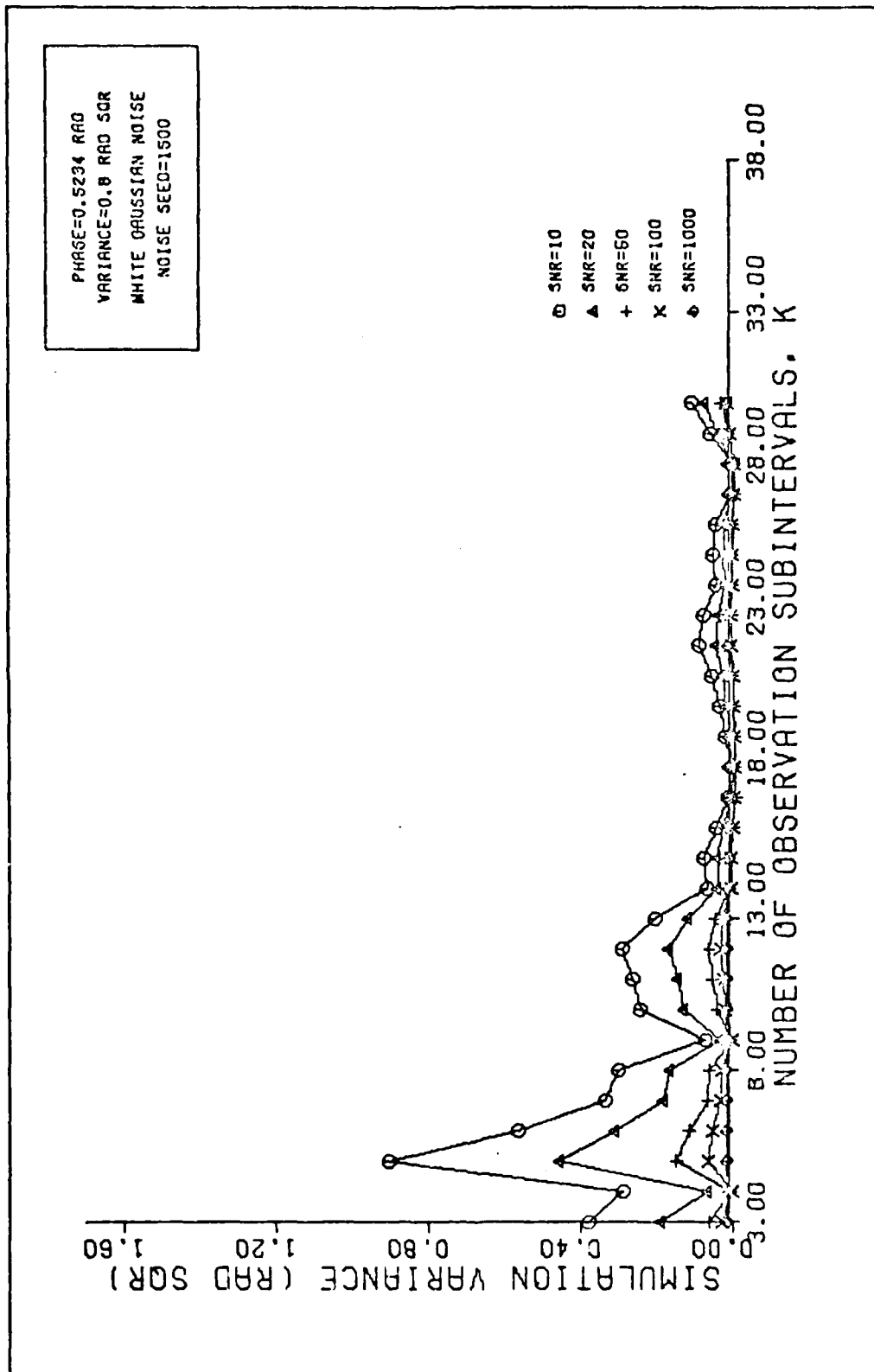


Fig 11. MAP Simulation Variance - Single Phase at Different SNR's

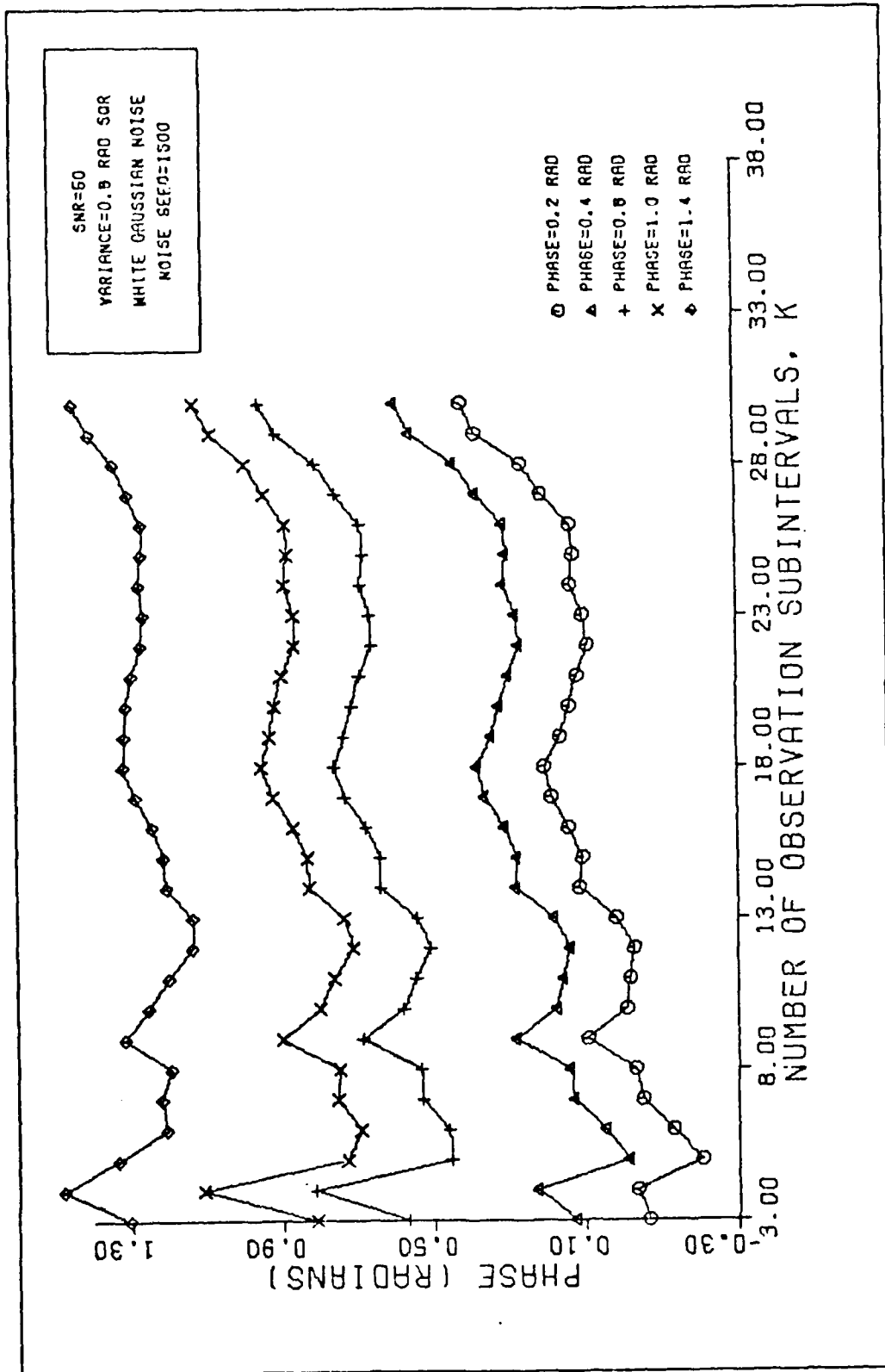


Fig 12. MAP Simulation Results - Multiple Phase Angles at a Fixed SNR

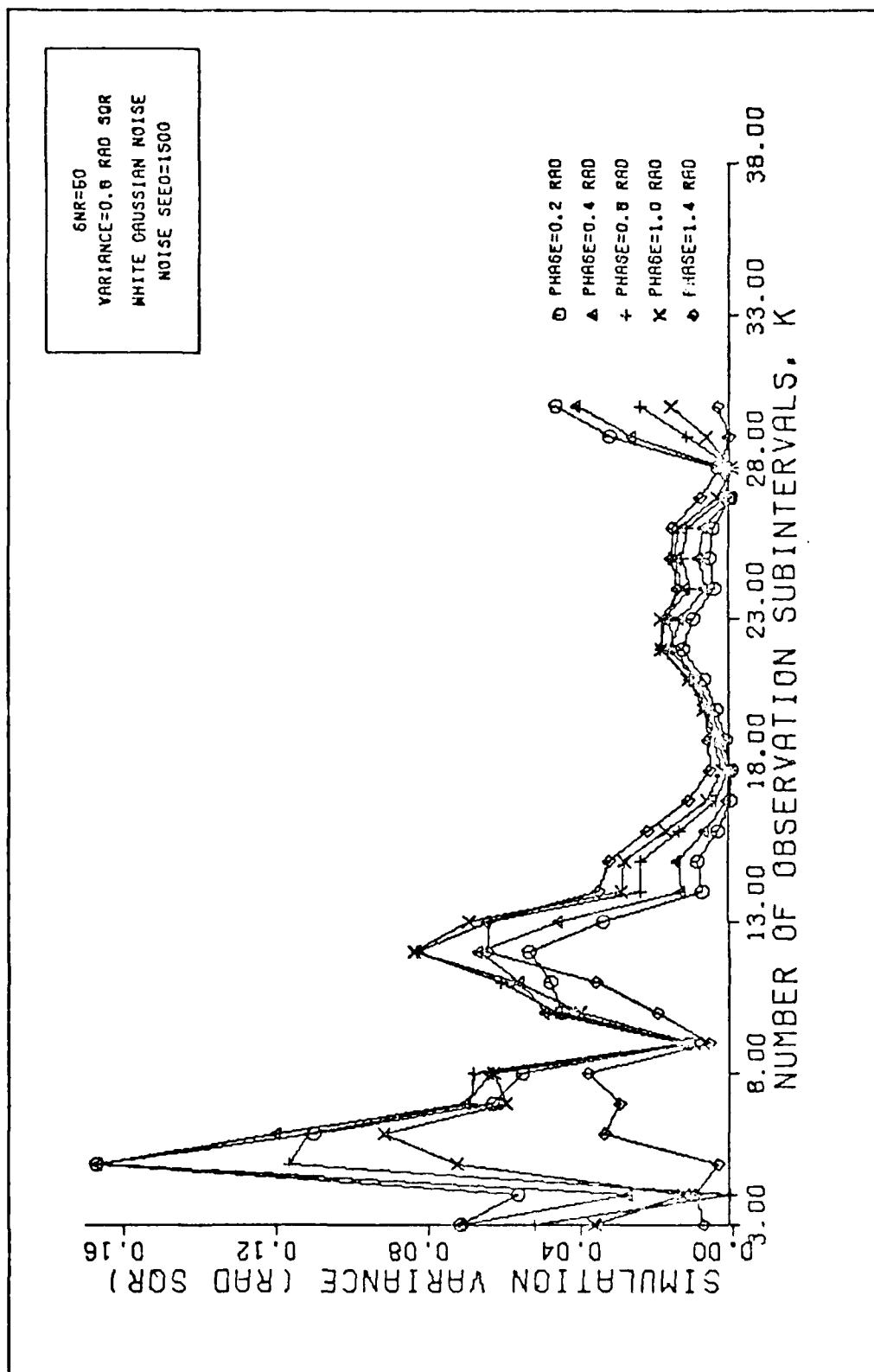


Fig 13. MAP Simulation Variance - Multiple Phase Angles at a Fixed SNR

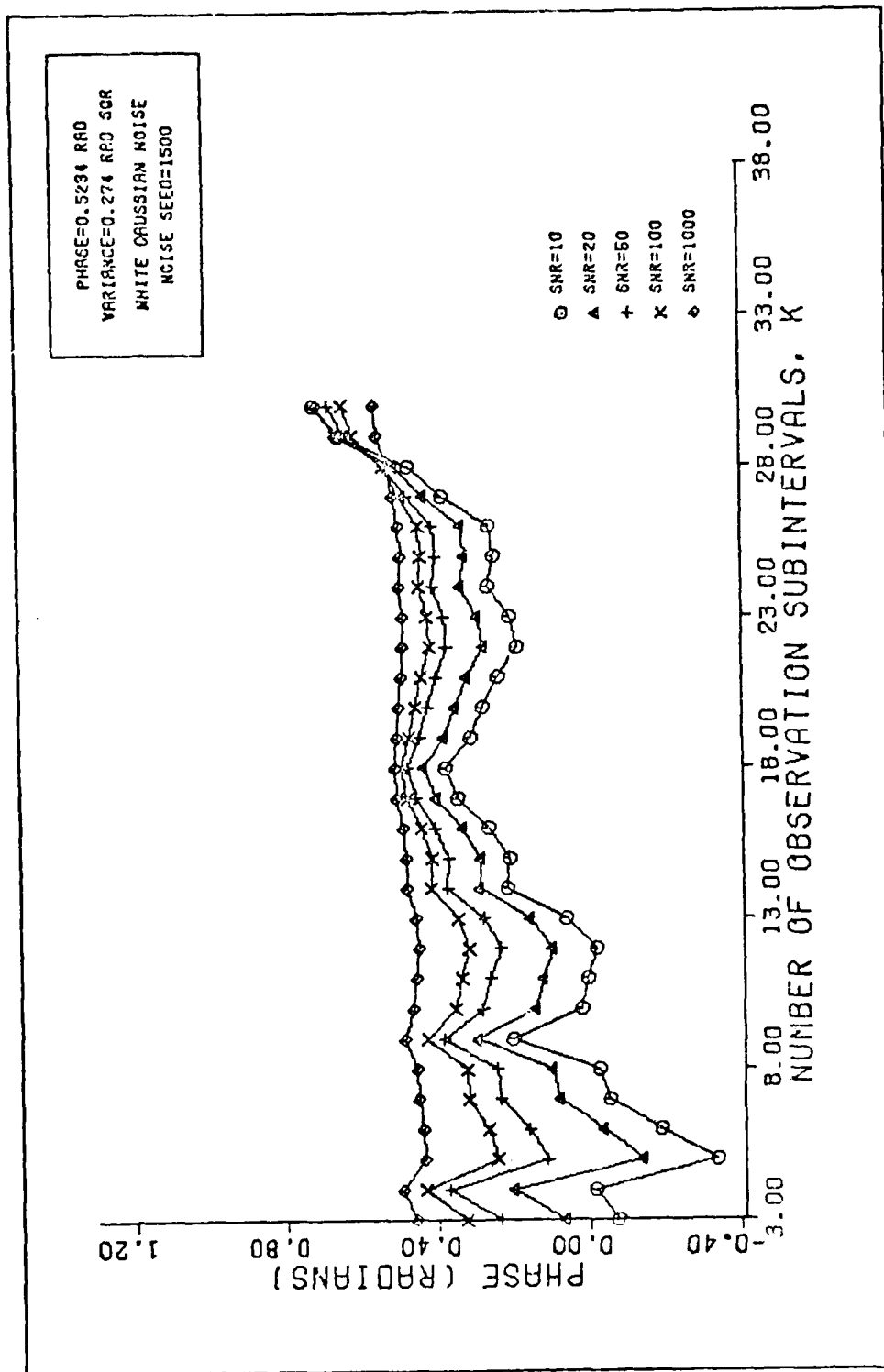


Fig 14. MAP Simulation Run with Improved Phase Variance

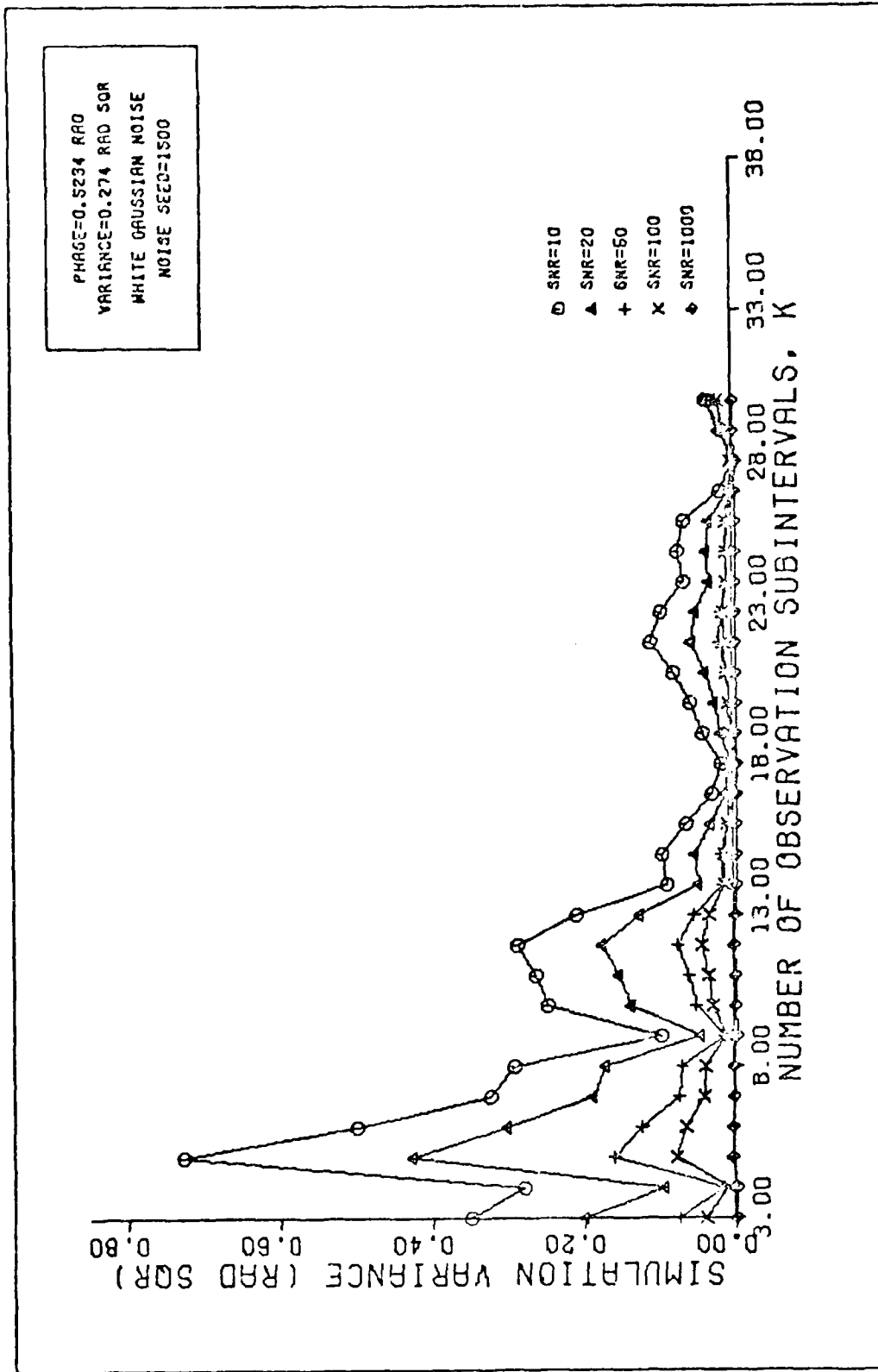


Fig 15. MAP Simulation Error Using Improved Phase Variance

for the estimates obtained with the smaller SNR used. This seems to confirm the discussion pertaining to Eq. (4-90), that estimates from noisy measurements are more dependent on the a priori information, a useful characteristic of the MAP estimator. Similar tests were also run to verify the ML algorithms, and are discussed in the following section.

Simulation Results for the ML Estimator. The ML estimator simulation is a series of tests performed on Eq. (4-48), similar to the ones performed on the MAP estimator. The main difference lies in the straightforward computation given by the inverse tangent form of Eq. (4-48). Here, no a priori information (phase variance) is used. The results, shown in Figures 16-19, are surprisingly close to the MAP results already discussed, especially as k increases. Thus, the ML approach can be used to advantage when the signal-to-noise ratios are high enough to perform nearly as well as the MAP estimator. From these results, Figures 10-19, it can be seen that high enough may be 10 dB and higher. Thus, given SNR's better than 10 dB, the ML algorithm of Eq. (4-48) seems to be a good estimator. Its use, when warranted, has the advantage of avoiding solving equations of the form of Eq. (4-41) which are time consuming. The MAP estimator, on the other hand, is more useful under noisy conditions, where the estimator weights more heavily on the a priori information.

In the analysis presented in this chapter, the ultimate noise limited condition was assumed: that of the detector.

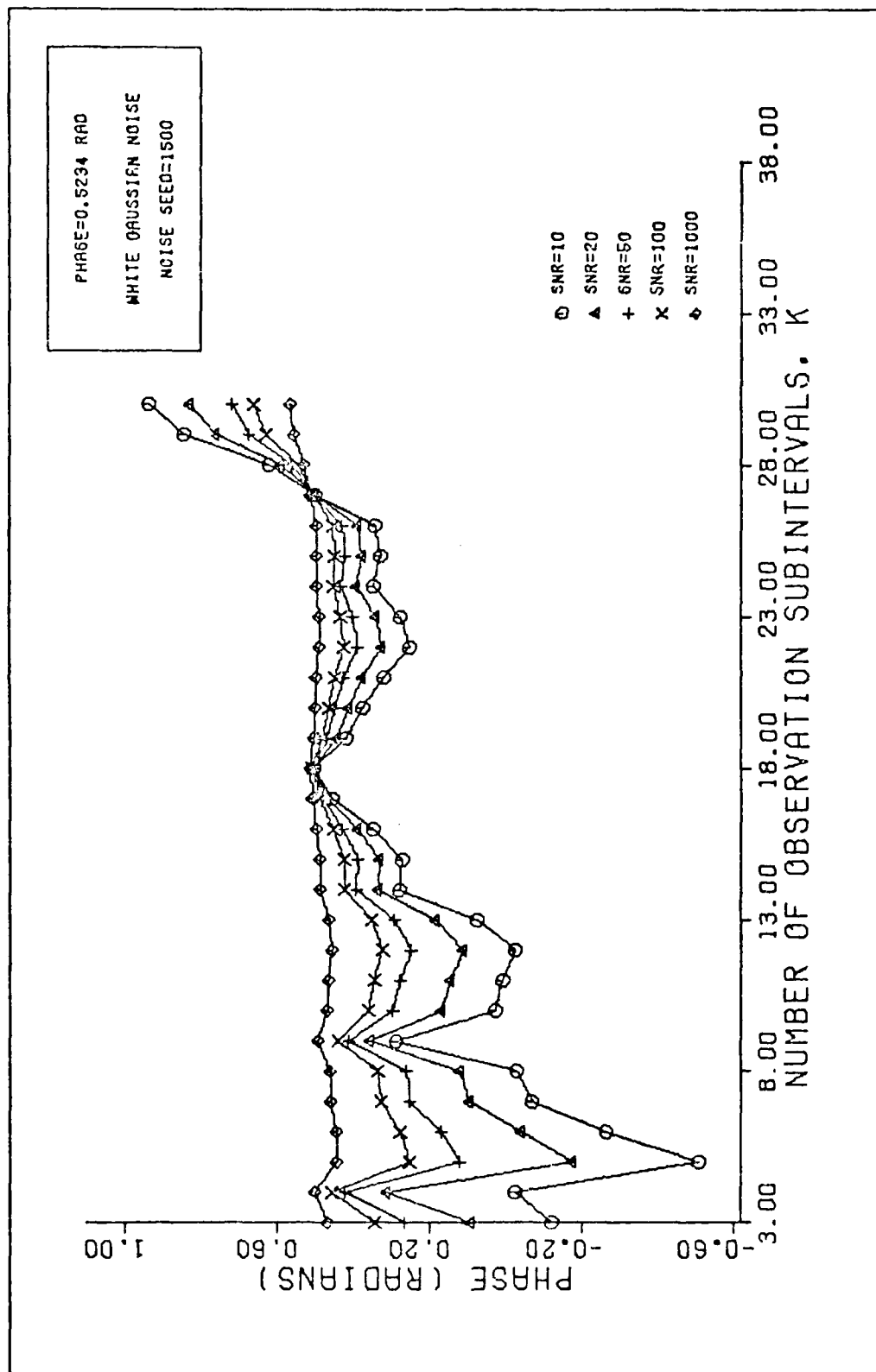


Fig 16. ML Simulation Results - Single Phase at Different SNR's

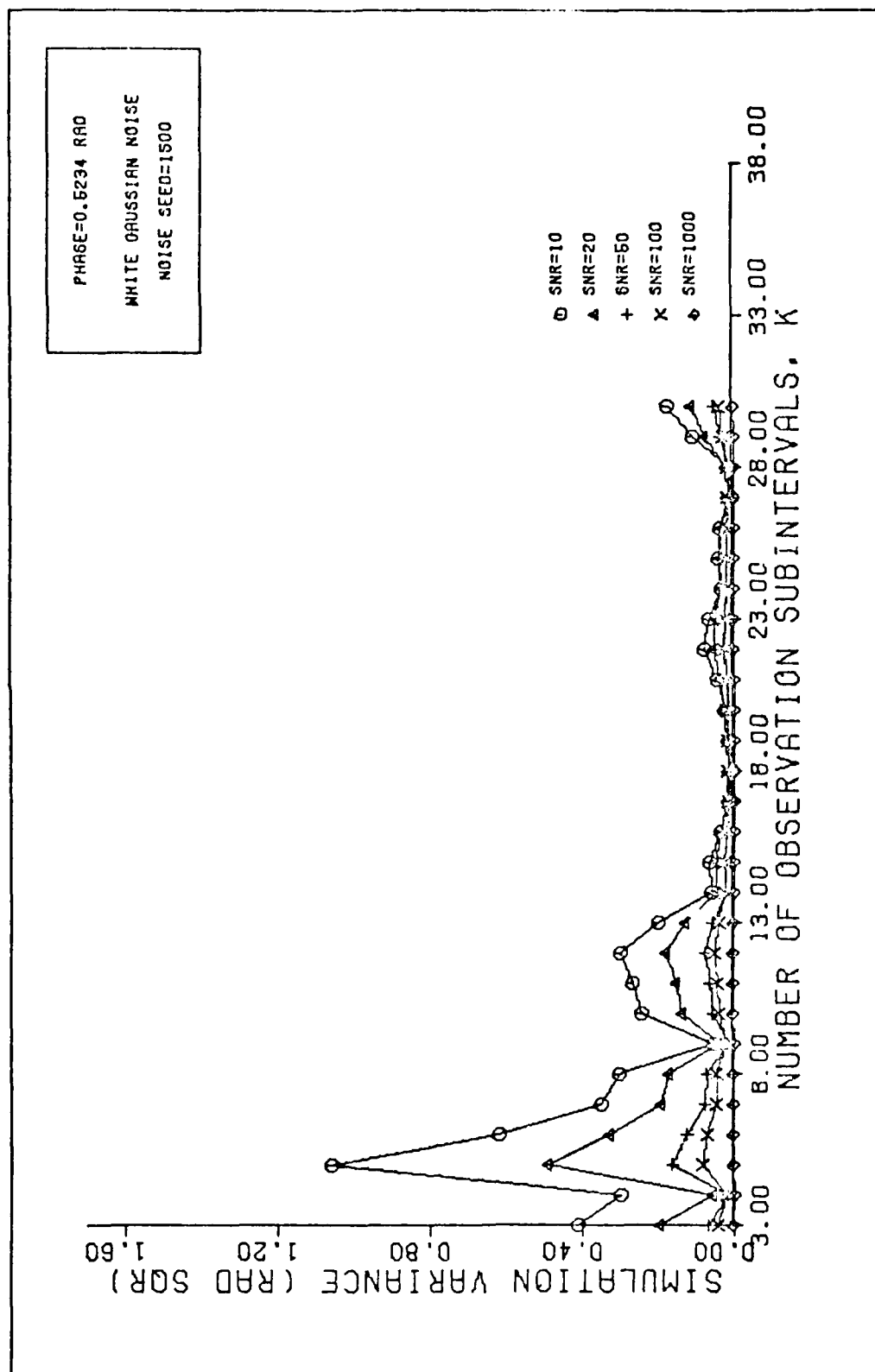


Fig 17. ML Simulation Variance - Single Phase at Different SNR's

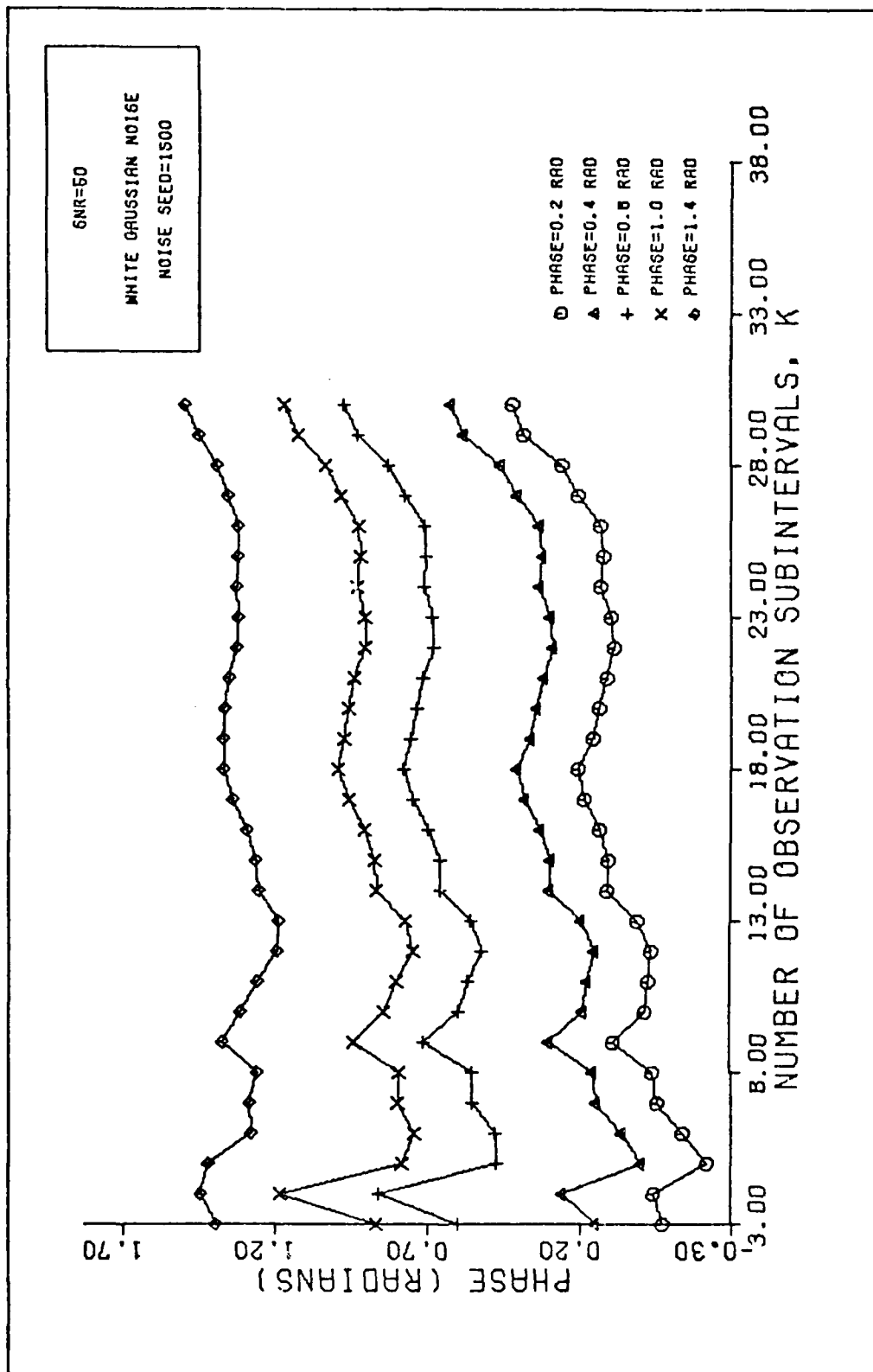


Fig 18. ML Simulation Results - Multiple Phase Angles at a Fixed SNR

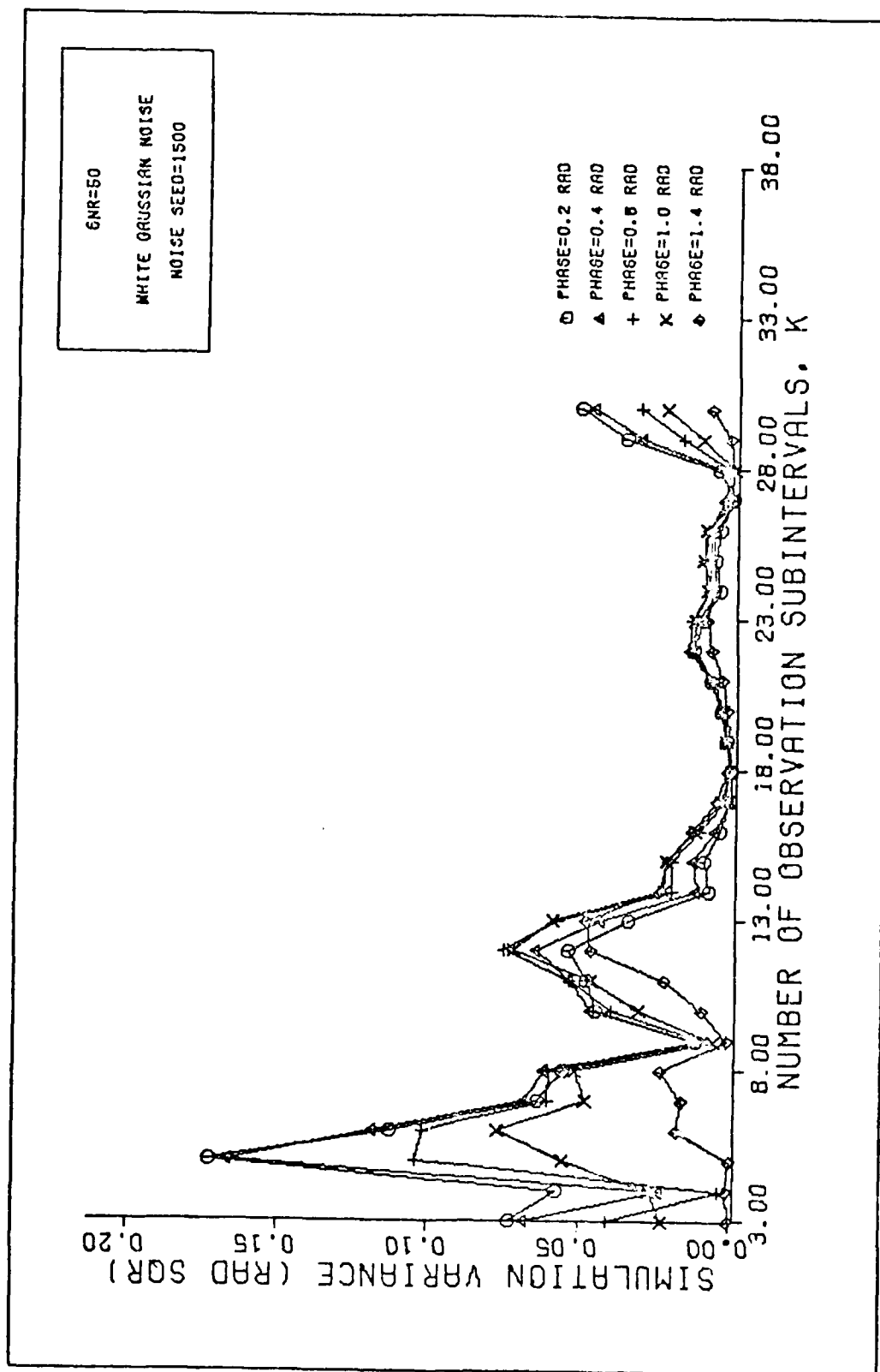


Fig 19. ML Simulation Variance - Multiple Phase Angles at a Fixed SNR

In reality, and particularly for low light levels, when the signal-to-thermal noise energy ratio is indeed very large as may be the case of the CC devices, then the effects of the signal shot noise predominate. Therefore, it is necessary to consider the predominant shot noise case in order to have a more complete analysis. When the phase θ is the only random parameter in Eq. (2-9) and consequently in Eq. (4-23), the problem can be treated in the Poisson context. An explicit use of the Poisson statistical description of shot noise, ignored by Wyant, will be the basis of the developments of the next chapter.

V Phase Estimation in Shot Noise

When detector thermal noise is negligible, the process is signal shot noise limited. For a multimode field (Ref 2: 87-94, 212), the process is well modeled as having conditionally Poisson statistics. When the field is single mode, then it is governed by Laquerre (Ref 2:304) statistics and will not be considered here. The analysis is identical to the one made in Chapter IV after Eqs. (3-32) and (3-33). For multimode detection, the counts r_j in the observation interval (t_1, t_1+T) are independent and Poisson distributed when conditioned on the field intensity (Ref 2:295). The density function of the observables in $(t_j, t_j+\tau)$ conditioned on θ is the probability density of the events (photons received), assuming that all the events equal the observations (photoelectrons produced) in each observation sub-interval τ . Therefore, the density function of the shot process is

$$P[N_\tau = r_j | \theta] = \frac{\mu_j^{r_j}}{r_j!} e^{-\mu_j} \triangleq f_{r_j | \theta}, \quad (5-1)$$

where

$$\mu_j = \int_{t_j}^{t_j+\tau} \frac{E[r(t)]}{q} dt. \quad (5-2)$$

The observation $r(t)$ has the form

$$r(t) = s(t, \theta) + q(\lambda_{sn}(t) + \lambda_b + \lambda_d(t)), \quad (5-3)$$

where the noise count (photon) rates have the following statistics: (1) the signal shot noise $\lambda_{sn}(t)$ is a non-stationary, zero-mean process with covariance $\lambda(t)\delta(t-t')$; (2) the background is assumed constant and infinite with correlation function $N_{ob}\delta(\bar{r}_a - \bar{r}_a')\delta(t-t')$ and a stationary count rate $\lambda_b = N_{ob}B_oD_o\eta/hf_o$, where N_{ob} is the spectral background noise strength, B_o is the optical bandwidth and D_o is the number of spatial modes (Ref 2:212,213,298); and (3) the stationary detector dark current has dc content λ_d and covariance $\lambda_d\delta(t-t')$.

Maximum A Posteriori and Maximum Likelihood Estimates

With the above conditions established, the MAP and ML phase estimates can be found using Eq. (5-1) as the starting point. Thus, Eq. (5-1) becomes

$$f_{r_j|\theta}(r_j|\theta) = \frac{(s_j(\theta) + (\lambda_b + \lambda_d)T/k)^{r_j}}{r_j!} \exp[-(s_j(\theta) + (\lambda_b + \lambda_d)T/k)] \quad (5-4)$$

In a manner analogous to Eq. (4-14), the observation vector \underline{r} has a conditional density function given by

$$\begin{aligned} f_{\underline{r}|\theta}(\underline{r}|\theta) &= \prod_{j=1}^k f_{r_j|\theta} \\ &= \left\{ \prod_{j=1}^k \frac{(s_j(\theta) + (\lambda_b + \lambda_d)T/k)^{r_j}}{r_j!} \right\} \exp[-\sum_{j=1}^k (s_j(\theta) + (\lambda_b + \lambda_d)T/k)] \quad (5-5) \end{aligned}$$

Unlike Eq. (4-14), Eq. (5-5) contains a constant noise term $(\lambda_b + \lambda_d)T/k$ that represents deviation from ideal behavior. Use of Eq. (5-5) in Eq. (3-32) yields the MAP estimator equation

$$\sum_{j=1}^k \frac{r_j}{s_j(\theta) + (\lambda_b + \lambda_d)T/k} \frac{\partial s_j(\theta)}{\partial \theta} - \frac{1}{q} \int_0^T \frac{\partial}{\partial \theta} s(t, \theta) dt + F(\theta) = 0, \quad (5-6)$$

where the substitution

$$\sum_{j=1}^k \frac{\partial s_j(\theta)}{\partial \theta} = \sum_{j=1}^k \int_{t_j}^{t_{j+1}} \frac{\partial}{\partial \theta} \frac{s(t, \theta)}{q} dt = \frac{1}{q} \int_0^T \frac{\partial s(t, \theta)}{\partial \theta} dt \quad (5-7)$$

and the definition of Eq. (4-26) were used.

Use of Eqs. (3-25)-(3-27) and (4-24) in Eq. (5-6) with

$\int_0^T \frac{\partial}{\partial \theta} s(t, \theta) dt = 0$, where $s(t, \theta)$ is given by Eq. (2-9), yields the MAP estimate

$$\sum_{j=1}^k r_j \frac{[\alpha_j \sin \hat{\theta}(\underline{r}) + \beta_j \cos \hat{\theta}(\underline{r})]k/2\pi}{[\alpha_j \cos \hat{\theta}(\underline{r}) - \beta_j \sin \hat{\theta}(\underline{r})]k/2\pi + (a + i_b + i_d)/b} - F(\theta) = 0, \quad (5-8)$$

where the substitution (Ref 2:113) $(i_b + i_d) = q(\lambda_b + \lambda_d)$ was made to convert constant photon count rates to dc noise current. The ratio

$$\gamma = \frac{\Delta}{a + i_b} \quad (5-9)$$

is the fringe visibility and depends on the radiance of the source. The dark current i_d is usually negligible.

Equation (5-8) is the MAP discrete estimator of phase measured under Poisson shot noise conditions. It can be reduced further under special conditions, but before specializing its results and following the practice of previous sections, Eqs. (5-6) and (5-8) can be put in the form of continuous waveform equations. Thus, in the limit as k becomes very large, Eq. (5-6) becomes (Ref 2:298)

$$\frac{1}{q} \int_0^T \frac{r(t)}{s(t, \theta) + (i_b + i_d)} \frac{\partial s(t, \theta)}{\partial \theta} dt - \frac{1}{q} \int_0^T \frac{\partial s(t, \theta)}{\partial \theta} dt + F(\theta) = 0, \quad (5-10)$$

and the MAP phase estimator of Eq. (5-8) becomes

$$\frac{1}{q} \int_0^T \frac{r(t) \cos(\omega t + \hat{\theta})}{\sin(\omega t + \hat{\theta}) + (a + i_b + i_d)/b} dt - F(\theta) = 0. \quad (5-11)$$

The first case to be considered is when the fringe visibility is approximately unity. This is more or less what is found from the output of the shearing interferometer, as can be determined from Eqs. (2-10) and (2-11). Thus, from these two equations, $a/b \approx 0.711$; so, $(a + i_b) \approx b$, considering the presence of a small background current. Thus, by setting $(a + i_b + i_d)/b = 1$, Eq. (5-8) can be transformed using simple trigonometric identities (Ref 11:225-241) into

$$\sum_{j=1}^k r_j \{ \tan[\sin^{-1}(\alpha_j / \sqrt{\alpha_j^2 + \beta_j^2}) - \hat{\theta}(\underline{r})] \\ + 2\pi / [(\alpha_j \sin \hat{\theta}(\underline{r}) + \beta_j \cos \hat{\theta}(\underline{r})) / k] \}^{-1}$$

$$- F(\theta) = 0$$

for $\gamma = i_d \approx 1$

and $\gamma \gg i_d$, (5-12)

where the substitution

$$\tan^{-1}(\alpha_j / \beta_j) = \sin^{-1}(\alpha_j / \sqrt{\alpha_j^2 + \beta_j^2}) \quad (5-13)$$

was made to avoid dividing by zero as some β_j 's are found to be. Equation (5-12) is therefore the discrete MAP phase estimator given Poisson shot noise conditions and equal amplitude dc and ac components. It is noteworthy to observe that if k is large, the second term in Eq. (5-12) can be neglected so the estimate becomes approximately

$$\sum_{j=1}^k r_j \cot[\sin^{-1}(\alpha_j / \sqrt{\alpha_j^2 + \beta_j^2}) - \hat{\theta}(\underline{r})] \\ - F(\theta) = 0 , \quad k \rightarrow \text{large} . \quad (5-14)$$

Finally as k becomes very large, from Eq. (5-11), the continuous measurement estimate is found to be

$$\int_0^T r(t) \cot\left(\frac{\omega t + \hat{\theta}}{2} + \frac{\pi}{4}\right) dt - q F(\theta) = 0 ,$$

$$\text{for } \gamma + i_d \approx 1 , \quad \gamma \gg i_d . \quad (5-15)$$

The second case to be considered is when $(a+i_b+i_d) = 0$, dc components blocked (capacitively perhaps). For this case, Eq. (5-8) becomes

$$\sum_{j=1}^k r_j \frac{\alpha_j \sin \hat{\theta}(\underline{r}) + \beta_j \cos \hat{\theta}(\underline{r})}{\alpha_j \cos \hat{\theta}(\underline{r}) - \beta_j \sin \hat{\theta}(\underline{r})} - F(\theta) = 0 . \quad (5-16)$$

Equation (5-16) can be also transformed using simple trigonometric identities into

$$\begin{aligned} \sum_{j=1}^k r_j \tan[\sin^{-1}(\beta_j / \sqrt{\alpha_j^2 + \beta_j^2}) + \hat{\theta}(\underline{r})] \\ - F(\theta) = 0 , \quad \text{dc blocked.} \end{aligned} \quad (5-17)$$

This is the discrete MAP phase estimator given Poisson shot noise conditions and dc components (signal and noise) blocked. In the limit as k becomes large, the continuous measurement estimators found to be from Eq. (5-11)

$$\int_0^T r(t) \cot(\omega t + \hat{\theta}) dt - q F(\theta) = 0 ,$$

dc blocked . (5-18)

The last case to be considered is for a very low fringe visibility such that $(a+i_b) \gg b$. This condition is given

under a strong infinite background competing with the source (target), and is referred to as background limited. Thus, for background limited conditions,

$$(a+i_b+i_d)/b \gg [\alpha_j \cos \hat{\theta}(\underline{r}) - \beta_j \sin \hat{\theta}(\underline{r})]k/2\pi$$

and Eq. (5-8) becomes

$$\sum_{j=1}^k r_j [\alpha_j \sin \hat{\theta}(\underline{r}) + \beta_j \cos \hat{\theta}(\underline{r})] - \frac{2\pi(a+i_b+i_d)}{kb} F(\theta) = 0 \quad (5-19)$$

Equation (5-19) is of the same form as Eq. (4-36) with the term $2\pi(a+i_b+i_d)/kb$ in place of $\pi N_0/gkb$. Thus, an equivalent noise can be defined as $N_0 \triangleq 2q(a+i_b+i_d)$. The phase estimator in multimode shot noise under background limited conditions is thus the same as the estimator obtained in the Gaussian analysis with equivalent noise $2q(a+i_b+i_d)$. Therefore, if $F(\theta) = -\theta/\sigma_\theta^2$, the MAP estimate is after Eq. (4-39)

$$\hat{\theta}(\underline{r}) = \frac{k b \sigma_\theta^2}{2\pi(a+i_b+i_d)} \left\{ - \sum_{j=1}^k \beta_j r_j \cos \hat{\theta}(\underline{r}) - \sum_{j=1}^k \alpha_j r_j \sin \hat{\theta}(\underline{r}) \right\},$$

for $i_b \gg b$, (5-20)

and the ML estimate is the same one given by Eq. (4-48).

In order to illustrate how Eqs. (5-12) and (5-17) change

AIR FORCE INST OF TECH WRIGHT-PATTERSON AFB OH SCHOO--ETC F/B 20/6
PHASE ESTIMATION TECHNIQUES FOR ACTIVE OPTICS SYSTEMS USED IN R--ETC (11)
DEC 80 F P ROJAS

DEC 80 P P RUJAS
AFIT/GEO/EE/80D-4

24

2 of 2
ADDOCO

END
DATE
FILMED
7-8
DTIC

with k and to compare them to Eqs. (5-20) and (4-48), some examples are given in Tables IV and V.

Performance of the Phase Estimators in Shot Noise

Considering that the phase estimates found in the Gaussian noise analysis are asymptotically unbiased for high SNR, the Cramer-Rao inequality seems to be also an appropriate measure of performance of the shot noise phase estimator under the same SNR restrictions. From Eqs. (4-78) and (5-6), the MAP-CRB bound is given by

$$\text{CRB} = \left\{ E \left[\sum_{j=1}^k \frac{\frac{\partial}{\partial \theta} s_j(\theta)^2}{s_j(\theta) + (\lambda_b + \lambda_d)T/k} - \frac{\partial F(\theta)}{\partial \theta} \right] \right\}^{-1} \quad (5-21)$$

By making the substitutions of Eqs. (3-25) and (4-85) into Eq. (5-21), the bound transforms into

$$\begin{aligned} \text{CRB} = & \left\{ E \left[\frac{bT}{2\pi q} \sum_{j=1}^k \frac{[\alpha_j^2 \sin\theta + \beta_j \cos\theta]^2 k/2\pi}{[\alpha_j \cos\theta - \beta_j \sin\theta] k/2\pi + (a + i_b + i_d)/b} \right] \right. \\ & \left. - E \left[\frac{\partial F(\theta)}{\partial \theta} \right] \right\}^{-1} \quad (5-22) \end{aligned}$$

For Gaussian phase, Eq. (5-22) becomes

$$\begin{aligned} \text{CRB} &= \left\{ \frac{bT}{2\pi q} E \left[\sum_{j=1}^k \frac{(\alpha_j \sin\theta + \beta_j \cos\theta)^2}{(\alpha_j \cos\theta - \beta_j \sin\theta) + 2\pi(a + i_b + i_d)/k_b} \right] + \frac{1}{\sigma_\theta^2} \right\} \\ &\triangleq \left\{ \frac{bT}{2\pi q} A_O + \frac{1}{\sigma_\theta^2} \right\}^{-1} \\ &= \frac{\sigma_\theta^2}{1 + \sigma_\theta^2 b T A_O / 2\pi q} \quad (5-23) \end{aligned}$$

TABLE IV

Examples of the MAP Phase Estimator Form
Under Multimode Shot Noise Conditions

DC Blocked, Eq. (5-17), $F(\theta) = -\theta/\sigma_\theta^2$

k	$\hat{\theta}(r_1 \dots r_k)$
3	$\sigma_\theta^2 \{ r_1 \cot \hat{\theta}(\underline{r}) - (r_2 + r_3) \tan(\hat{\theta}(\underline{r}) + \frac{\pi}{6}) \}$
4	$\sigma_\theta^2 \{ (r_1 + r_3) \cot \hat{\theta}(\underline{r}) - (r_2 + r_4) \tan \hat{\theta}(\underline{r}) \}$
∞	$\sigma_\theta^2 \int_0^T dt r(t) \cot(\omega t + \hat{\theta})$

Background Limited, Eq. (5-20), $F(\theta) = -\theta/\sigma_\theta^2$

k	$\hat{\theta}(r_1 \dots r_k)$
3	$\frac{3\sqrt{3}}{4} (2r_1 - r_2 - r_3) k_1 \cos \hat{\theta}(\underline{r}) - \frac{3}{2} (r_2 - r_3) k_1 \sin \hat{\theta}(\underline{r})$
4	$\sqrt{2} (r_1 - r_3) k_1 \cos \hat{\theta}(\underline{r}) - \sqrt{2} (r_2 - r_4) k_1 \sin \hat{\theta}(\underline{r})$
∞	$[\int_0^T r(t) \cos \omega t dt] k_q \cos \hat{\theta} - [\int_0^T r(t) \sin \omega t dt] k_q \sin \hat{\theta}$

$$k_1 \triangleq \frac{k b \sigma_\theta^2}{2\pi(a + i_b + i_d)}$$

$$k_q \triangleq \frac{b \sigma_\theta^2}{q(a + i_b + i_d)}$$

TABLE V

Examples of the ML Phase Estimator
Under Multimode Shot Noise Conditions

DC Blocked, Eq. (5-17), $F(\theta) = 0$

k	$\tan \hat{\theta}(r_1 \dots r_k)$
3	$\frac{r_1}{r_2 + r_3} \frac{\sqrt{3} - \tan \hat{\theta}(\underline{r})}{\sqrt{3} + \tan \hat{\theta}(\underline{r})}$
4	$\sqrt{\frac{r_1 + r_3}{r_2 + r_4}}$
∞	$\int_0^T r(t) \cot(\omega t + \hat{\theta}) dt = 0$

Background Limited, Eq. (4-48)

k	$\tan \hat{\theta}(r_1 \dots r_k)$
3	$\frac{\sqrt{3}}{3} \frac{2r_1 - r_2 - r_3}{r_2 - r_3}$
4	$\frac{r_1 - r_3}{r_2 - r_4}$
∞	$\frac{\int_0^T r(t) \cos \omega t dt}{\int_0^T r(t) \sin \omega t dt}$

TABLE V
(Continued)

$\gamma \approx 1, i_d \approx 0, \text{Eq. (5-12)}, F(\theta) = 0$

k	$\tan \hat{\theta}(r_1 \dots r_k)$
4	$\frac{r_1/(\sin \hat{\theta}(\underline{r})+1.11) - r_3/(\sin \hat{\theta}(\underline{r})-1.11)}{r_2/(\cos \hat{\theta}(\underline{r})+1.11) - r_3/(\cos \hat{\theta}(\underline{r})-1.11)}$
∞	$\int_0^T dt \, r(t) \cot\left(\frac{\omega t + \hat{\theta}}{2} + \frac{\pi}{4}\right) = 0$

where A_0 is the expected value of the sum with respect to θ .

For $(a+i_b+i_d) = b$ and k very large, Eq. (5-23) reduces to

(Ref 2:300)

$$V_{ar}(\epsilon_r) \geq \frac{\sigma_\theta^2}{1 + \sigma_\theta^2 bT/q} \quad (5-24)$$

The ML bound is on the other hand (σ_θ^2 large)

$$V_{ar}(\epsilon_r) \geq \frac{q}{bT} \quad (5-25)$$

the reciprocal of the collected count energy. The perform-

ance of Eq. (5-20) as given by the CRB bound is, from Eq.

(5-22) with $F(\theta) = -\theta/\sigma_\theta^2$,

$$CRB = \left\{ \frac{bT}{2\pi q} E \left[\sum_{j=1}^k \frac{(\alpha_j \sin\theta + \beta_j \cos\theta)^2 k/2\pi}{(a+i_b+i_d)/b} \right] + \frac{1}{\sigma_\theta^2} \right\}^{-1} \quad (5-26)$$

Invoking the identities of Eqs. (4-29) and (4-30), Eq.

(5-26) simplifies to

$$CRB = \left\{ \frac{b^2 T k}{4\pi^2 q (a+i_b+i_d)} \sum_{j=1}^k \alpha_j^2 + \frac{1}{\sigma_\theta^2} \right\}^{-1} \quad (5-27)$$

Finally, the definitions of Eqs. (4-59), (4-60) and (4-77)

can be used to write the error variance as

$$E[\epsilon_r^2] \geq \frac{\sigma_\theta^2}{1 + E_a \sigma_\theta^2 / [2\pi^2 q (a+i_b+i_d) \gamma_k]} \quad (5-28)$$

$$(a+i_b+i_d) \gg b \quad ,$$

or in the limit as k becomes very large

$$\lim_{k \rightarrow \infty} E[\epsilon_r^2] \geq \frac{\sigma_\theta^2}{1 + E_a \sigma_\theta^2 / q(a+i_b+i_d)}, \quad i_b \gg b. \quad (5-29)$$

Because of the requirement that $i_b \gg b$, small SNR, the error is limited by the variance. Furthermore, the actual error variance may be much higher due to the inherent SNR restrictions needed to apply Eq. (5-22). For the ML estimate, Eq. (5-28) becomes

$$V_{ar}(\epsilon_r) \geq \frac{2\pi^2 q(a+i_b+i_d)}{E_a}, \quad i_b \gg b, \quad (5-30)$$

and Eq. (5-29) becomes

$$\lim_{k \rightarrow \infty} V_{ar}(\epsilon_r) \geq \frac{q(a+i_b+i_d)}{E_a} \triangleq \frac{N_o}{2E_a}, \quad i_b > b. \quad (5-31)$$

Equation (5-31) tells that the ML estimate obtained from Eq. (4-48), when used as an approximation for background limited conditions, results in a bad estimate.

The foregoing discussion is based on Wyant's assertion (Ref 16:2624) that for shot noise limited conditions, a better method for measuring phase is as given by Eq. (5-19), $F(\theta) = 0$, easily implemented by letting $k = 4$. (See Table V, Background Limited.) The performance of Eq. (4-48) analogous to Eq. (5-19) for ML, was proven to be exclusively SNR dependent. The equivalent noise $2q(a+i_b+i_d)$ also makes the result of Eq. (5-19) SNR dependent, and the estimate is likely to be erroneous. (See Eq. (5-31).) A better

equation is given also in Table V for $\gamma \approx 1$, but the solution is not so straightforward. The analysis performed by Wyant gives an error variance (dark current neglected)

$$V_{ar}(\epsilon_r) \triangleq (\Delta\phi)^2 = \frac{\pi^2}{4\gamma^2 \sum_{j=1}^k r_j}, \quad (5-32)$$

where the photon counts can be evaluated from external parameters. Comparison of Eq. (5-32) to Eq. (5-30) using Eq. (5-9) gives the following inequality:

$$\frac{\pi^2 (a+i_b)^2}{4b^2 \sum_{j=1}^k r_j} \geq \frac{4\pi^2 q (a+i_b)}{b^2 T k \sum_{j=1}^k \alpha_j^2}, \quad (a+i_b) \gg b. \quad (5-33)$$

For the particular case of $k = 4$, Eq. (5-33) yields

$$(a+i_b) \geq \frac{q}{T} (r_1 + r_2 + r_3 + r_4) \gg b. \quad (5-34)$$

From Eqs. (5-32) and (5-9), Wyant's approach is found to be also SNR dependent. Any good performance thus depends on the condition that

$$\sum_{j=1}^k r_j \gg (a+i_b). \quad (5-35)$$

From Eq. (5-34), obviously Eq. (5-35) is not true.

The foregoing results clearly indicate that phase estimation requires a strong signal regardless of the noise process. It can be noted that under low light level conditions, the SNR constraints are more difficult to meet, and large errors may be expected. With these conclusions, the

analysis of phase difference estimation from measurements from a single detector are completed within the scope of this thesis. Given the added complexity of Eq. (5-8) and time constraints, a simulation as performed in Chapter IV is not included. Estimation of the actual phase components ϕ in Eq. (2-3) will be performed in the next chapter using the measurements of the detector array as a whole.

VI Joint Processing of Array Signals for Wavefront Estimation

The problem of phase difference estimation was addressed in Chapters IV and V. Ideally what is desired are the actual phases at specific points across the aperture rather than slopes between points. The methods usually employed to find these phases consist of mappings of data given by the measured wavefront difference functions $\Delta\phi(\bar{r}_a)$ and the geometry of the data points. These mappings use the concepts of least squares fitting and are discussed by Fried (Ref 1), Hardy et al (Ref 4), Hudgin (Ref 5), Rimmer (Ref 10), and Wyant (Ref 16) among others. The general result given by these mappings is an average of phases and measurements about a single point, requiring a recursive solution.

A different approach will be used in this thesis which uses the fact that the phases across the aperture are spatially correlated due to slow spatial variation of the wavefront, and the assumption that a spatial covariance matrix is available from experimental measurements. Therefore, by jointly processing the outputs of the two detector arrays discussed in Chapter II, a phase estimate can be made in real time. Because of the a priori information supplied by the covariance matrix, an improvement is expected over mappings of data points.

The criteria of Maximum A Posteriori estimation will be used in this chapter, but the algorithm so obtained will

be in continuous waveform rather than discrete counts. Because of the difficulty in applying the MAP theory, several assumptions need to be made in order to simplify the algorithm derivation. The problem will be worked out in the Gaussian context or second moment models only, where detector thermal noise is the predominant noise source. The noise waveforms from each detector are samples from independent white Gaussian processes with zero-mean and strength $N_k/2$. The subscript k will be used to index the $k^{(th)}$ detector. The phases $\phi(\vec{r}, t)$ will be assumed to be stepwise constant in the interval sequence $(0, T, 2T, \dots)$ as presented in Chapter I. The covariance matrix is, therefore, constant in each interval, but needs to be updated every T seconds. This is the sequential problem which is beyond the scope of this thesis. A suggestion, however, will be given later for sequential estimation by quantizing $\theta(\vec{r}, t)$ when it is continuous in time. The final assumption to be made is that of a jointly Gaussian random phase distribution over the aperture. The time-space problem fitted to the above description is one of multiple channel, multiple parameter estimation in Gaussian noise.

Multidimensional Estimator Formulation

Derivation of the required time-space estimator equation will be made in this section. The next section will treat the specific application to the shearing interferometer output. So, the multiple observation model can be written in vector form as

$$\underline{r}(t) = \underline{s}(t, \underline{a}) + \underline{n}(t) , \quad 0 \leq t \leq T , \quad (6-1)$$

where $\underline{r}(t)$ is a column vector of the outputs from a two-dimensional detector array, indexed with a single subscript $1 \leq \kappa \leq m$. A vector of phase parameters \underline{a} over the aperture, indexed also with a single subscript $1 \leq p \leq n$, is to be estimated jointly using all available outputs. The formulation needed for array processing is a direct extension of the single element case. Let the output from the κ^{th} detector be

$$r_{\kappa}(t) = s_{\kappa}(t, \underline{a}) + n_{\kappa}(t) . \quad (6-2)$$

The noise statistics are given, from Eqs. (4-2)-(4-6), as

$$E[n_{\kappa}(t)] = 0 \quad (6-3)$$

and

$$E[n_{\kappa}(t)n_{\kappa}(t')] = \frac{2kT}{R_{\kappa}} \delta(t-t') \\ \triangleq \frac{W_{\kappa}}{2} \delta(t-t') . \quad (6-4)$$

It is assumed that the noises in the detectors are statistically independent of each other. The detector outputs \underline{r}_{κ} are also statistically independent as was shown in Eqs. (4-9)-(4-13). Therefore, an array output vector can be defined as

$$\underline{R} \triangleq [\underline{r}_1 \dots \underline{r}_{\kappa} \dots \underline{r}_m]^T , \quad (6-5)$$

and the conditional density of the observations given the phase vector is found from

$$f_{\underline{R}|\underline{a}}(\underline{R}|\underline{a}) = \prod_{k=1}^m f_{\underline{r}_k|\underline{a}}(\underline{r}_k|\underline{a}) , \quad (6-6)$$

where $f_{\underline{r}_k|\underline{a}}(\underline{r}_k|\underline{a})$ is given by Eq. (4-14). The likelihood function defined by the ratio

$$\Lambda \triangleq [\ln f_{\underline{R}|\underline{a}}(\underline{R}|\underline{a})] / [\ln f_{\underline{R}}(\underline{R})] \quad (6-7)$$

is therefore given by

$$\Lambda = \frac{2q^2k}{T} \sum_{k=1}^m \sum_{j=1}^k \left[\frac{r_j^{(k)}}{W_k} s_j^{(k)}(\underline{a}) - \frac{1}{2W_k} (s_j^{(k)}(\underline{a}))^2 \right] . \quad (6-8)$$

Equation (6-8) must be maximized by the proper choice of all the elements a_p in \underline{a} . Since the phases across the aperture are assumed jointly Gaussian and spatially correlated, they can be represented in a different coordinate system where the new elements a_i are independent Gaussian random variables, each with density

$$f_{a_i}(a_i) = [2\pi\sigma_{a_i}^2]^{1/2} \exp[-a_i^2/2\sigma_{a_i}^2] . \quad (6-9)$$

Beginning the estimator derivation with Eq. (6-9), the MAP estimate of a_i can be obtained by maximizing $\{\Lambda + \ln f_{a_i}(a_i)\}$ with respect to a_i . The result in vector form is

$$\frac{2q^2k}{T} \sum_{j=1}^k \frac{\partial s_j^T(\underline{a})}{\partial a_j} W^{-1} [\underline{r}_j - \underline{s}_j(\underline{a})] - \frac{a_i}{\sigma_{a_i}^2} = 0 , \quad (6-10)$$

where \underline{W} is a positive definite diagonal matrix of terms W_p . To convert Eq. (6-10) to the actual parameter system, a_p is expanded into a set of orthogonal unit vectors ϕ_i such that

$$\hat{a}_p \triangleq \lim_{N \rightarrow \infty} \sum_{j=1}^N a_j \phi_j^{(p)} \quad (6-11)$$

and

$$\hat{a} = \lim_{N \rightarrow \infty} \sum_{j=1}^N a_j \phi_j, \quad (6-12)$$

where a_i is obtained in a manner analogous to Eq. (3-14)

from

$$a_i = \sum_{p=1}^n a_p \phi_i^{(p)}. \quad (6-13)$$

In the same manner, it is also true that

$$\frac{\partial \underline{s}_j^T(\underline{a})}{\partial a_i} = \sum_{p=1}^n \frac{\partial \underline{s}_j(\underline{a})}{\partial a_p} \phi_i^{(p)}. \quad (6-14)$$

Equation (6-14) can be simplified by defining in vector notation

$$\sum_{j=1}^n \phi_i^{(p)} \frac{\partial \underline{s}_j(\underline{a})}{\partial a_p} = \phi_i^T \begin{bmatrix} \frac{\partial \underline{s}_j^{(1)}(\underline{a})}{\partial a_1} & \dots & \frac{\partial \underline{s}_j^{(m)}(\underline{a})}{\partial a_1} \\ \vdots & \ddots & \vdots \\ \frac{\partial \underline{s}_j^{(1)}(\underline{a})}{\partial a_n} & \dots & \frac{\partial \underline{s}_j^{(m)}(\underline{a})}{\partial a_n} \end{bmatrix}$$

$$\triangleq \phi_i^T \underline{D}_j(\underline{a}). \quad (6-15)$$

By using Eqs. (6-14) and (6-15), Eq. (6-10) becomes

$$a_i = \frac{2q^2 k}{T} \sigma_{a_i}^2 \sum_{j=1}^k \phi_{i-j}^T D_j(\underline{a}) \underline{W}^{-1} [\underline{r}_j - \underline{s}_j(\underline{a})] \quad (6-16)$$

By using Eq. (6-16) in Eq. (6-12), the joint estimate is

$$\hat{\underline{a}} = \frac{2q^2 k}{T} \left[\begin{array}{c} \text{l.i.m.} \\ N \rightarrow \infty \end{array} \sum_{i=1}^N \sigma_{a_i}^2 \phi_i \phi_i^T \right] \sum_{j=1}^k D_j(\underline{a}) \underline{W}^{-1} [\underline{r}_j - \underline{s}_j(\underline{a})] \quad (6-17)$$

The covariance matrix is given by (Ref 12:222)

$$\underline{k}_a = \begin{array}{c} \text{l.i.m.} \\ N \rightarrow \infty \end{array} \sum_{i=1}^N \sigma_{a_i}^2 \phi_i \phi_i^T \quad (6-18)$$

and is assumed to be known in the interval (t_1, t_1+T) . It is further defined by

$$\underline{k}_a \triangleq E[\underline{a} \underline{a}^T] = \begin{bmatrix} k_1 & \dots & k_{1n} \\ \vdots & \ddots & \vdots \\ k_{n1} & & k_n \end{bmatrix} \quad (6-19)$$

Therefore, the discrete joint MAP estimate of \underline{a} is given by

$$\hat{\underline{a}}(\underline{r}) = \frac{2q^2 k}{T} \underline{k}_a \sum_{j=1}^k D_j(\underline{a}) \underline{W}^{-1} [\underline{r}_j - \underline{s}_j(\underline{a})], \quad t_1 \leq t \leq t_1+T \quad (6-20)$$

Equation (6-20) can be converted into a continuous form by substituting for the definition of Eq. (3-14). By observing that, for a set $\underline{\zeta}(t)$ of complete orthonormal functions,

$$\lim_{k \rightarrow \infty} \sum_{j=1}^k \zeta_j(t) \zeta_j(u) = \delta(t-u) \quad (6-21)$$

then Eq. (6-20) becomes

$$\hat{\underline{a}} = 2k_a \int_0^T \underline{D}(t, \underline{a}) \underline{W}^{-1} [\underline{r}(t) - \underline{s}(t, \underline{a})] dt$$

for $0 \leq t \leq T$, (6-22)

where

$$\underline{D}(t, \underline{a}) \triangleq \begin{bmatrix} \frac{\partial s_1(t, \underline{a})}{\partial a_1} & \dots & \frac{\partial s_m(t, \underline{a})}{\partial a_1} \\ \vdots & \ddots & \vdots \\ \frac{\partial s_1(t, \underline{a})}{\partial a_n} & \dots & \frac{\partial s_m(t, \underline{a})}{\partial a_n} \end{bmatrix} \quad (6-23)$$

Equation (6-22) is the joint MAP estimate from a continuous measurement of a Gaussian random vector \underline{a} observed in Gaussian noise. This is the result that will be used in the forthcoming developments to process jointly the outputs of a shearing interferometer. Equation (6-22) can also be obtained in a manner analogous to the single detector by performing a correlation-summing operation as shown in Figure 20 (Ref 14:367,452,453).

Wavefront Estimation from the Shearing Interferometers

The output fields of the interferometers at the focal planes are received and processed by two separate detector arrays, one each for the X and Y sheared fields as depicted in Figure 2. Therefore, it will be convenient to keep

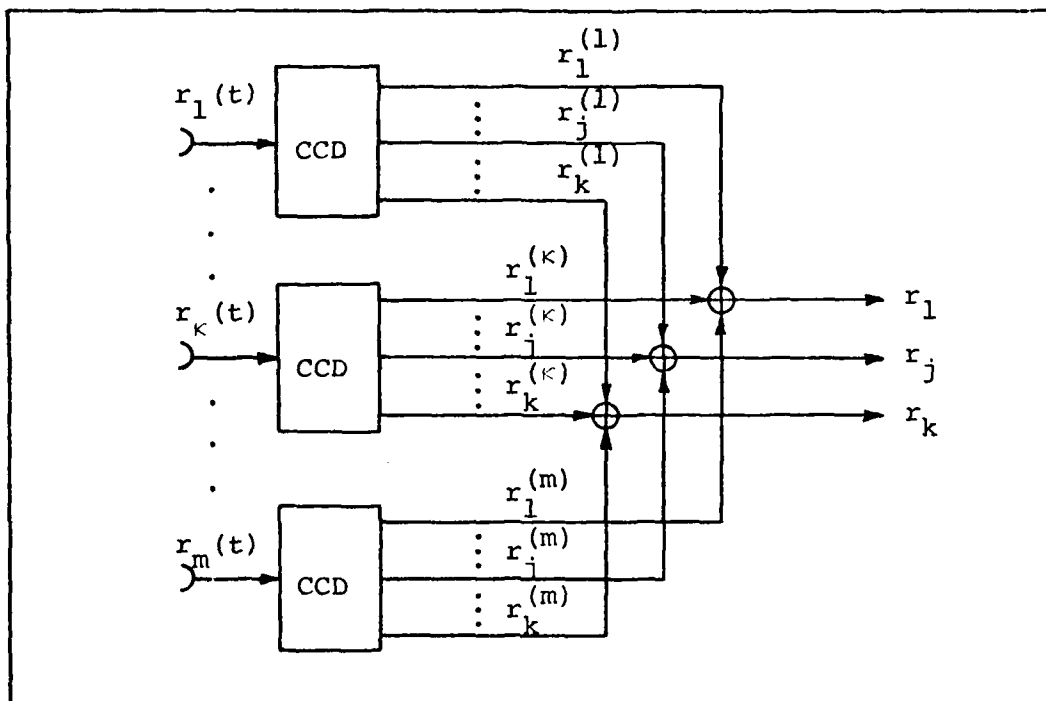


Fig 20. Correlator-Summer Model for Joint Processing

track of the observations by use of appropriate subscripted notation. Define

$$w_{\kappa\ell}(t) \triangleq x_{\kappa\ell}(t, \theta) + m_{\kappa\ell}(t) \quad (6-24)$$

$$z_{\kappa\ell}(t) \triangleq y_{\kappa\ell}(t, \theta) + n_{\kappa\ell}(t) \quad , \quad (6-25)$$

where $w_{\kappa\ell}(t)$ and $z_{\kappa\ell}(t)$ are the outputs of the $\kappa\ell^{(th)}$ detector in each of the x- and y-arrays. The subscripts κ and ℓ index the rows and columns respectively. For any one detector, the signals can be written as

$$y(t, \theta) = a + b \sin(\omega t + \theta(y_a))$$

for x_a fixed,

(6-26)

and

$$x(t, \theta) = d + c \sin(\omega t + \theta(x_a))$$

for y_a fixed,

(6-27)

where the difference functions are, from Eqs. (2-3) and (3-1)-(3-5), given by

$$\theta(x_a) = \frac{1}{2} \{ \phi(x_a - M_{s_d}, y_a) - \phi(x_a + M_{s_d}, y_a) \} \quad (6-28)$$

$$\theta(y_a) = \frac{1}{2} \{ \phi(x_a, y_a - M_{s_d}) - \phi(x_a, y_a + M_{s_d}) \} \quad (6-29)$$

Further notational simplification can be made by defining

$$\phi(x^-) \triangleq \phi(x_a - M_{s_d}, y_a) \quad (6-30)$$

$$\phi(x^+) \triangleq \phi(x_a + M_{s_d}, y_a) \quad (6-31)$$

$$\phi(y^-) \triangleq \phi(x_a, y_a - M_{s_d}) \quad (6-32)$$

$$\phi(y^+) \triangleq \phi(x_a, y_a + M_{s_d}) \quad (6-33)$$

so that Eqs. (6-26) and (6-27) can be written as

$$y(t, \theta) = a + b \sin(\omega t + \frac{\phi(y^-) - \phi(y^+)}{2})$$

for x_a fixed,

(6-34)

$$\text{and } x(t, \theta) = d + c \sin(\omega t + \frac{\phi(x^-) - \phi(x^+)}{2})$$

for y_a fixed.

(6-35)

Equation (6-22) can now be applied using Eqs. (6-24) through (6-35) to perform the joint estimate of the wavefront phases

using two plane detector arrays properly interfaced to couple the x- and y-measurements with the same wavefront points. But the two-array configuration must be set up before proceeding to perform the joint phase estimation.

Configuration of the Detector Arrays. The need for the use of two detector plane arrays for actual phase estimation is a consequence of the structure of the difference functions in Eqs. (6-30) through (6-35), obtained from the use of lateral shearing instead of radial shearing interferometry. As is the case in the approach of data mappings, processing of the observations $r(t)$ requires a specific detector arrangement. In order to make full utilization of the information collected, the detectors (and the arrays) must be arranged so that each wavefront point be measured by as many detectors as possible in order to provide a strong deterministic relationship between the measurements over the aperture. All other coupling is provided statistically by the covariance matrix of the phases.

In order to provide redundancy of measurements, the best possible detector arrangement is as shown in Figure 21. This arrangement allows each phase point to be measured by four detectors, two from each one of the arrays, and has the advantage that only one reference phase is required to determine the entire phase distribution. It is assumed that such phase point is measured by another means or is set arbitrarily equal to zero. The X's and Y's in Figure 21 denote the detector locations and the ϕ 's denote the phase

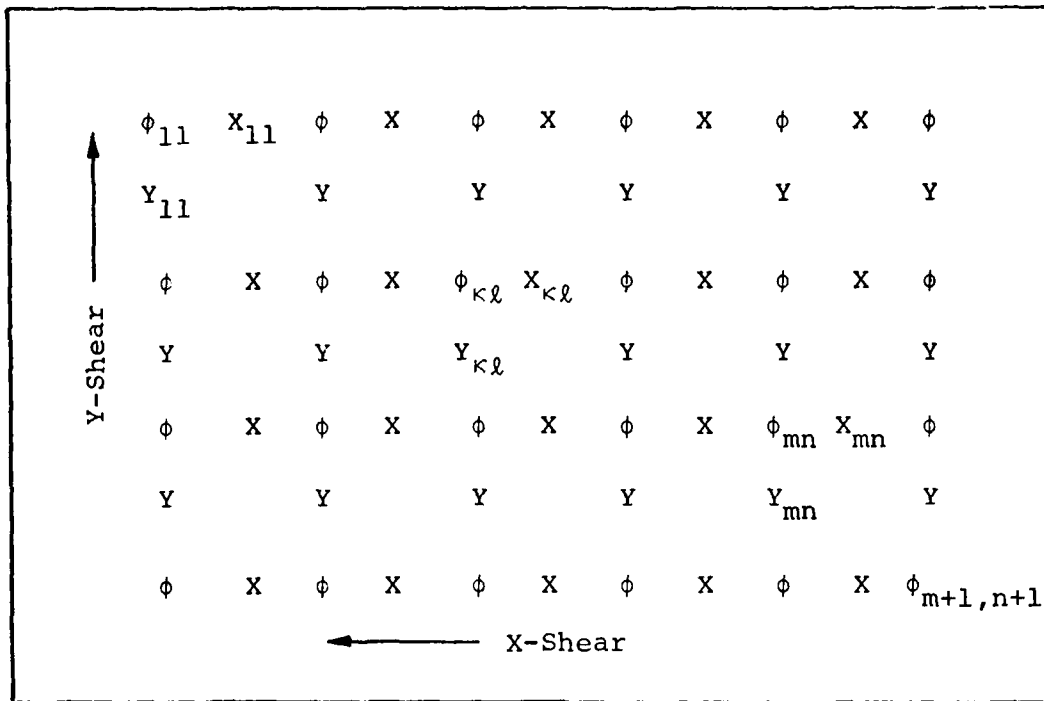


Fig 21. Arrangement of Two Detector Arrays to Measure $(m+1) \times (n+1)$ Phase Points with $(m+1) \times n$ X- and $m \times (n+1)$ Y-Detectors

points being measured. Except for the edge phase points, each phase ϕ_{kl} is measured by detectors x_{kl} , $x_{k-1,l}$, y_{kl} , and $y_{k,l-1}$, ϕ_{kl} being a common phase point of the four difference functions $\theta_{kl}(x_a)$, $\theta_{k-1,l}(x_a)$, $\theta_{kl}(y_a)$, and $\theta_{k,l-1}(y_a)$. The grid shown in Figure 21 is formed by overlapping the two arrays to indicate the relative positions of the X- and Y-shear detector. The corresponding detectors x_{kl} and y_{kl} are not located at the same point on the field. They are displaced 45° instead so that both can measure the same phase ϕ_{kl} . The direction of the shear has been chosen from right to left and bottom up to correspond to the notation adopted in Eqs. (6-34) through (6-37). In this arrangement the

detector spacing has been chosen so that

$$\phi_{\kappa\ell}(y^-) = \phi_{\kappa+1,\ell}(y^+) \quad (6-36)$$

and
$$\phi_{\kappa\ell}(x^-) = \phi_{\kappa,\ell+1}(x^+) \quad (6-37)$$

in Eqs. (6-30) through (6-35). The detectors must then be spaced $2M$ shear distances s_d apart (s_{dx} and s_{dy} may not necessarily be equal). This is depicted in Figure 22 for a column array.

In general, for a non-square array of phase points, the number of detectors is different in each array. Thus, referring to Figure 21, there are $[m+1] \times n$ X-detectors and $m \times [n+1]$ Y-detectors, and $[m+1][n+1]$ measured phases. The ratio of detector to phase points is

$$\frac{[m+1] \times n + m \times [n+1]}{[m+1] \times [n+1]}$$

and ranges from unity, when a minimum of four phases are measured with two each X- and Y-detectors, up to the value of two, in the limit when a very large number of phase points are being measured. Thus, in the best possible arrangement of Figure 21, the number of detectors required tends to double as more wavefront points are measured simultaneously. With these preliminaries completed, derivation of the algorithm for wavefront estimation by jointly processing the two detector array outputs can be initiated.

Joint Wavefront Estimation with Two Detector Arrays.

The observations $\underline{r}(t)$ can be arranged in a column vector of

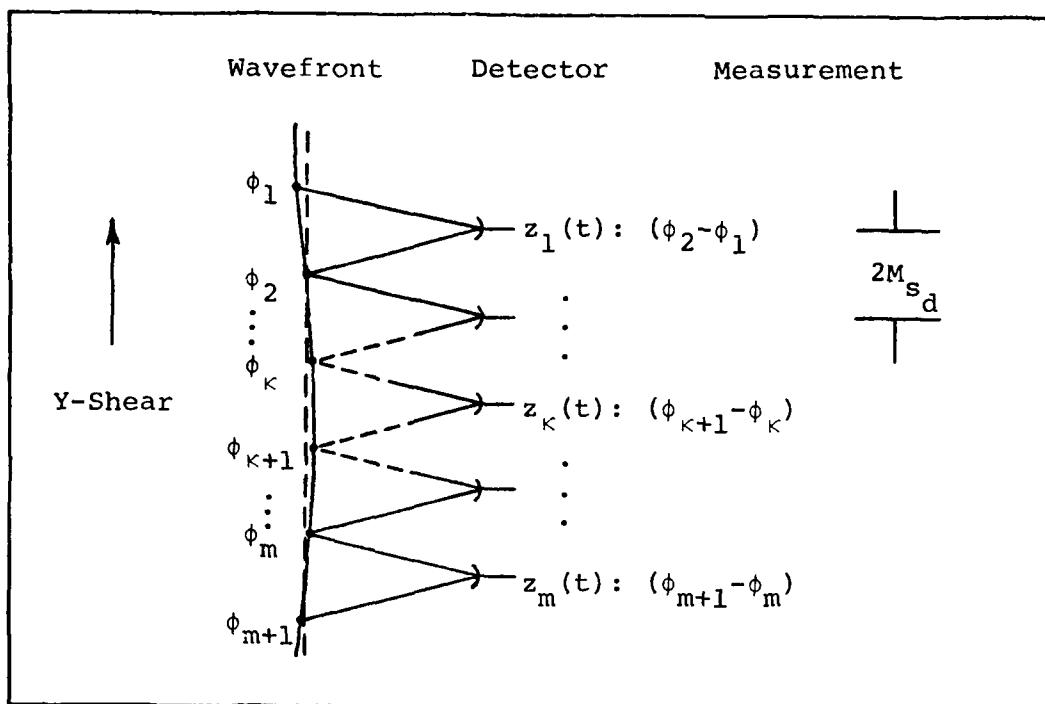


Fig 22. Arrangement of Detector Column Array for Joint Processing

dimension $(m[2n+1]+n)$, using the notation of Eqs. (6-24) and (6-25). Thus,

$$\begin{aligned} \underline{r}(t) = & [z_{11}(t), w_{11}(t) \dots z_{mn}(t), w_{mn}(t) \\ & \dots w_{m+1,n}(t)]^T, \end{aligned} \quad (6-38)$$

where $z_{kl}(t)$ and $w_{kl}(t)$ are the observations with signal components given, after Eqs. (6-34) through (6-37), by

$$y_{kl}(t, \phi) = a_{kl} + b_{kl} \sin(\omega t + \frac{\phi_{k+1,l} - \phi_{k,l}}{2})$$

for $0 \leq t \leq T$,

$1 \leq k \leq m$,

$1 \leq l \leq n+1$,

(6-39)

$$\begin{aligned}
\text{and } x_{\kappa\ell}(t, \underline{\phi}) &= d_{\kappa\ell} + c_{\kappa\ell} \sin(\omega t + \frac{\phi_{\kappa, \ell+1} - \phi_{\kappa\ell}}{2}) \\
\text{for } 0 \leq t \leq T, \\
1 \leq \kappa \leq m+1, \\
1 \leq \ell \leq n.
\end{aligned} \tag{6-40}$$

The arguments (x^+) and (y^+) used in Eqs. (6-34) and (6-35) are dropped from Eqs. (6-39) and (6-40) since the ambiguity is taken care of by the subscripts $\kappa+1, \ell$ and $\kappa, \ell+1$, and because $\phi_{\kappa\ell}(x^+) = \phi_{\kappa\ell}(y^+)$.

The phase vector is also a $([m+1][n+1])$ column matrix

$$\underline{\phi} = [\phi_{11} \dots \phi_{pq} \dots \phi_{m+1, n+1}]^T, \tag{6-41}$$

and has a $([m+1][n+1])$ symmetrical covariance matrix with terms from $k_{11,11}$ to $k_{m+1, n+1; m+1, n+1}$. The noise covariance matrix, on the other hand, is $(m[2n+1]+n)$ diagonal (noises were assumed spatially uncorrelated) given by

$$\underline{W} = \begin{bmatrix} N_{11} & & & & \\ & M_{11} & & & \underline{0} \\ & & \ddots & & \\ & \underline{0} & & N_{n, n+1} & \\ & & & \ddots & \\ & & & & M_{m+1, n} \end{bmatrix}, \tag{6-42}$$

where the N's and M's make reference to X- and Y-detector noises respectively. With the observation and covariance matrices defined in Eqs. (6-38) through (6-42), Eqs. (6-22) and (6-23) can be applied directly to perform the joint estimation of the vector $\underline{\phi}$.

Thus, the product $\underline{W}^{-1}[\underline{r}(t) - \underline{s}(t, \underline{\phi})]$ in Eq. (6-22) is a $(n[2n+1]+n)$ column matrix with general terms

$$\frac{1}{N_{k\ell}} [z_{k\ell}(t) - y_{k\ell}(t, \underline{\phi})]$$

for $1 \leq k \leq m$,

$$1 \leq \ell \leq n+1, \quad (6-43)$$

and

$$\frac{1}{M_{k\ell}} [w_{k\ell}(t) - x_{k\ell}(t, \underline{\phi})]$$

for $1 \leq k \leq m+1$,

$$1 \leq \ell \leq n. \quad (6-44)$$

The signal derivative matrix is $([m+1][n+1]) \times (m[2n+1]+n)$ dimensional given by

$$\underline{D}(t, \underline{\phi}) = \begin{bmatrix} \frac{\partial y_{11}(t, \underline{\phi})}{\partial \phi_{11}} & \frac{\partial x_{11}(t, \underline{\phi})}{\partial \phi_{11}} & \dots & \frac{\partial x_{m+1,n}(t, \underline{\phi})}{\partial \phi_{11}} \\ \vdots & \vdots & \ddots & \vdots \\ \frac{\partial y_{11}(t, \underline{\phi})}{\partial \phi_{m+1,n+1}} & \frac{\partial x_{11}(t, \underline{\phi})}{\partial \phi_{m+1,n+1}} & \dots & \frac{\partial x_{m+1,n}(t, \underline{\phi})}{\partial \phi_{m+1,n+1}} \end{bmatrix} \cdot \quad (6-45)$$

By carrying out the matrix multiplications of Eq. (6-22), the MAP estimate of the $pq^{(th)}$ phase is found in general terms to be given by

$$\hat{\phi}_{pq} = \sum_{i=1}^{m+1} \sum_{j=1}^{n+1} \left\{ \sum_{\kappa=1}^m \sum_{\ell=1}^{n+1} \frac{2k_{pq,ij}}{N_{\kappa\ell}} \int_0^T \frac{\partial y_{\kappa\ell}(t, \underline{\phi})}{\partial \phi_{ij}} [z_{\kappa\ell}(t) - y_{\kappa\ell}(t, \underline{\phi})] dt \right. \\ \left. + \sum_{\kappa=1}^{m+1} \sum_{\ell=1}^n \int_0^T \frac{\partial x_{\kappa\ell}(t, \underline{\phi})}{\partial \phi_{ij}} [w_{\kappa\ell}(t) - x_{\kappa\ell}(t, \underline{\phi})] dt \right\} \quad (6-46)$$

Finally, when Eqs. (6-39) and (6-40) are used in Eq. (6-46), the general $pq^{(th)}$ member of the $\underline{\phi}$ vector of Eq. (6-41) is obtained. The result is given by

$$\hat{\phi}_{pq} = \sum_{\kappa=1}^m \sum_{\ell=1}^{n+1} \frac{b_{\kappa\ell}}{N_{\kappa\ell}} [k_{pq;\kappa+1,\ell} - k_{pq,\kappa\ell}] \\ \int_0^T z_{\kappa\ell}(t) \cos(\omega t + \frac{\hat{\phi}_{\kappa+1,\ell} - \hat{\phi}_{\kappa\ell}}{2}) dt \\ + \sum_{\kappa=1}^{m+1} \sum_{\ell=1}^n \frac{c_{\kappa\ell}}{M_{\kappa\ell}} [k_{pq;\kappa,\ell+1} - k_{pq,\kappa\ell}] \\ \int_0^T w_{\kappa}(t) \cos(\omega t + \frac{\hat{\phi}_{\kappa,\ell+1} - \hat{\phi}_{\kappa\ell}}{2}) dt$$

for $0 \leq t \leq T$,

$$1 \leq p \leq m+1,$$

$$1 \leq q \leq n+1,$$

(6-47)

Equation (6-47) is the joint Maximum A Posteriori phase estimator using measurements of two orthogonal, lateral shearing interferometers and their detector arrays. The phase estimate distribution over the aperture is shown in Figure 23.

$\hat{\phi}_{11}$...	$\hat{\phi}_{1q}$...	$\hat{\phi}_{1n}$	$\hat{\phi}_{1,n+1}$
\vdots		\vdots		\vdots	\vdots
$\hat{\phi}_{p1}$...	$\hat{\phi}_{pq}$...	$\hat{\phi}_{pn}$	$\hat{\phi}_{p,n+1}$
\vdots		\vdots		\vdots	\vdots
$\hat{\phi}_{m1}$...	$\hat{\phi}_{mq}$...	$\hat{\phi}_{mn}$	$\hat{\phi}_{m,n+1}$
$\hat{\phi}_{m+1,1}$...	$\hat{\phi}_{m+1,q}$...	$\hat{\phi}_{m+1,n}$	$\hat{\phi}_{m+1,n+1}$

Fig 23. Phase Estimate Distribution Over the Aperture

The algorithm given by Eq. (6-47) is applicable only when the phases ϕ being measured are jointly Gaussian random variables and the a priori information represented by \underline{k}_a is available. The distinction between $\hat{\phi}_{pq}$ and $\hat{\phi}_{rs}$ in Eq. (6-47) is made, observing the structural form of Eq. (6-46), by the covariance terms $k_{pq,ij}$ and $k_{rs,ij}$ only, where i and j take on all values from 1 to $m+1$, and 1 to $n+1$ respectively. Therefore, the joint phase estimates are weighted accordingly by the a priori information. This will be further explained in a forthcoming example.

Solution of Eq. (6-47) is to be obtained recursively with numerical methods on a digital computer. However, to

illustrate the estimator, Eq. (6-47) can be implemented with a heuristic correlator-summer of considerable complexity as will be seen in the following example.

Illustrative Example. The simplest example to illustrate a hardware implementation of Eq. (6-47) is given by the joint estimate of a wavefront at four locations using two (2x2) detector arrays. The arrangement is shown in Figure 24. The notation is so chosen for simplicity. Detector Y_2 corresponds to Y_{12} and phase ϕ_4 corresponds to ϕ_{22} in the notation of Eq. (6-47). It will also be assumed that the noises are of equal strength N_0 and the signals have equal amplitude $\sqrt{2E_a/T}$. With the problem so defined, the $p^{(th)}$ phase estimate is given, from Eq. (6-47), by

$$\begin{aligned} \hat{\phi}_p = \frac{1}{N_0} \sqrt{\frac{2E_a}{T}} \left\{ (k_{p3} - k_{p1}) \int_0^T z_1(t) \cos\left(\omega t + \frac{\hat{\phi}_3 - \hat{\phi}_1}{2}\right) dt \right. \\ + (k_{p4} - k_{p2}) \int_0^T z_2(t) \cos\left(\omega t + \frac{\hat{\phi}_4 - \hat{\phi}_2}{2}\right) dt \\ + (k_{p2} - k_{p1}) \int_0^T w_1(t) \cos\left(\omega t + \frac{\hat{\phi}_2 - \hat{\phi}_1}{2}\right) dt \\ \left. + (k_{p4} - k_{p3}) \int_0^T w_2(t) \cos\left(\omega t + \frac{\hat{\phi}_4 - \hat{\phi}_3}{2}\right) dt \right\}, \quad (6-48) \end{aligned}$$

where any $\hat{\phi}_r$ is set as the zero reference. Equation (6-48) can be implemented with a correlator-summer as shown in Figure 25, where $\cos(\omega t + \frac{\hat{\phi}_i - \hat{\phi}_j}{2})$ is denoted by $\sim \hat{\phi}_i - \hat{\phi}_j$. The structure of Figure 25 is a feedback system in which the

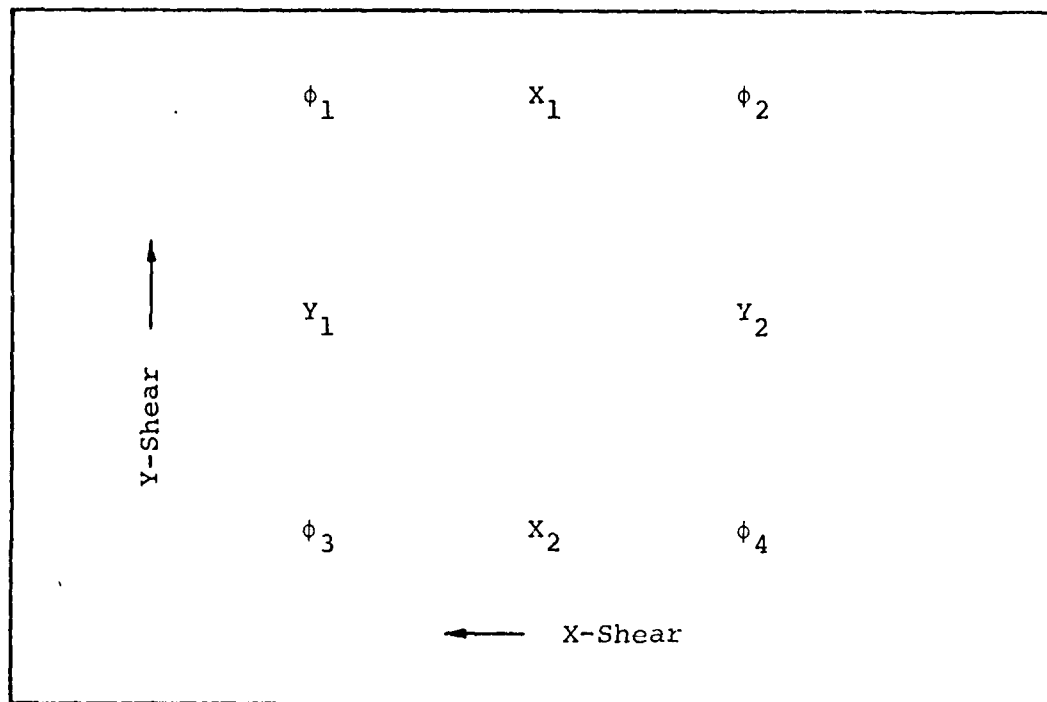


Fig 24. Phase-Detector Grid for Joint Processing of Four Detectors to Estimate Four Wavefront Phases

detector outputs are weighted by the covariance terms so that each phase estimate has a contribution from each measurement. Three feedback loops from the estimate outputs $\hat{\phi}_2$, $\hat{\phi}_3$ and $\hat{\phi}_4$ are returned to the detector inputs. The estimate $\hat{\phi}_1$ does not provide any feedback for being the starting point of the spatially recursive estimation. The phase output $\hat{\phi}_3$ has been arbitrarily set as the zero reference.

To better understand how this formidable structure weighs the measurements, or better yet, what Eq. (6-48) really does, the underlying mechanism is shown in Figure 26. Here, the phase points have been replaced by the covariance

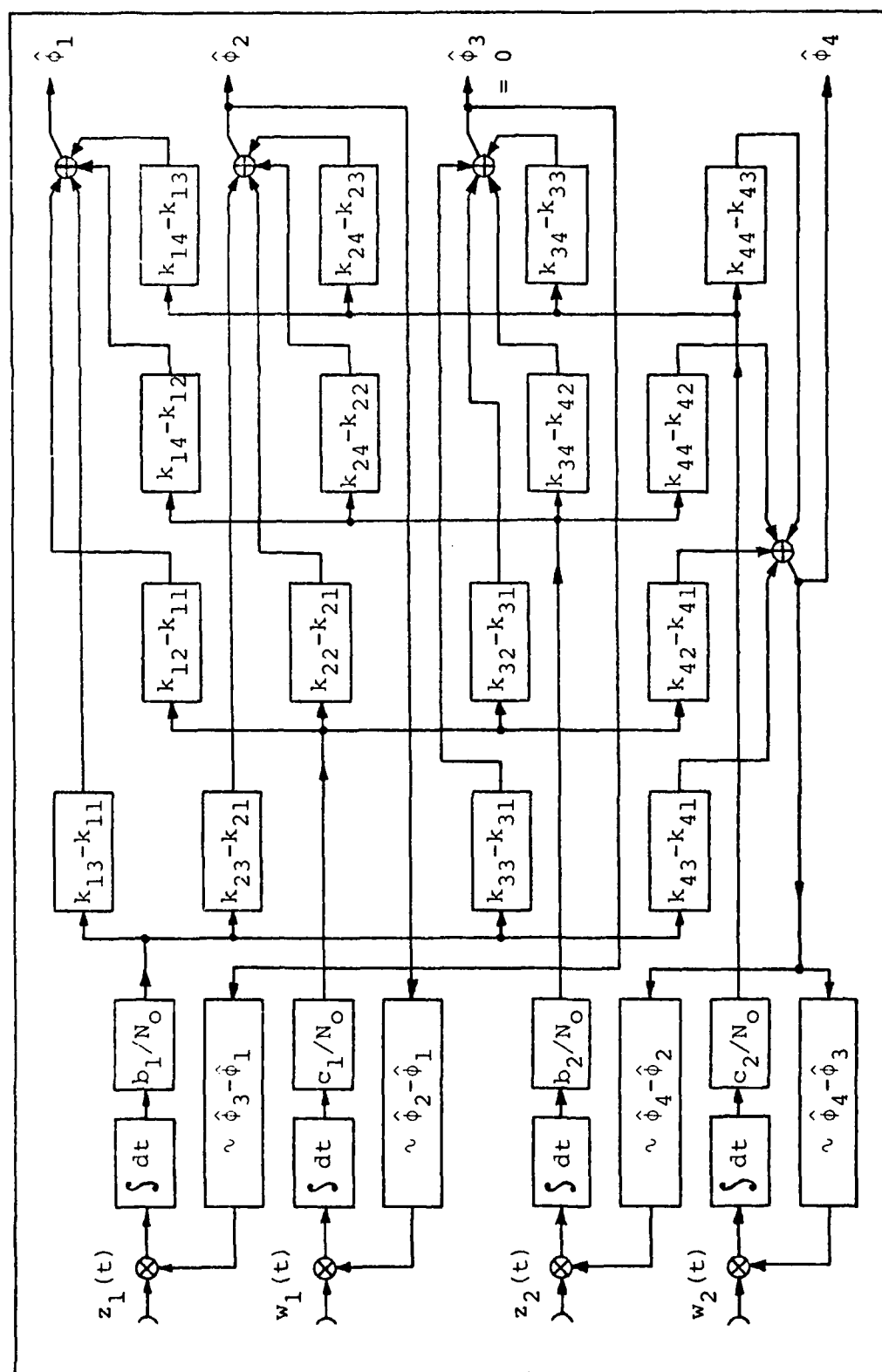


Fig 25. Correlator-Summer to Estimate Four Phases

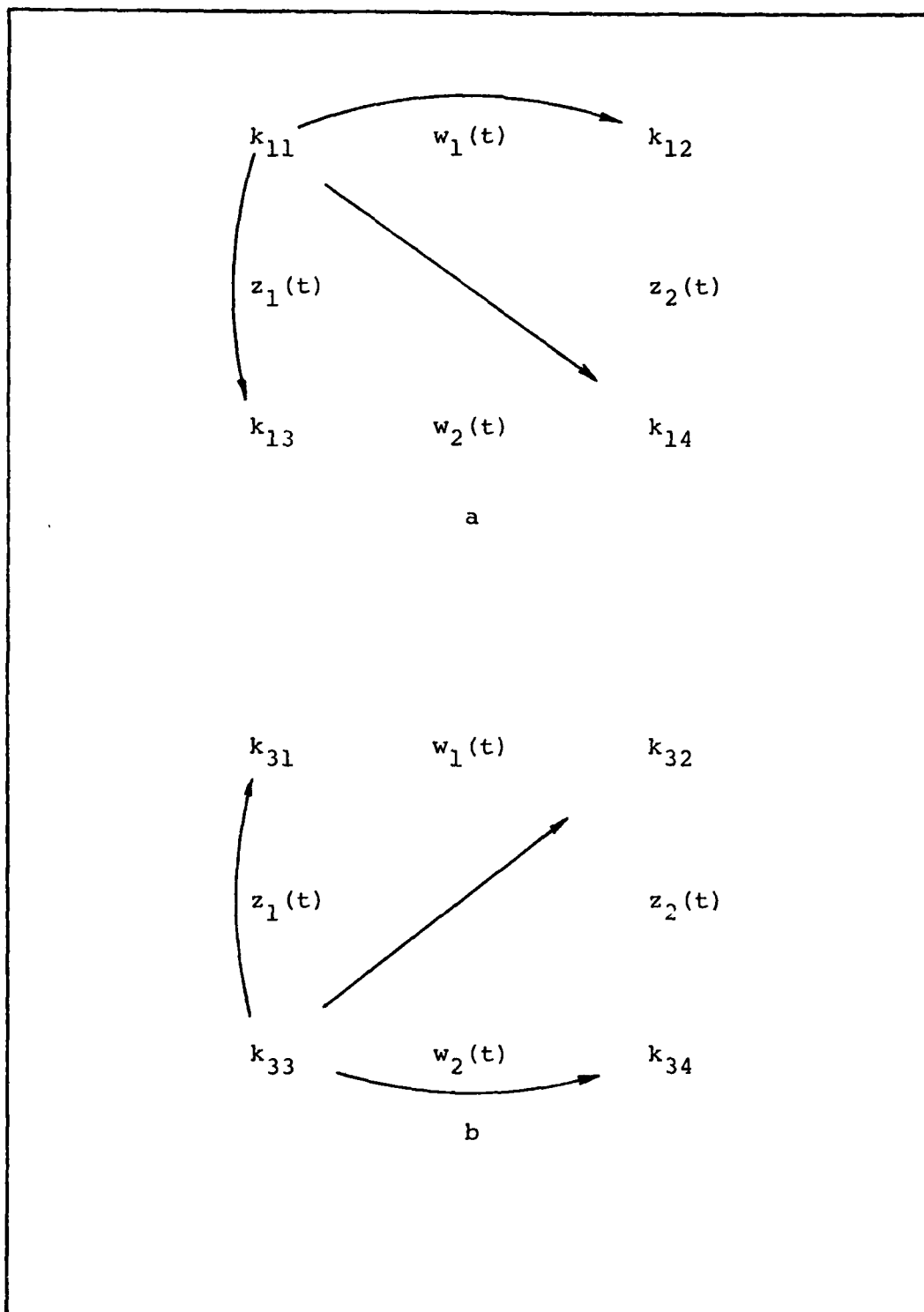


Fig 26. Underlying Mechanism to Estimate ϕ_1 and ϕ_3

terms of ϕ_p with respect to the other phases. The detector locations have been denoted by their measurements $z(t)$ and $w(t)$. Figure 26-a shows the mechanism involved in estimating ϕ_1 . Each phase location has the covariance term involving ϕ_1 and the phase at each point; this is the meaning of the arrows. The operation involves taking pairwise the difference between the covariance terms at all points and multiplying by the measurement made between each two points (this means the output of the integrator). Thus, the difference between k_{11} and k_{14} is multiplied by zero because there is no detector in between. In the same manner, Figure 26-b shows the same mechanism used to evaluate ϕ_3 . Here, the covariance terms are k_{33} , k_{31} , k_{32} and k_{34} . This can be generalized for any number of array elements.

From this example, it is evident that the algorithm indeed provides a means for jointly processing spatially correlated phase measurements. It also implies a simultaneous evaluation of all phase points and a recursive substitution. The difficulty involved in solving Eq. (6-47) numerically is also evident due to the redundancy provided by the feedback loops. Therefore, such a solution goes beyond the scope of this paper.

Estimator Performance

The performance of the estimator of Eq. (6-22) is more easily described in terms of the Cramer-Rao bounds, provided that the signal-to-noise ratio is large and biases are

negligible. Then, the lower bounds on the error matrix are the diagonal terms of the matrix

$$\underline{R}_B = \underline{k}_a [\underline{I} + \underline{D}_a \underline{k}_a]^{-1} \quad (6-49)$$

adapted from a more general case given by Van Trees (Ref 13: 454). Simplification to the point of Eq. (6-49) is possible because the matrix

$$\begin{aligned} \underline{D}_a(u, \phi) &\triangleq \int_0^T E[\underline{D}(t, \phi) \underline{W}^{-1} \underline{D}^T(t, \phi)] dt \\ &\triangleq \underline{D}_a \end{aligned} \quad (6-50)$$

is constant over $(0, T)$ for $s(t, \phi)$ defined as $[a + b \sin(\omega t + \phi)]$.

To find the MS error bounds, the matrix operations of Eqs. (6-50) and (6-49) must be performed. Carrying out these matrix multiplications is a rather cumbersome task. After some work, the matrix $\underline{D}_a(u, \phi)$ is found to have a diagonal band form with dimensions $(m[2n+1] + n) \times ([m+1][n+1])$ as illustrated in Figure 27. The five X's in each column are given by

$$\frac{2}{N_{p-1,q}} \left(\frac{\partial y_{p-1,q}}{\partial \phi_{p-1,q}} \frac{\partial y_{p-1,q}}{\partial \phi_{pq}} \right) \quad (6-51)$$

$$\frac{2}{M_{p,q-1}} \left(\frac{\partial x_{p,q-1}}{\partial \phi_{p,q-1}} \frac{\partial x_{p,q-1}}{\partial \phi_{pq}} \right) \quad (6-52)$$

$$\begin{bmatrix}
 X & X & & & X & & & & & & \\
 X & X & X & & & & X & & & & \\
 & X & X & X & & & X & & & & \\
 & & X & X & X & & & & X & & \\
 & & & X & X & & & & & X & \\
 X & & & & & X & X & & & X & \\
 & X & & & & X & X & X & & & X \\
 & & X & & & & X & X & X & & X \\
 & & & X & & & X & X & X & & X \\
 & & & & X & & & X & X & & X \\
 & & & & & X & & & X & X & X \\
 & & & & & & X & & & X & X \\
 & & & & & & & X & & X & X \\
 & & & & & & & & X & X & X \\
 & & & & & & & & & X & X
 \end{bmatrix}$$

Fig 27. The Form of the Matrix $\underline{D}_a(u, \phi)$

$$\frac{2}{N_{pq}} \left(\frac{\partial y_{pq}}{\partial \phi_{pq}} \right)^2 + \frac{2}{N_{p-1,q}} \left(\frac{\partial y_{p-1,q}}{\partial \phi_{pq}} \right)^2 + \frac{2}{M_{pq}} \left(\frac{\partial x_{pq}}{\partial \phi_{pq}} \right)^2 + \frac{2}{M_{p,q-1}} \left(\frac{\partial x_{p,q-1}}{\partial \phi_{pq}} \right)^2 \quad (6-53)$$

$$\frac{2}{M_{pq}} \left(\frac{\partial x_{pq}}{\partial \phi_{p,q+1}} \frac{\partial x_{pq}}{\partial \phi_{pq}} \right) \quad (6-54)$$

$$\frac{2}{N_{pq}} \left(\frac{\partial y_{pq}}{\partial \phi_{p+1,q}} \frac{\partial y_{pq}}{\partial \phi_{pq}} \right) \quad (6-55)$$

The product $\underline{D}_a(u, \phi) \underline{k}_a$ is a $([m+1][n+1])$ square matrix. The general term at location pq, ij is given by

$$\begin{aligned}
& \frac{2}{N_{p-1,q}} \left(\frac{\partial y_{p-1,q}}{\partial \phi_{pq}} \frac{\partial y_{p-1,q}}{\partial \phi_{p-1,q}} \right) k_{p-1,q;ij} \\
& + \frac{2}{M_{p,q-1}} \left(\frac{\partial x_{p,q-1}}{\partial \phi_{pq}} \frac{\partial x_{p,q-1}}{\partial \phi_{p,q-1}} \right) k_{p,q-1;ij} \\
& + \left\{ \frac{2}{N_{pq}} \left(\frac{\partial y_{pq}}{\partial \phi_{pq}} \right)^2 + \frac{2}{N_{p-1,q}} \left(\frac{\partial y_{p-1,q}}{\partial \phi_{pq}} \right)^2 + \frac{2}{M_{pq}} \left(\frac{\partial x_{pq}}{\partial \phi_{pq}} \right)^2 + \frac{2}{M_{p,q-1}} \left(\frac{\partial x_{p,q-1}}{\partial \phi_{pq}} \right)^2 \right\} k_{pq;ij} \\
& + \frac{2}{M_{pq}} \left(\frac{\partial x_{pq}}{\partial \phi_{pq}} \frac{\partial x_{pq}}{\partial \phi_{p,q+1}} \right) k_{p,q+1;ij} \\
& + \frac{2}{N_{pq}} \left(\frac{\partial y_{pq}}{\partial \phi_{pq}} \frac{\partial y_{pq}}{\partial \phi_{p+1,q}} \right) k_{p+1,q;ij}
\end{aligned}$$

for

$$N, y: \quad 1 \leq p \leq m, \quad 1 \leq q \leq n+1$$

$$M, x: \quad 1 \leq p \leq m+1, \quad 1 \leq q \leq n$$

$$1 \leq i \leq m+1, \quad 1 \leq j \leq n+1. \quad (6-56)$$

Integration of the matrix with general term given by Eq.

(6-56) gives a constant matrix $\underline{D}_a k_a$ whose general term at location pq, ij is given by

$$\begin{aligned}
& - \frac{b_{p-1,q}^2}{4N_{p-1,q}} k_{p-1,q;ij} - \frac{c_{p,q-1}^2}{4M_{p,q-1}} \\
& + \frac{1}{4} \left\{ \frac{b_{pq}^2}{N_{pq}} + \frac{b_{p-1,q}^2}{N_{p-1,q}} + \frac{c_{pq}^2}{M_{pq}} + \frac{c_{p,q-1}^2}{M_{p,q-1}} \right\} k_{pq,ij} \\
& - \frac{c_{pq}^2}{M_{pq}} k_{p,q+1;ij} - \frac{b_{pq}^2}{4N_{pq}} k_{p+1,q;ij}
\end{aligned} \quad (6-57)$$

The matrix \underline{D}_a is $([m+1][n+1])$ square and $p, q, i,$ and j are bounded as in Eq. (6-56). Further evaluation of the error matrix is to be done numerically to yield the diagonal values of \underline{R}_B defined by Eq. (6-49). This evaluation as well as a numerical solution of Eq. (6-47) are not included in this paper due to the difficulties encountered in undertaking that task. This, however, does not discourage further study since Eqs. (6-47) and (6-57) are believed to be correct.

VII Conclusions and Recommendations

Conclusions

The purpose of this work was twofold: (1) perform a discrete phase estimation analysis for a single detector measurement, and (2) perform a joint phase estimation analysis for multiple detector measurements. This work was prompted by the need for improved processing techniques directly applicable to shearing interferometry and wave-front correction systems.

The first workfront motivation was to determine in a stochastic sense if phase estimation algorithms with the simplicity of the form of

$$\phi = \tan^{-1} \left[\frac{A-D}{B-C} \right] , \quad (7-1)$$

from Reference 16, intended for use with low level signals, could be obtained using Maximum A Posteriori and Maximum Likelihood estimation theories, and the conditions for which they would give good phase estimates. A family of such algorithms was found and is given by the ML estimator Eq. (4-48), which is a specialized result of the MAP Eq. (4-36), derived under the white Gaussian noise assumption. A similar result is also given by Eq. (5-8), derived under the Poisson shot noise assumption, for the case of low fringe visibility. It is shown, however, without empirical verification (computer simulation), that this algorithm form will result in poor estimates under those modeling conditions.

The performance analyses carried out in Chapters IV and V (both theory and simulation) show that the only factor affecting phase estimation performance is the SNR regardless of the noise process involved and the technique used. In fact, the performance of both MAP and ML estimators is asymptotically given by the reciprocal SNR with an appropriate scaling factor for the particular algorithm form used (given k). Emphasis is made on this point to clear up Wyant's implication that Eq. (7-1) might be free from the SNR restrictions.

The estimators of Eqs. (4-39) and (4-48) were verified with a simple computer simulation with results presented in Figures 10-19. The similarity of performance between the MAP and ML estimators particularly for $\text{SNR} > 10$ dB follows directly from the implications of Eqs. (4-91) and (4-95), which predict the same asymptotic performance of the MAP and ML phase estimators for large SNR, and the implication of Eq. (4-90), which tends to ignore a priori information as the noise in the measurement decreases.

For a given SNR, there exists a tradeoff between algorithm simplicity and algorithm performance of the discrete estimators. The increased structural complexity as k increases from $k = 3$ to infinity is illustrated with a few examples in Tables I, II, IV and V. This complexity is particularly noticeable in the Poisson analysis equations. The return of using the more complex forms is an improved performance as shown in Table III and plotted on a relative

basis in Figure 9. The difference in theoretical performance between the worst ($k = 3$) and the best ($k = \infty$) possible estimator forms is 1.65 dB according to the definition of Eq. (4-76), and decreases quite rapidly as the number of counts (k) increases. On the basis of this performance-complexity tradeoff, the photon counting technique ($k < \infty$) is suboptimal (but acceptable) with respect to current-measurement ($k = \infty$) based phase estimation.

The second motivation of this work was the analysis of a time-space problem intended to provide a joint estimate of the phases across the aperture of the interferometer. Such joint processing had not been addressed in the light of MAP theory, where the fact that the phases were spatially correlated could be used to improve performance. The algorithm derived is given by Eq. (6-47) and is restricted to the assumption of a Gaussian phase distribution. The weighting between measurements is explicitly shown by the covariance terms in Eq. (6-47). The difficulty with this algorithm is the mathematical form of simultaneous nonlinear integral equations for which a solution is not readily available. The performance equations were carried out up to the point of numerical evaluation, which is not included due to time constraints imposed by the difficulties encountered in deriving the algorithms. Thus, a direct comparison to other estimators such as the one derived by Hudgin (Ref 5) is not possible given the form of Eqs. (6-47) and (6-57).

Recommendations

The study contained in Chapters IV through VI was performed for the extreme cases of detector limited and signal limited noise statistics. It is not unreasonable to think that the intermediate cases are also encountered in the reception of optical fields, where both thermal and shot noise occur together. These noise processes are independent of each other, and the density of the observables is then a convolution of Gaussian and Poisson functions. Estimation under these conditions should be tried.

The random phase in the argument of the sine function represented both target and turbulence. Going beyond the application of wavefront correction systems, it may be desirable to distinguish target and noise induced phases. This is estimation in the presence of unwanted parameters and should also be considered.

The basic assumption of the analyses presented in this paper was the time invariance of the phase in the measurement interval. Although the staircase approximation to the phase process may be suitable for slowly varying fields, it requires an update of the covariance matrix in each interval. A procedure should be tried for which $\theta(t)$ is time-dependent throughout the measurement, thus freeing the estimation problem from the requirement of short observation intervals. This could be done by homodyning the detector signal and filtering the frequency domain components with a low pass filter. The output signal would then have the form

$$r(t) = B \frac{b}{2} \sin \theta(t) + \frac{B}{\sqrt{2}} n_c(t) \quad (7-2)$$

where B is a gain factor given by the amplitude of the mixing signal, and $n_c(t)$ is filtered white Gaussian noise.

This waveform can now be used in Eq. (3-15) to obtain

$$r_j = \frac{Ab}{2} \sin \theta_j + \frac{A}{\sqrt{2}} n_j \quad (7-3)$$

The signal has now been quantized and is in a suitable form for recursive parameter estimation (Ref 2:319).

The joint processing algorithms of Eqs. (6-23) and (6-47) were derived using the assumption of independent detector noise processes. Development of an algorithm to include the case of spatially correlated noise should also be considered. Finally, the algorithm of Eq. (6-47) needs to be worked out to an implementable form, and tested through a performance evaluation by means of Monte Carlo simulation.

Bibliography

1. Fried, D. L. "Least Square Fitting a Wavefront Distortion Estimate to an Array of Phase Difference Measurements," Journal of the Optical Society of America, 67(3): 370-382 (March 1977).
2. Gagliardy, R. M. and S. Karp Optical Communications, New York: John Wiley and Sons, 1976.
3. Hardy, J. W. "Active Optics: A New Technology for the Control of Light," Proceedings of the IEEE, 66(6): 651-696 (June 1978).
4. Hardy, J. W., et al "Real-Time Atmospheric Compensation," Journal of the Optical Society of America, 67(3): 360-369 (March 1977).
5. Hudgin, R. H. "Wavefront Reconstruction for Compensated Imaging," Journal of the Optical Society of America, 67(3): 375-378 (March 1977).
6. Idell, P. S. Coherence Properties of Broadband Optical Fields with Applications to White-Light Shearing Interferometry, MS thesis, Wright-Patterson AFB, Ohio: School of Engineering, Air Force Institute of Technology, December 1978. (AD A064404)
7. Martoni, P. J. Signal Processing for Shearing Interferometer Measurements, MS thesis, Wright-Patterson AFB, Ohio: School of Engineering, Air Force Institute of Technology, December 1978. (AD A064043)
8. Papoulis, A. Probability, Random Variables, and Stochastic Processes, New York: McGraw-Hill Book Company, 1965.
9. Raemer, H. R. Statistical Communication Theory and Applications, Englewood Cliffs, New Jersey: Prentice-Hall, 1969.
10. Rimmer, M. P. "Method for Evaluating Lateral Shearing Interferograms," Applied Optics, 13(3): 623-629 (March 1974).
11. Sage, A. P. and J. L. Melsa Estimation Theory with Applications to Communications and Control, New York: McGraw-Hill Book Company, 1971.
12. Standard Mathematical Tables, 21st Edition, Cleveland: The Chemical Rubber Company, 1973.

13. The Infrared Handbook, Office of Naval Research, Department of the Navy, Arlington, Virginia: United States Government Printing Office, 1978.
14. Van Trees, H. L. Detection, Estimation and Modulation Theory, Part I, New York: John Wiley and Sons, 1968.
15. Viterbi, A. J. Principles of Coherent Communication, New York: McGraw-Hill Book Company, 1966.
16. Wyant, J. C. "Use of an AC Heterodyne Lateral Shear Interferometer with Real-Time Wavefront Correction Systems," Applied Optics, 14(11): 2622-2626 (November 1975).
17. Ziemer, R. E. and W. H. Tranter Principles of Communications: Systems, Modulation, and Noise, Boston: Houghton Miffling Company, 1976.

VITA

Fernando Pinzón Rojas was born on 4 September 1952 in Bogotá, Colombia. He graduated from Camilo Torres National High School in Bogotá in 1971 and in 1972 he established residence in the State of New Jersey. He attended Newark College of Engineering, now New Jersey Institute of Technology, from which he received the degree of Bachelor of Science in Electrical Engineering in 1977. Upon graduation he received a commission as a second lieutenant in the United States Air Force. He then served his first active duty assignment as a support engineer at the San Antonio Air Logistics Center, Kelly Air Force Base, Texas, until he was assigned to the School of Engineering, Air Force Institute of Technology, in 1979. He is a member of Tau Beta Pi.

Permanent address: 3 Walter Drive

Woodbridge, New Jersey 07095

UNCLASSIFIED

SECURITY CLASSIFICATION OF THIS PAGE (When Data Entered)

REPORT DOCUMENTATION PAGE		READ INSTRUCTIONS BEFORE COMPLETING FORM
1. REPORT NUMBER AFIT/GEO/EE/80D-4	2. GOVT ACCESSION NO.	3. RECIPIENT'S CATALOG NUMBER
4. TITLE (and Subtitle) PHASE ESTIMATION TECHNIQUES FOR ACTIVE OPTICS SYSTEMS USED IN REAL-TIME WAVEFRONT CORRECTION SYSTEMS		5. TYPE OF REPORT & PERIOD COVERED MS Thesis
		6. PERFORMING ORG. REPORT NUMBER
7. AUTHOR(s) Fernando F. Rojas 1st Lt USAF		8. CONTRACT OR GRANT NUMBER(s)
9. PERFORMING ORGANIZATION NAME AND ADDRESS Air Force Institute of Technology (AFIT/EN) Wright-Patterson AFB, Ohio 45433		10. PROGRAM ELEMENT PROJECT, TASK AREA & WORK UNIT NUMBERS
11. CONTROLLING OFFICE NAME AND ADDRESS Advance Radiation Technology Office (AFWL/AR) Air Force Weapons Laboratory Kirtland AFB NM 87115		12. REPORT DATE December 1980
		13. NUMBER OF PAGES 138
14. MONITORING AGENCY NAME & ADDRESS (if different from Controlling Office)		15. SECURITY CLASS. (of this report) Unclassified
		15a. DECLASSIFICATION DOWNGRADING SCHEDULE
16. DISTRIBUTION STATEMENT (of this Report) Approved for public release; distribution unlimited.		
17. DISTRIBUTION STATEMENT (of the abstract entered in Block 20, if different from Report)		
18. SUPPLEMENTARY NOTES Approved for public release; IAW AFR 190-17 <i>Fredric C. Lynch</i> FREDRIC C. LYNCH, Maj, USAF Director of Public Affairs 16 JUN 1981		
19. KEY WORDS (Continue on reverse side if necessary and identify by block number) Phase Estimation Array Processing Shearing Interferometry Active Optics Systems		
20. ABSTRACT (Continue on reverse side if necessary and identify by block number) Two analyses are presented, which involve estimation of constant phase from single detector and detector array measurements. The single detector analysis is carried out in a discrete mode to obtain algorithms based on photon counting. The method used follows the Maximum A Posteriori and Maximum Likelihood estimation theories. Both white Gaussian noise and Poisson Shot noise limited conditions are considered. Simulation results show that signal-to-noise ratios of 17 dB or better are needed to produce adequate estimates. Estimate improvement is obtained as more photon counts are performed. In this sense, photon counting		

DD FORM 1473
1 JAN 73

EDITION OF 1 NOV 65 IS OBSOLETE

UNCLASSIFIED

SECURITY CLASSIFICATION OF THIS PAGE (When Data Entered)

UNCLASSIFIED

SECURITY CLASSIFICATION OF THIS PAGE (When Data Entered)

20. (Continued)

seems to be inferior to current measuring, but the error variance is only 1.65 dB larger in the worst case, where three photon counts are performed. An extension of the single detector analysis is made, using only the Gaussian noise assumption, to derive an algorithm that jointly estimates the phase distribution over an optical wavefront. The procedure is based on a parametric dependence between the measurements performed by adjacent detectors, and on the a priori knowledge available through a covariance matrix. An algorithm for processing continuous waveform measurements is developed, but no computer simulation is included due to difficulties encountered in solving the feedback system equations.

UNCLASSIFIED

SECURITY CLASSIFICATION OF THIS PAGE (When Data Entered)

END

DATE
FILMED

7-81

DTIC